THESIS

STUDY ON ENERGETIC DEUTERIUM BEHAVIOR IN GRAPHITE CRYSYAL FROM THE VIEWPOINT OF HIGH ENERGY CHEMISTRY

グラファイト結晶中に注入された重水素の挙動に関する高エネルギー化学的観点からの研究

森 本 泰 臣

静 岡 大 学
大学院理工学研究科
物質科学専攻
放射化学研究施設

平成 15 年 12 月

PREFACE

The presented work was conducted as main theme of my studies from April 1998 to March 2004 at Radiochemistry Research Laboratory in Shizuoka University. Graphite material has been the most fascinating nuclear material. This is no exception in the case of materials for fusion reactors. In the present study, Highly Oriented Pyrolytic Graphite (HOPG) was used as a sample and chemical interactions between it and energetic deuterium were focused from the high energy chemistry point of view.

My personal involvement in research on high energy chemistry began when I belonged to Okuno's Laboratory at the Radiochemical Research Laboratory and since that time I have been involved to the various collaborative research on behaviors of hydrogen isotopes in fusion reactor materials. It remain to believe that this work of the thesis reflects my many experiences stored in the researches and is not concluded without connecting to many teachers, researchers and students in several research institutes and universities through the researches and meetings.

I wish that this work become the lodestar for the puisne studies and the high energy chemical behavior of hydrogen isotopes implanted into materials is revealed in detail.

Shizuoka, February 2004

Y. MORIMOTO

ACKNOWLEDGEMENTS

This work would have not been possible without the help, support and understanding of so many people, who made my life so much easier and enjoyable.

Acknowledgement with respects goes to:

Professor Kenji Okuno as my boss who provides many chances for studies and experience. He also guides me in the right direction for my campus life. The reason for acknowledgement is too many to be written down here

Prof. Mitsutoshi Tanimoto as my second boss proper guidance and valuable discussion.

Prof. Hideo Suganuma, Prof. Hiroe Yoshioka and Prof. Makoto Yanaga as team of professors at Radiochemistry Research Laboratory who had an open ear and the desire to give scientific advice and help.

Dr. Tsuyoshi Takeda for his help in cording of the TDS spectrum-fitting program.

Ms. Takako Ishida for office works and care for my private life.

Prof. Tetsuro Tanabe in Nagoya University for his lecture and discussion for this work.

Ass. Yasuhisa Oya in The University of Tokyo for their many useful advices in progressing my research, who is my greatest senior

Prof. Yuko Hirohata in Hokkaido University for many advices and encouragements.

Dr. Naoyuki Miya, Dr. Yoshitaka Gotoh and co-workers at JT-60 Facilities Division II in JAERI for setting and discussion for the collaborative research in JT-60U.

ULVAC-PHI Inc. for construction, improvements and repairs of the apparatus in Shizuoka University.

Special thanks goes to:

Prof. N. Yoshida, Ass. H. Iwakiri and Dr. M. Miyamoto, Prof. M. Nishikawa, Prof. K. Munakata, Prof. S. Fukada, Dr. A. Baba and Mr. Y. Yokoyama in Kyushu University.

Prof. M. Matsuyama and Prof. Y. Hatano in Toyama University.

Ass. T. Yoshida in Nagoya University.

Prof. K. Morita in Meijo University.

Prof. H. Moriyama, Prof. M. Okada and Ass. K. Kawamoto in KUR.

Dr. M. Nishi and co-workers at TPL, Dr. H. Tanigawa Dr. S. O'hira and Dr. T. Imai, Dr. K. Takahashi, Dr. T. Inoue in JAERI.

Prof. N. Noda, Prof. A. Sagara, Ass. Prof. Y. Hirooka, Prof. Y. Asakura and Prof. T. Uda in NIFS.

Prof. K. Kondo and Prof. S. Sasaki in KEK.

Mr. M. Numata in JGC co.

They are my best teachers and grate senior for the life and works. I thanks to their discussion anywhere.

Mr. N. Inudzuka, Dr. K. Iguchi, Mr. S. Akahori, Mr. T. Sugiyama, Mr. H. Kodama, Ms. E. Tega, Mr. M. Oyaidu, Mr. M. Sasaki, Ms. H. Kimura, Mr. T. Nunome and Mr. A. Yoshikawa at Okuno's Laboratory in Shizuoka University, Mr. Y. Onishi in Tokyo University of Science and the colleagues in Radiochemistry Research Laboratory of Shizuoka University.

They are my best colleagues and make me have an enjoyable campus life.

To my family, my parents and brother,
I am grateful for supporting everything and greatly respect in all my life.

CONTENTS

CHAPTER II

EXPERIMENTAL

CHAPTER III

STUDY ON CHEMICAL STATE OF DEUTERIUM IMPLANTED INTO HIGHLY ORIENTED GRAPHITE CRYSTAL

CHAPTER IV

STUDY ON DESORPTION BEHAVIOR OF IMPLANTED DEUTERIUM FROM HIGHLY ORIENTED PYROLYTIC GRAPHITE

CHAPTER V

STUDY ON TEMPERATURE DEPENDENCE OF TRAPPING FOR DEUTERIUM IMPLANTED INTO HIGHLY ORIENTED GRAPHITE CRYSTAL

CHAPTER VI

ANALYSIS OF PLASMA FACING GRAPHITE TILE IN JT-60U

CHAPTER VII

CONCLUSION

ATTACHMENT

CHAPTER I

INTRODUCTION

1.1 Demand for Energy

Energy is an indispensable ingredient of material prosperity and a source of many of the largest impacts of human beings on their environment [1].

As the population is increasing, the demand for energy is increasing rapidly. Since the Industrial Revolution, the human being has required the energy. The fossil resource such as coal, petroleum and so on has supplied the low-cost energy. However we have nearly run out the low-cost energy that has fueled the industrial development of today's developed countries and has shaped the expectations of the developing ones.

New energy sources will demand the safe and steady supply, low-cost and energy efficiency [1,2]. An additional point will be "cleanness" which is the most important [2]. The fossil energy has led to the environmental problem, especially greenhouse gas emission. The greenhouse gases, which include water vapor, carbon dioxide (CO_2), nitrous oxide (N_2O), methane (CH_4), chlorofluorocarbons, and tropospheric ozone, do not contribute equally to the risk of rapid climate change [3]. If this gas emission trend continues, the atmospheric buildup of these gases may lead to rapid and dangerous changes in global and regional climates [3]. Alternative energy sources in the future should be "clean" to the environment.

Alternative sources of energy that do not rely on fossil fuels have been proposed and demonstrated; these include photovoltaic solar cells, solar thermal energy, geothermal energy, wind power, biomass, ocean thermal differential, fuel cells, fusion and solar power satellites [4]. These energy sources have several problems [5], while they are expected very much. For energy sources, the human demands not only cost-effectiveness but also cleanness in the future. No "CO_2 free" energy resources exist [2]. The most important thing is the balance among the environment, economy, and energy for the activity of human being.

Nuclear fusion has been said to represent the ultimate in energy technologies in several different ways. It is potentially a clean technology in which it does not emit great amount of gaseous or solid wastes and its nuclear by-products are far less hazardous than that of nuclear fission technologies. Because of its enormous potential, by far the largest long-term research

and development have been carried out intensively [5].

1.2 Fusion Promising Energy Source

Nuclear fusion has potential to give an essentially inexhaustible source of energy in the future. Under proper conditions, low atomic number elements react each other to convert mass into energy via nuclear fusion. It is the common knowledge that the energy source of the sun is the nuclear fusion reactions. Eddington and Perrin proposed this hypothesis for the first time [6].

Now, the human being is challenging a making the sun on the earth. However, it is difficult that the human being controls the nuclear fusion reactions in the sun. In the present day, the human being is interested in several nuclear fusion reactions, described below. The cross sections of these nuclear reactions are shown in Fig. 1.1 [7].

$$D + T \rightarrow {}^{4}He + n + 17.58\ MeV \quad (1\text{-}1)$$

$$D + D \rightarrow {}^{3}He + n + 3.27\ MeV \quad (1\text{-}2)$$

$$D + D \rightarrow T + H + 4.04\ MeV \quad (1\text{-}3)$$

$$D + {}^{3}He \rightarrow {}^{4}He + H + 18.34\ MeV \quad (1\text{-}4)$$

The reaction (1-1) is the most possible nuclear fusion reaction considered for fusion reactors in the present day. The deuterium-tritium (D-T) reaction gives a 14.06 MeV neutron and a 3.52 MeV α particle. The reaction has the highest cross section at low energies indicated in Fig. 1.1 and the highest Q value [8]. The Q value is an energy multiplication factor, which is the ratio of input power to produce high temperature plasma and out put power generated by the nuclear fusion reaction.

The fusion reaction of 1g of tritium (together with 2/3g of deuterium) produces 1.6×10^{5} kW hr of neutron energy. This energy corresponds to about 8 ton of oil. Deuterium exists in the natural water at 0.015% of isotope abundance [9] and the extraction technique of deuterium has been established. Accordingly, deuterium can be considered to constitute an essentially infinite fuel resource. Tritium is a radioisotope emitting β radiation with half-life of 12.33 years and its isotope abundance is 10^{-16}%. Tritium can be produced with the neutron capture reaction of lithium as follows.

$$n + {}^{6}Li \rightarrow T + {}^{4}He + 4.78\ MeV \quad (1\text{-}5)$$

$$n + {}^{7}Li \rightarrow T + {}^{4}He + n' - 2.82\ MeV \quad (1\text{-}6)$$

The natural lithium consists of ^{6}Li (isotope abundance of 7.42%) and ^{7}Li (isotope abundance of 92.58%) [9] and can be considered to constitute an essentially infinite resource for tritium production in the nature when the recovery technology of Li from the seawater will be established [10]. Lithium-6 has the large reaction cross section (945 barn) for thermal neutron, while the reaction cross section of ^{7}Li for fast neutron (for example, 5 and 14 MeV) is 0.21 and 0.055 barn, respectively [9]. When the fusion chamber is blanketed with the lithium compounds, the 14.06 MeV neutron formed by D-T reaction can produce tritium by Reaction (1-5) and (1-6), accordingly inducing the possibility of a fusion reactor "breeding" its own fuel.

In the nuclear energy source, such as fission and fusion, radioactive waste is very huge problem. The nuclear fusion, however, has the potential attraction since it produces not only no high-level radioactive waste but also no possibility of reckless driving for fusion reaction, a little amount of released CO_2, and even distribution and unlimited fuel resource [11]. Inabe *et al.* discussed the radioactive waste in the literature [12]. They calculated the contact dose rate from conventional stainless steel and advanced materials (low-activation martensitic steel, V-Cr-Ti alloy, SiC composites, and Ti-Al alloy) as a function of time after the end of irradiation in a conceptual fusion reactor studied under the European SEAL (Safety and Environment Assessment of fusion power, Long-term) [12, 13]. According to a study under the SEAL program it is indicated that the low-activation radioactive materials and their recycling can reduce the wastes to be disposed to a significantly small amount [14]. The fusion energy will not run out and be wonderful energy source in the future.

However, to realize the fusion energy there are many problems. One of them is an economical problem. How about the cost of power generation for the nuclear fusion is? For example, when the cost of power generation including recovery of released CO_2 is considered, it is 1.3-2.0 times larger than that of various present generation [11]. The generation cost needs to reduce on the nuclear fusion. And if the fusion reactor is a significantly safe and the cost of building is lower than that of the fission reactor, there is possibility of alternative energy source of fossil energy. And many engineering problems are also still remained, today.

1.3 Fusion Reactor

1.3.1 Plasma Confinement

It was described above that most possible nuclear fusion reaction is D-T reaction in the present day. Even for the D-T reaction, however, the necessary temperature for ignition and maintaining the burning condition is of the order of 10^8 K or 10 keV. There are no known materials that could be used for a containment vessel that could withstand the solar temperature of the plasma. To confine the plasma, the special techniques are required. The two major plasma confinement ways are inertial confinement and magnetic confinement.

An Inertial Confined Fusion (ICF) concept is an "implosion" system. Targets are small capsules containing the fuel, and the ignition and burning are achieved at its center with imploded and highly compressed fuel [15]. The inertial confinement was suggested by J. Dawson who expressed "On the production of Plasma by Giant Pulse Laser" in 1964 [16]. In 1968, Bascov *et al.* observed the neutron by inertial confinement fusion reaction for the first time [17]. In Japan, ICF have been studied since 1972 at Institute of Laser Engineering of Osaka University. However, we will focus on the Magnetic Confined Fusion (MCF) rather than ICF, because it is the primary thrust of fusion research today.

The leading design configuration for the magnetic confinement is the tokamak, an example of which is shown in Fig. 1.2 [7]. The "tokamak" means the torus (a donut-shaped ring) vessel and magnetic coil (toroidalnya kamera ee magnetnaya katushka: tokamak) and this idea was expressed by Igor Tamm and Andrei Sakharov in 1951 [18, 19]. The toloidal field (TF), which is generated by the toloidal coil, is weak at the outside of the torus and strong at inside of it. So the plasma expands to outside of torus due to self-pressure. To depress this phenomenon, the proidal coil is used. This coil is flowed the current and then generates the proidal field (PF) which is vertical for TF. By the TF and PF, the plasma in the torus is confined. This way is more stable than other confinement way in the present day. In fact, the tokamak concept represents today the mainline experimental device in the field of MCF research throughout the world.

The tokamak is the approach that has obtained the most promising results to date, and is expected to be vehicle by which energy breakeven will be first demonstrated for fusion energy in near future. On Dec. 5, 2000, the Japan Atomic Energy Research Institute (JAERI) announced to the press that JT-60, which is the large tokamak device in JAERI, achieved the plasma

condition of the high density and high confinement for ITER operation.

1.3.2 Concept of Fusion Reactor

Figure 1.3 shows the basic concept of fusion reactor. The fusion reactor consists of the magnet component and vacuum vessel to confine the plasma, energy conversion system, and tritium processing system for the recovery of tritium, isotope separation, fuel storage, and so on. The fusion reactor is power multiplier, but not power generator [7]. It is reason why the fusion reactor needs the much energy to generate the energy.

In the reactor, the energy resource is the fast neutron produced by D-T reaction. The kinetic energy of it is converted into the heat in the blanket. Thermalized neutron reacts with lithium atom of tritium breeder and tritium is produced. The tritium is recovered in a tritium recovery system (see Fig. 1.3). In addition, the blanket shields the neutron and other radiation. On the other hand the energetic α particle produced by D-T reaction is trapped by the magnetic field and its energy is used to plasma heating [20]. Then thermalized α particle is pumped out as waste, however, a fuel is pumped out at same time and the pumped fuel is recycled (see Fig. 1.3). Therefore the fusion reactor is the fuel recycling reactor and the fuel generator.

1.3.3 International Thermonuclear Experimental Reactor (ITER)

The latest design of tokamak type D-T fusion reactor is International Thermonuclear Experimental Reactor project, called ITER. Because Europe Union, Japan, Russia, and so on. are cooperating to develop ITER, it is called 'International' reactor. ITER is envisioned to be the next major step in the world fusion program. As 'next-step' device on the development path defined by nearly thirty year of improvement of the tokamak fusion concept, ITER will combine a capability for achieving sustained ignition and extended-duration fusion barn in D-T plasma with reactor-relevant engineering features. Key features of main plasma with the nominal inductive operation are presented in Table 1.1 [21]. In terms of fusion power, ITER is designed to produce a normal fusion power of 500 MW for a pulse length of ≥400 seconds. The ITER project is unique and successful model for effective international collaboration in science and technology. It is scheduled to become operational early in the 21st century and will be the first fusion device to produce more energy than it consumes.

1.4 Plasma Surface Interaction (PSI)

Recently, the plasma confinement has been improved sufficiently. On the other hand, to realize fusion reactors, the reactor engineering becomes to be more important. The engineering about reactors materials is strongly needed to construct the fusion reactors. In the fusion reactors, the materials are exposed to the serious condition of radiation, energetic particles. Especially, the materials of Plasma Facing Components (PFCs), such as First Wall, Divertor, and so on, are exposed to most serious conditions such as heavy irradiation of fast neutron, α particles, and escaped energetic fuel particles (D and T). The PFCs is inner components of the vacuum vessel for enclosing D-T plasma. PFMs are wall facing the plasma directly and exists in more inner position than the blanket as shown in Fig. 1.3. Divertor is the pumping port which is exposed directly to plasma. Especially the divertor is called High Heat Flux Component. The materials of both PFCs are generally called Plasma Facing Materials (PFMs).

1.4.1 Candidates for Plasma Facing Materials (PFMs)

Plasma Facing Materials (PFMs) cannot avoid the interaction with the escaped energetic fuel particles from plasma, called Plasma Surface Interaction (PSI). PSI leads to damages of the material and release of surface species resulting in contamination of plasma, which is then cooled down via energy radiation [22]. Basic processes inducing the modification of PFMs surfaces are physical sputtering, chemical sputtering, and sublimation [22, 23]. Taking into account all these events, the desired properties of PFMs are followings; (1) high thermal conductivity and resistance to thermal shock, (2) non-magnetism, (3) low activation by neutrons, (4) high enthalpy of sublimation, (5) low reactivity with hydrogen towards formation of volatile compounds, and (6) gettering of oxygen (formation of stable surface oxides) which is one of serious plasma impurity species [20, 22]. So in general, low Z materials are used as PFMs, such as carbon materials, in the tokamak devices [24]. For example, graphites have been widely used for PFC of large powerful devices like TFTR, JET and JT-60U, because of their good outgassing property, low Z character and capability of handling high heat fluxes [25]. However, in the present day, high Z materials are reviewed because the plasma confinement is improved better. Yoshida has reported the review of high Z plasma facing materials, especially W and W alloy [26]. In fact, Be, CFC (carbon fiber composite), and W alloy (including 3% Re) have selected as candidates of PFMs in ITER design [21, 27, 28]. The required properties of

PFMs are not depending always on the plasma maintenance in recent day. Both the low Z and high Z materials have merits and demerits. To choose the best materials, the various studies on the interaction between the materials and plasma should be needed.

1.4.2 Plasma Surface Interaction (PSI)

In the most present, as PFMs of tokamak device, the carbon materials are chosen because of its ability to withstand high heat fluxes and its high sublimation temperature [24]. PFMs could be exposed not only to the fast neutrons but also by fuel particles, such as tritium and deuterium, and impurities, such as helium. They escape from the plasma and have high energy and high flux. Fast-neutron induces irradiation damages and activation and helium the irradiation damages of PFMs. However, the escaped fuel particles behavior in complicate manners, in PFMs materials such as carbon composites, that is, PSI, such as trapping, diffusion, chemical sputtering, and so on, is occurred as shown in Fig. 1.4 [29].

The important phenomenon of PSI from viewpoint of plasma maintenance is erosion of PFMs, such as the sputtering, chemical sputtering (only carbon materials), sublimation, and evaporation. Especially, in the present day, the chemical sputtering of the carbon materials is much studied because the carbon is chosen in PFMs of many tokamak devices. The chemical sputtering is the erosion phenomenon in which the hydrocarbon and/or carbon oxides are produced when the hydrogen and/or oxygen is irradiated to the carbon materials. This phenomenon has been studied by ion beam analyzed the mass since 1970's [30, 31] and the many information was obtained by experiments in the wide energy region [23, 32]. Ueda reviewed the erosion processes and suggested their models [33].

Another important phenomenon in PSI from viewpoint of the fusion safety is trapping of tritium in PFMs. Tritium is one of most dangerous atom for the human being because it is easy to permeate the metals at high temperature, to leak, to change the various chemical forms, and so on [34]. There is a possibility that tritium distribute to various parts in fusion reactor by the adsorption, dissolution, diffusion, and so on [34]. In case of accident, tritium would leak to the environment. The tritium inventory and the information of its trapping state need to estimate the behavior and amounts of tritium leaked from PFMs at accident.

1.5 High Energy Chemistry [35, 36, 37, 38]

1.5.1 Outline of High energy Chemistry

What is "High energy chemistry"? The high energy chemistry is defined as the interaction of high energy particles with matter, the nature and reactivity of short-lived species induced by the action of particle and electromagnetic radiation or hot atoms on substances in their gaseous and condensed states, and chemical processes initiated in organic and inorganic systems by high energy radiation.

The high energy chemistry began from "Hot atom chemistry" which have been used as informal synonym for "recoil chemistry" or "chemical effects of nuclear transformations". From the beginning, a hot atom means an atom formed with energy well in excess of ambient thermal energy or highly charged via a nuclear event. Recently, it has been available to study on the hot atom reaction that the hot atom can be formed by the non-nuclear reaction as well as by the nuclear event. The hot atom chemistry have become to include not only the chemistry induced via the nuclear event but also via non-nuclear reactions using beam method and/or photolysis, with the energy scale in the range from several tens to hundreds eV as shown in Fig. 1-5, thus it is called as the "High energy chemistry".

The high energy chemistry deals with chemical events caused by the deposition in single atoms of energy, which is much greater than chemical bond and ionization energies. Therefore the high energy chemical reaction progresses without any other energies such as activation energy in thermal chemical reactions. The type of energy conveyed to the atom, and thence to the surrounding atoms and molecules are: (1) the kinetic energy of recoil from gamma ray or energetic particle emissions (for example, typically of the order of 100 eV from the (n, γ) process and 100,000 eV from the (n, p) process), (2) the energy of Coulomb repulsion generated when the high positive charge acquired by an atom as a result of internal conversion of γ rays, excitation and/or emission of inner shell electron by X-ray absorption, followed by Auger electron emission, spreads over the atom in a molecules and (3) the energy of ionization and molecular excitation conveyed to molecule of the medium by γ rays, X rays and high energy electrons emitted. The recoil energy and massive Coulomb repulsion are different initiators of reactions than those found in radiation chemistry, but the reactions of electrons, atoms, radicals, and ions following the primary energy deposition are similar.

1.5.2 History of High energy Chemistry

While the final goal of the high energy chemistry is the elucidation of the mechanisms of reactions involving highly excited chemical species, more or less empirical approaches were employed in its early days with appreciable interest in its applications such as the production of enriched radioisotopes and labeled compounds. A history of high energy chemistry is summarized in Table 1.2 [35-51]. Early studies were introduced as several examples in high energy chemistry when it was still called as the hot atom chemistry, in this section.

The substantial recoil accompanying a particle emission in radioactive decay was observed early in the study of radioactivity at first time [39]. In 1904, H. Brooks, working under the guidance of Ernest Rutherford at McGill University in Montreal, reported that the decay products of the emanation "X" of radium, when deposited on a solid body, appears slightly volatile even at ordinary temperature [39]. Thus, when a copper plate on which the daughter nuclides of radon were deposited from a hydrochloric acid solution was placed inside a testing vessel and removed after one minute, a temporal activity, as high as one or two percent of the plate activity, was found on the walls of the vessel. The explanation of this phenomenon was reported in the next year by E. Ratherford in his book [40]: "Since radium A breaks up with an expulsion of an α particle, some of the residual atoms constituting radium B, may acquire sufficient velocity to escape into the gas and are then transferred by diffusion to the walls of the vessel". In modern terms, due to the recoil effect following α decay of ^{218}Po (radium A) the hot daughter atoms ^{214}Pb (radium B) are projected onto the walls of the vessel. Hot atom chemistry started from these studies.

In 1934, Szilard and Chalmers found that, when they irradiated C_2H_5I with neutrons, the ^{128}I atoms produced by ^{127}I (n, γ) ^{128}I reaction in liquid C_2H_5I were extracted in water phase [41]. This phenomenon is called "Szilard-Chalmers reaction", which is one of the most famous hot atom chemical reactions. The first step toward a better understanding came when Fermi and co-workers suggested that it must result from recoil from the γ ray emitted in the (n, γ) process in 1934 and 1935 [42, 43]. This concept, that the atom is ejected with high translational energy, led to the "billiard ball collision hypothesis" of Lobby in 1940 [44] which postulated that the radioactive recoiling atom may reenter stable combination as the result of a head-on collision with a bound atom of the same mass, leaving the recoil atom in the solvent cage vacated by the knocked-on atom. Thus, ^{128}I was thought to rupture its parent C-I bond and then lose its large excess energy by head-on collision with I in another C_2H_5I molecules, leaving the ^{128}I in the cage

with the C_2H_5 to form $C_2H_5{}^{128}I$. Conservation of momentum considerations preclude the recoil I atom from remaining in the cage after giving enough energy to an H atom to break a C-H bond.

Another important discovery in 1939 was that deep ionization, such as arises after internal conversion, could also lead to chemical changes, even when any associated recoil appeared to be negligible [45].

In 1968, R. Wolfgang and co-workers constructed a chemical accelerator [38, 50]. This prototype named "ADAM" was just a simple ion accelerator. However, they reported the non-nuclear hot atom reaction at first time. The non-nuclear hot atom have been studied and applied until the present day.

Until the present day, many studies have been investigated and the subjects have been subdivided. It is reason why the high energy chemical reaction correlates with various reactions such as the sputtering process and irradiation damage of solids, radioactive decay, analysis methods (Secondary Ion Mass spectrometry (SIMS) *etc.*) and so on. The investigation of high energy chemistry have contributed to not only clarification of the mechanism of chemical reaction caused by high energy, but also application of these reactions to concentration of radioisotope, to synthesis of labeled compounds.

1.5.3 Application of High energy Chemistry to Fusion Reactor Research [35, 36]

The amount of tritium required for a fusion reactor is estimated to be a kg order. On safe handling of tritium, various kinds of radiochemical research subjects as well as technological ones should be solved in the course of fusion reactor development.

In the blanket, the recoil tritium is produced by the ^6Li (n, α) T and ^7Li (n, n'α) T reactions. Its final states would be independent of primary species, and classical thermodynamics and kinetics of thermal species will govern the behavior of the tritium, although the chemical effects of nuclear transformation obviously enter the scene in the very first stage of exposure to neutron. For example, the tritium produced in neutron-irradiated Li_2O, which is one of the candidate materials for the tritium breeder, was three chemical forms such as T^+, T^-, and T^0, and the presence of positive damage in the crystal, that is, F^+-centers (oxygen-ion vacancy occupied by one neutron) was observed [52, 53]. The tritium release from Li_2O crystal irradiated with neutrons was correlated with the F^+ center annihilation. In the recent day, it was reported that the defects annihilation by annealing after the neutron irradiation correlated with the tritium release from several lithium ceramics [54-57]. These all results indicate that the defects related

with the oxygen vacancy would play important roles on tritium release. However, it is expected to investigate that what kind of tritium chemical form is induced by high energy chemical reaction during neutron irradiation. These informations are important to consider the tritium recovery concepts from the blanket.

The PFCs are exposed with the electromagnetic radiation, neutrons with kinetic energy of ~14 MeV, and the neutral particles of T, D and He with kinetic energies up to the keV range whose charge would be changed to atoms on plasma edge, and the energetic ions and/or atoms implanted directly along magnetic field lines or by ripple loss. The energy range of T, D, and He atoms is almost in the high energy chemical region (the order of < keV). When they are implanted into PFMs, they will react high energy chemical reactions, directly and/or indirectly. In fact, the erosion induced by high-flux particles is one of problems to be solved for PFMs developments. The erosion progresses by not only physical sputtering but also chemical one. The chemical reaction on PFMs, as represented by the chemical sputtering, is not explained by only thermodynamics. T. Tanabe reported that the special chemistry, as presented by non-equilibrium chemistry, would need to be applied to resolve the problem on PFMs [58]. This special chemistry could mean the high energy chemistry. He also reported that it does not mean the reaction left much from thermodynamics [58]. However, it is a fact that the all reactions are not always resolved by only thermodynamics, and that is indicating the possibility for the high energy chemical reaction. Accordingly, the effects of the energetic T, D, and He ions should be investigated from the high energy chemical point of view. Especially, information on interaction between energetic T ion and PFMs is most important from fusion safety point of view. Particular attention will be paid for the chemistry of PFMs, such as chemical sputtering, chemical effects of implantation and plasma-driven permeation of hydrogen isotopes.

1.6 Outline of Present Study

Graphite materials have been promising for nuclear reactors, fission and fusion reactors, materials. For the graphite materials in the fusion reactor, over the last two decades, carbon has been the material of choice for lining the walls of fusion device [59, 60]. Carbon is a low-Z material, has a low vapor pressure, has excellent high temperature properties and is relatively inexpensive. The natures provided constitutionally to carbon meet requirements for the reactor

materials from the viewpoints of plasma confinement. In fact, using the graphite materials as PFMs have enhanced the plasma character [61]. Barriers to break down, however, have been demonstrated for the plasma confinement enhancing, tritium inventory in the materials, interaction with hydrogen isotopes on the surface and so on.

From fusion reactor safety point of view, the tritium inventory is one of the most important things and is governed by chemical interactions between carbon and tritium. Study on carbon interacting with hydrogen has been enormously reported as shown in some reviews [7, 20, 25, 29, 33, 58-61]. The retention of hydrogen in carbon saturates at the ratio (H/C) of 0.4 around RT. The hydrogen to carbon ratio in the saturated layers is controlled by the temperature. On the other hand, when hydrogen is implanted into carbon at temperatures below 800 K, it is effectively immobile. Although the hydrogen retained in carbon is not thermally desorbed below 800 K, the saturated ratio is decreased with increasing the temperature. Therefore the implantation temperature is one of the most important parameters for governing the tritium inventory and chemical interaction with carbon.

As a subject of the present study, the chemical behavior of deuterium with carbon in HOPG was investigated for the estimation of tritium safety, especially the tritium inventory, in fusion reactors. Chemical states and desorption processes of deuterium implanted into HOPG were revealed. Then effects of the temperature for those were discussed using deuterium implantation at various temperatures including the lower temperature than RT. The thermodynamics for chemical reactions depends on the temperature. In the present study, the temperature dependence of chemical behavior deuterium in HOPG is focused and investigated whether the difference from the thermo-chemical reaction is induced by the implantation, from view point of the non-equilibrium chemistry; that is high energy chemistry.

The chemical behavior of implanted deuterium ions in graphite crystal was investigated by means of Thermal Desorption Spectroscopy (TDS) and X-ray Photoelectron Spectroscopy (XPS). Outline of the present study is as follows:

Introduction for the thesis was given in chapter 1

Features of apparatus designed and constructed in this work were indicated and theories of XPS and TDS, and property of graphite are described in chapter 2.

In chapter 3, the results of investigations by XPS on chemical states of deuterium implanted into the graphite crystal were described. In the XPS measurements, the chemical peak shifts of C1s resulting from D_2^+ and Ar^+ ions implantation were measured and chemical state of the implanted deuterium in HOPG were discussed.

In chapter 4, the desorption behavior of the deuterium implanted into HOPG was investigated by TDS. The TDS measurements with various heating rates were carried out after deuterium D_2^+ ions implantation into HOPG with various fluences of D_2^+ implantation. From these experimental results, desorption kinetics of the implanted deuterium was analyzed and discussed.

In chapter 5, temperature dependence of deuterium retention was investigated using TDS. Annealing of disordered structure in HOPG was also discussed with XPS results after the implantation at various temperatures.

In chapter6, the plasma facing tiles in JT-60 was analyzed by XPS, Secondary Ion Mass Spectroscopy (SIMS) and Scanning Electron Microscope (SEM). The hydrogen isotopes behavior in the divertor tile was discussed.

In chapter7, the present study was concluded and discussed for application to fusion reactor.

References

[1] J. P. Holdren, *Population and Environment*, **12**, 231 (1991).

[2] P. E. Doerell, *Applied Energy*, **64**, 79 (1999).

[3] I. M. Mintzer, *MTS Jounal*, **25**, 25 (1991).

[4] J. C. Glenn and T. J. Gordon, *Technol. Forecast. Soc. Change*, **61**, 97 (1999).

[5] E. S. Cassedy and P. Z. Grossman, Introduction to Energy. Resources, Technology, and Society. 2nd ed., Cambridge University Press, Cambridge (1998).

[6] E. Rutherford, *Nature*, **112**, 409 (1923).

[7] H. Ikegami, *et al.*, Kakuyugo Kenkyu I Kakuyugo Purazuma, University of Nagoya Press, Nagoya (1996) [in Japanese].

[8] R. F. Post, *Ann. Rev. Nucl. Sci.*, **20**, 509 (1970).

[9] Y. Murakami, *et al.*, Housyasen Deta Bukku, TININSYOKAN, Tokyo (1982), [in Japanese].

[10] S. Kaneko and W. Takahashi, *Colloids surf.*, **47**, 69 (1990).

[11] K. Okano, *J. At. Energy Soc. Jpn.*, **41**, 731 (1999), [in Japanese].

[12] T. Isobe, *et al.*, *Fusion Eng. Des.*, **42**, 7 (1998).

[13] I. Cook, *et al.*, SEAL studies of variant blanket concepts and materials, Sixth IAEA Technical Committee Meeting on Developments in Fusion Technology, Naka (Japan), October 21-25, 1996.

[14] P. Rocco and M. Zucchetti, Management strategy to reduce the radioactive waste amount in fusion. Sixth IAEA Technical committee Meeting on Developments in fusion Technology, Naka (Japan), October 21-25, 1996.

[15] C. Rubbia, *Nucl. phys.*, **A553**, 375c (1993).

[16] J. M. Dawson, *Phys. Fluid.*, **7**, 981 (1964).

[17] N. Bosov, *et al.*, *J. Quant. Electron.*, **4**, 864 (1968).

[18] J. L. Bromberg, *Fusion*, The MIT Press, Cambridge, MA (1983).

[19] R. Herman, *Fusion*, The Cambridge Univ. Press, Cambridge (1990).

[20] H. Ikegami, *et al.*, Kakuyugo Kenkyu II. Kakuyugouro Kougaku, University of Nagoya Press, Nagoya [in Japanease]

[21] Summary of the ITER Final Design Report, presented by the ITER director, July 2001.

[22] M. Rubel, *et al*, *Mater. Sci. Eng.*, **A272**, 174 (1999).

[23] Physical Processes of Interaction of Fusion Plasma with Solids, ed. by W.O. Hofer and J.

Roth, Academic Press, San Diego (1996).

[24] R.-D. Penzhorn, *et al.*, *J. Nucl. Mater.*, **279**, 139 (2000).

[25] A. Miyahara and T. Tanabe, *J. Nucl. Mater.*, **155-157**, 49 (1988).

[26] N. Yosida, *J. Nucl. Mater.*, **266-269**, 197 (1999).

[27] R. Paker, *et al.*, *J. Nucl. Mater.*, **241-243**, 1 (1997).

[28] G. Fedrici, *et al.*, *J. Nucl. Mater.*, **266-269**, 14 (1999).

[29] K. Ashida, *J. Plasma Fusion Res.*, **75**, 394 (1999), [in Japanese].

[30] J. Roth, *et al.*, *J. Nucl. Mater.*, **63**, 222 (1976).

[31] S. K. Erents, *et al.*, *J. Nucl. Mater.*, **63**, 399 (1976).

[32] J. W. Davis and A. A. Haasz, *J. Nucl. Mater.*, **241-243**, 37 (1997).

[33] Y. Ueda, *J. Plasma Fusion Res.*, **75**, 384 (1999), [in Japanese].

[34] K. Kobayashi, *J. Plasma Fusion Res.*, **76**, 1051 (2000), [in Japanese].

[35] Handbook of Hot Atom Chemistry, ed. by J.-P. Adloff, *et al.*, VCH Publishers, New York (1992).

[36] T. Tominaga and E. Tachikawa, Modern Hot-Atom Chemistry and Its Applications, Springer-Verlag, Berlin, Heidelberg (1981).

[37] H. K. Yoshihara and T. Sekine, *J. Radioanal. Nucl. Chem.*, **243**, 267 (2000).

[38] K. Yoshihara, Hotto atomu kagaku, Kibo shoten, Kooriyama (1978), [in Japanese].

[39] H. Brooks, *Nature*, **70**, 270 (1904).

[40] E. Rutherford, Radioactivity, Cambridge University Press, Cambridge, (1904), pp. 392.

[41] L. Szilard and T.A. Chalmers, *Nature*, **134**, 462 (1934)

[42] E. Amaldi, *et al.*, *Proc. Roy. Soc.*, **A146**, 483 (1934).

[43] E. Amaldi, *et al.*, *Proc. Roy. Soc.*, **A149**, 522 (1935).

[44] W. F. Libby, *J. Am. Chem. Soc.*, **62**, 1930 (1940).

[45] G. T. Seaborg and J. W. Kennedy, *Phys. Rev.*, **55**, 410 (1939).

[46] E. Segre et al. *Phys. Rev.*, **55**, 321 (1939).

[47] J. E. Willard, Chemical Effects of Nuclear Transformations, Annual Review of Nuclear Science, Annual Reviews, Inc., Stanford, CA, 1953, p198.

[48] G. Harbottle and N., Sutin, *J. Phys. Chem.*, **62**, 1344 (1958).

[49] T.A. Carlson and R.M. White, *J. Chem. Phys.*, **48**, 5191 (1968).

[50] E. Tachikawa and F.S. Rowland, *J. Am. Chem. Soc.*, **90**, 4767 (1968).

[51] Y. T. Lee, Nobel Lectures in Chemistry 1991-1990, World Scientific, Singapore, 1992 p. 320

[52] H. Kudo and K. Okuno, *J. Nucl. Mater.*, **133&134**, 192 (1985).

[53] K. Okuno and H. kudo, *J. Nucl. Mater.*, **138**, 31 (1986).

[54] Y. Morimoto, *et al.*, *Fusion Sci. Technol.*, **39**, 634 (2001).

[55] S. Akahori *et al.*, *Proceedings of 6th Japan-China Symposium on Materials for Advanced Energy System and Fission & Fusion Engineering*, (2001).

[56] S. Akahori, *et al.*, *J. Radioanal. Nucl. Chem.*, **255**, 257 (2003).

[57] M. Oyaidzu *et al.*, *Phys. Scr.*, (2003) in press.

[58] T. Tanabe, *J. Plas. Fus. Res.*, **74**, 423 (1998), [in Japanese].

[59] R. A. Causey, *J. Nucl. Mater.*, **300**, 91 (2002).

[60] R. A. Causey *et al.*, *Fusion Eng. Des.*, **61-62**, 525 (2002).

[61] T. Tanabe and T. Maruyama, *J. Plas. Fus. Res.*, **69**, 415 (1993), [in Japanese].

Table 1.1 Main plasma parameters and dimensions [21].

Parameter	Value
Total Fusion Power	500 MW *(700 MW)*
Q — fusion power additional/heating power	≥10
Average neutron wall loading	0.57 MW m^2 (0.8 MW m^2)
Plasma inductive burn time	≥400 s
Plasma major radius	6.2 m
Plasma minor radius	2.0 m
Plasma current	15 MA (*17 MA*[1])
Vertical elongation @ 95% flux surface/separatrix	1.70/1.85
Triangularity @ 95% flux surface/separatrix	0.33/0.49
Safety factor @ 95% flux surface	3.0
Toroidal field	5.3 T
Plasma volume	837 m^3
Plasma surface area	678 m^2
Installed auxiliary heating/current drive power	73 MW

(1) The machine is capable of a plasma current up to 17 MA, with the parameters shown in parentheses) within some limitations over some other parameters (e.g., pulse length)

(2) A total plasma heating power up to 110 MW may be installed in subsequent operation phases.

Table 1.2 Chronological table of high energy chemistry.

Year	Worker	Matter
1904	H. Brooks	Discovery of the emanation "X" of radium on inside wall of ion chamber
1905	E. Ratherford	Explanation of Brooks's discovery
1934	L. Szilard, T.A. Chalmers	Confirmation of free radioactive iodine in water phase after neutron irradiation to CH_3I; Szilard-Chalmers reaction
1935	O. Fermi group	Explanation of Szilard-Chalmers reaction
1939	E. Segre et al.	Confirmation of Coulomb repulsion by high charged particle induced by isomeric transition of $^{80m}Br \rightarrow ^{80}Br$
1940	W.F. Libby	Billiard bell collision hypothesis
1953	J.E. Willard	Random fragmentation hypothesis
1958	G. Harbottle, N., Sutin	Proposition of hot zone model
1968	R. Wolfgang	Chemical accelerator (appearance of non-nuclear hot atom reaction)
1986	Y.T. Lee	Noble prize (neutral-neutral system for non-nuclear hot atom reaction using chemical accelerator)
Some interesting hot atom chemical studies have been performed recently.		

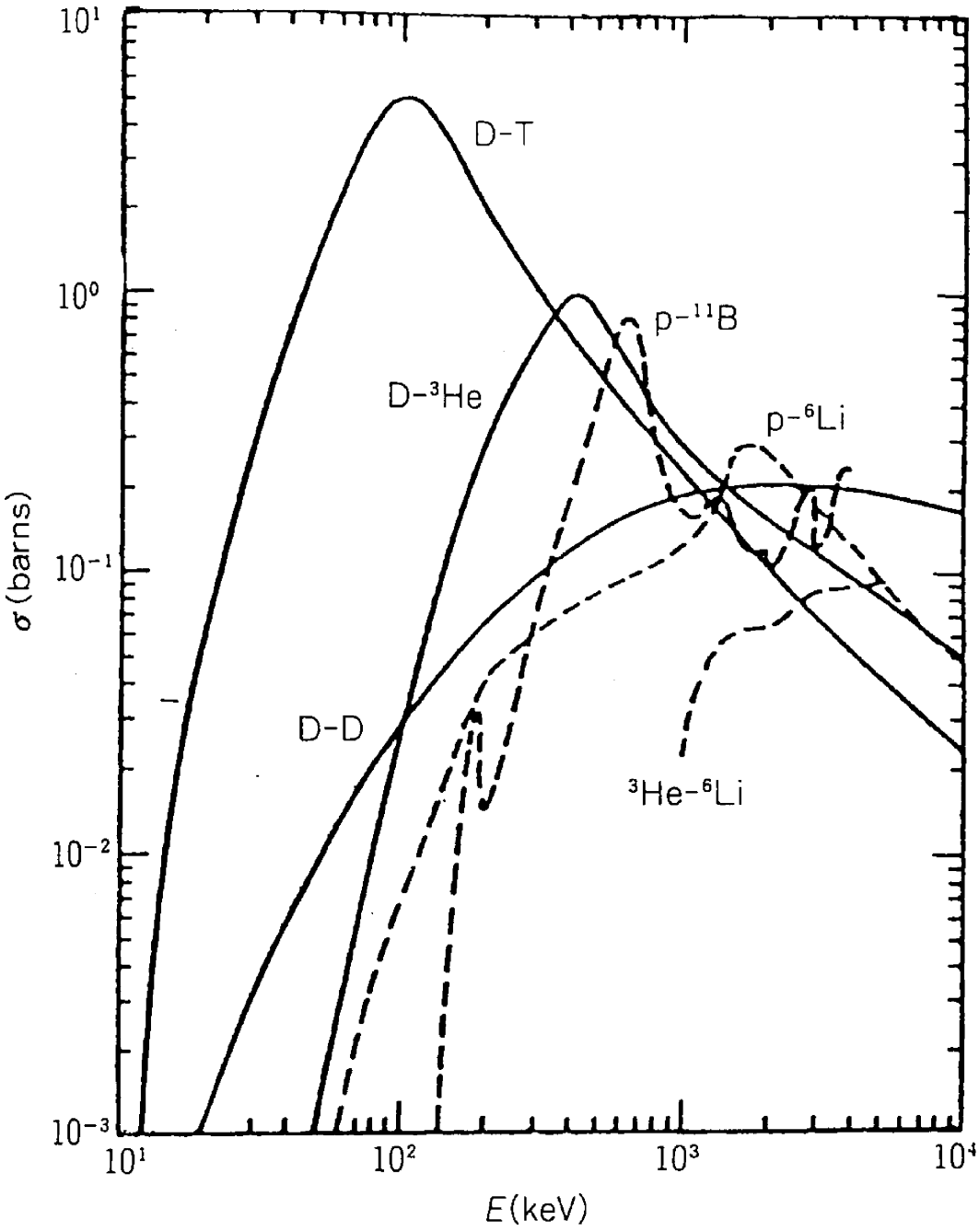

Fig. 1.1 Cross section of various nuclear fusion reactions [8].

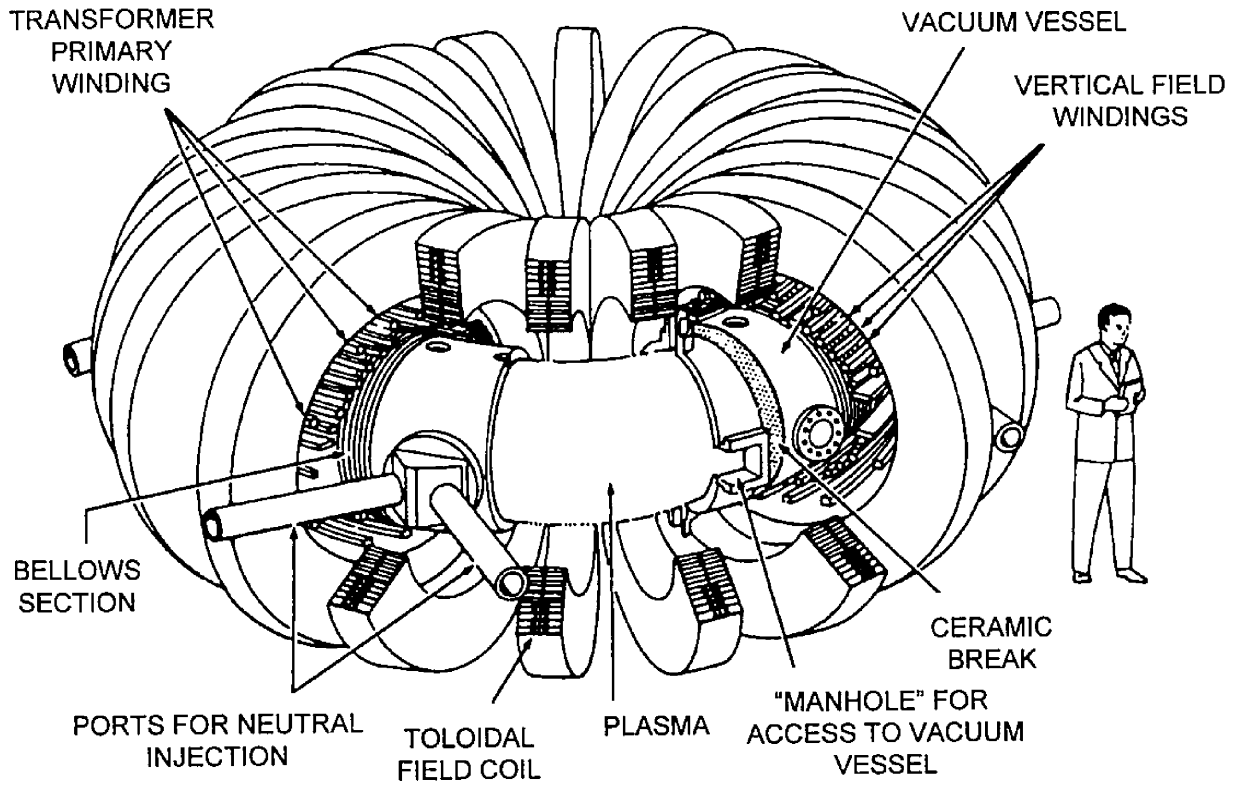

Fig. 1.2 Structure of the tokamak device [8].

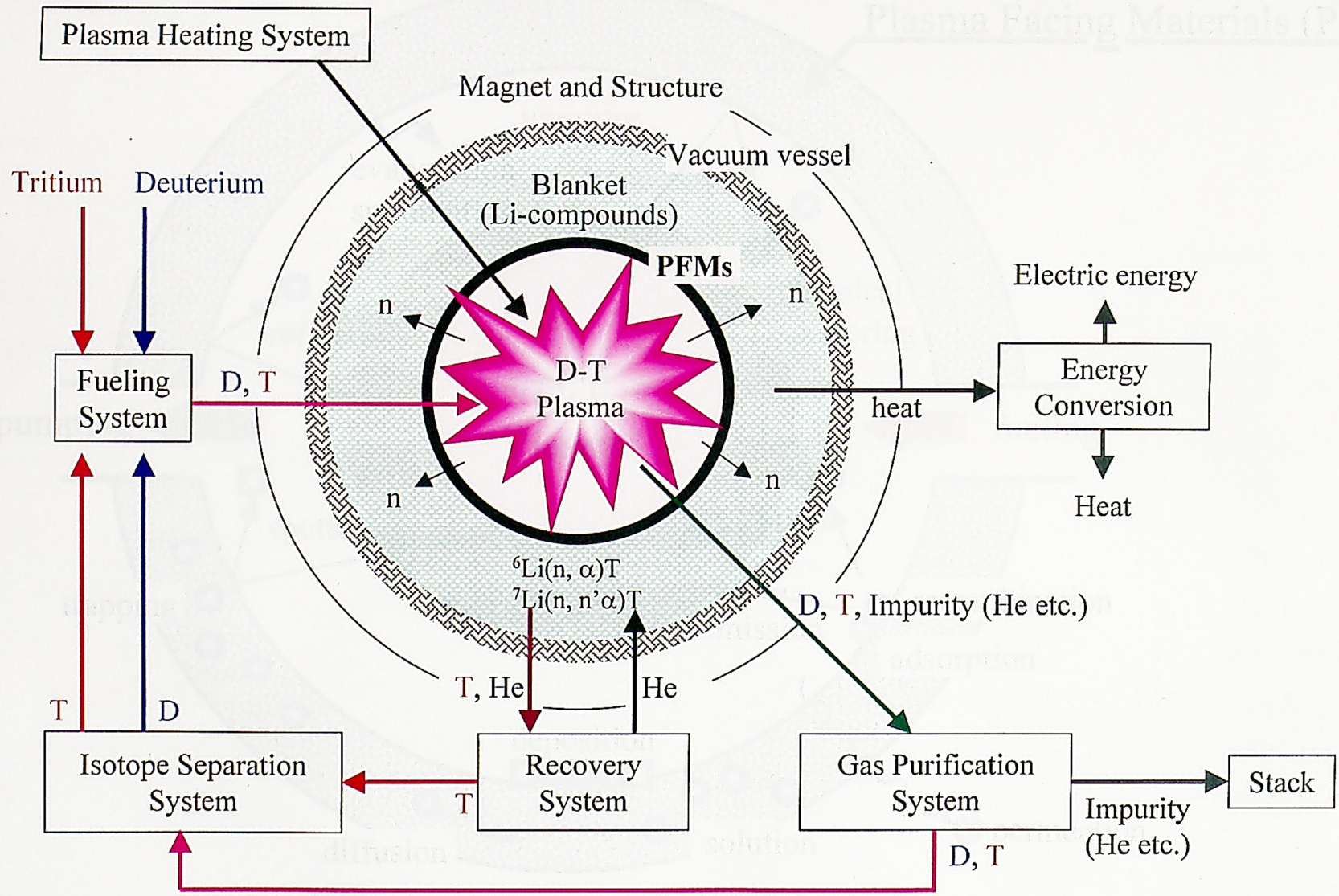

Fig.1.3 Basic concept of fusion reactor.

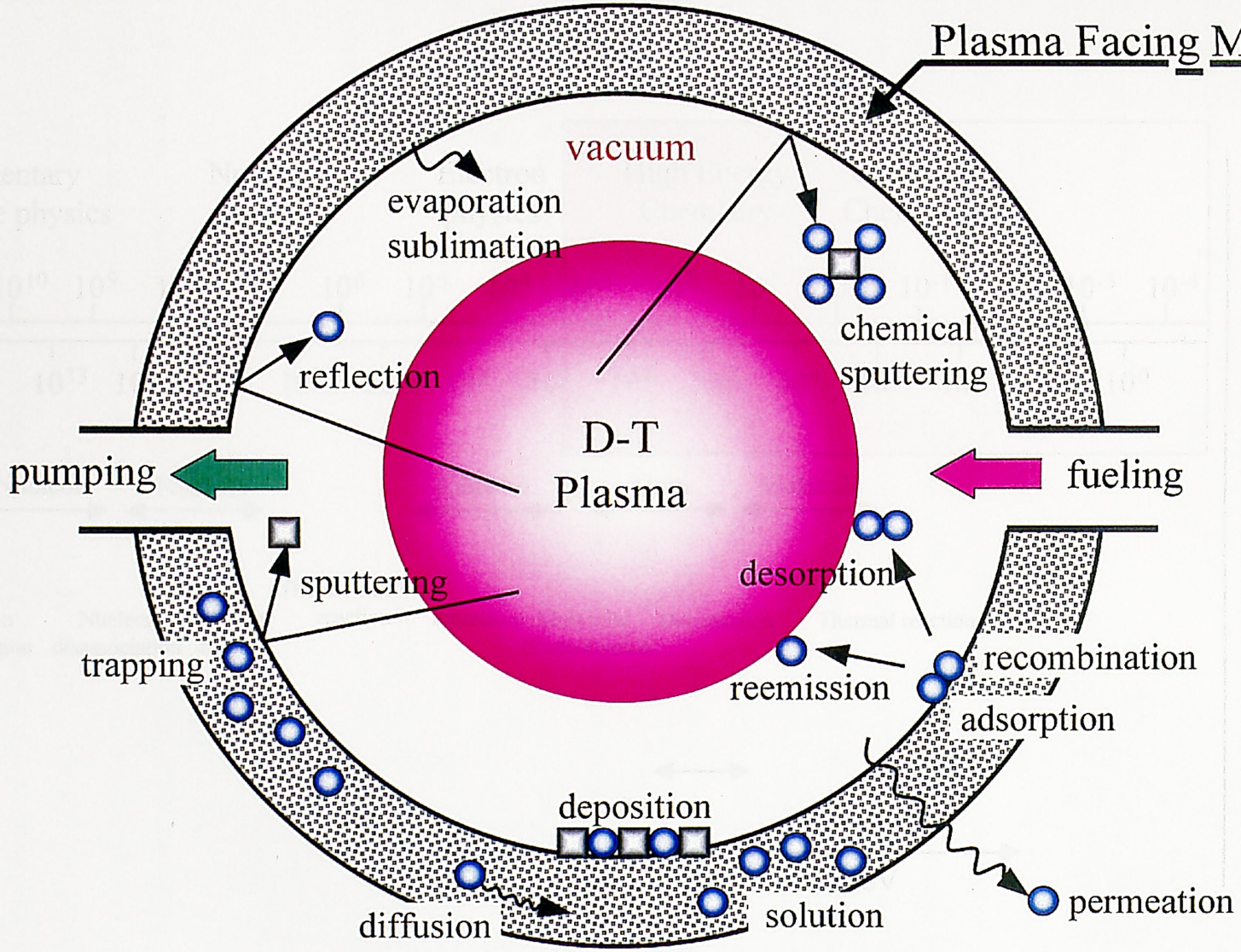

Fig. 1.4 Schematic drawing of plasma surface interaction (PSI).

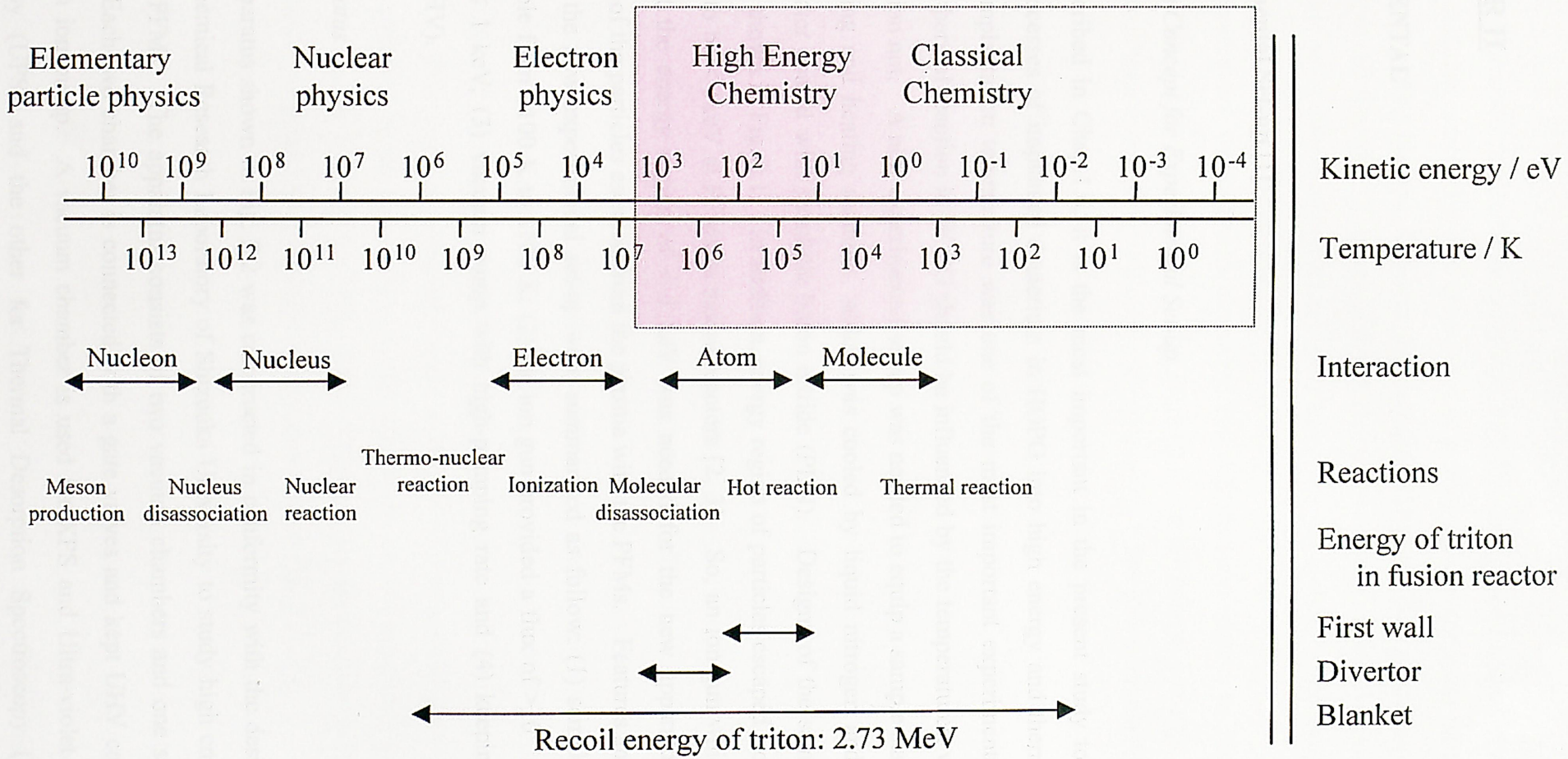

Fig. 1.5 Disciplinary and reactions classified from the viewpoint of energy scale.

CHAPTER II

EXPERIMENTAL

2.1 Experimental Set-up [1]

2.1.1 Design Concept for Experimental Set-up

As described in Chap.1.6, it is the most important in the present study to separate the chemical processes of implanted deuterium in HOPG into high energy and thermal reactions. Therefore, implantation temperature was one of the most important experimental parameters because the thermal reaction in HOPG should be influenced by the temperatures, while the high energy reaction not. A new experimental set-up was needed to equip a sample stage and holder with a cooling and heating modules, which was cooled by liquid nitrogen and heated by a ceramics heater coated with pyrolytic boron nitride (PBN). Designs of the sample stage and holder were shown in Fig. 2.1. In addition, energy region of particles escaped from the plasma is expected to be < 1keV at PFMs in fusion reactors [2, 3]. So, an ion gun which provided a high flux at the energy region of < 1 keV was needed for the new apparatus to simulate interactions of the particles escaped from the plasma with the PFMs. Features and components required to the new experimental set-up were summarized as follow: (1) sample temperature being variable from ~100 K to 1500 K; (2) the ion gun provided a flux of $>10^{18}$ m^{-2} s^{-1} and an energy of < 1 keV; (3) vacuum pump with high-pumping rate and (4) keeping Ultra High Vacuum (UHV).

2.1.2 Apparatus

An apparatus shown in Fig. 2.2 was constructed in conformity with the design concept at the Radiochemical Research Laboratory of Shizuoka University to study high energy chemical reaction in PFMs. The apparatus consists of two vacuum chambers and one sample-loading chamber. Each two chamber is connected with a gate valves and kept UHV condition ($\sim 10^{-8}$ Pa) by each ion pump. A vacuum chamber is used for XPS and Ultra-violet Photoelectron Spectroscopy (UPS) and the other for Thermal Desorption Spectroscopy (TDS). Each

spectrometer, which was fabricated from ULVAC PHI Inc., is equipped under the same vacuum system. In addition, each XPS and TDS chamber is respectively equipped with an ion gun. Therefore, the ion implantation, XPS and UPS measurements and TDS experiments are carried out in same vacuum system. This means the all chambers existing in same vacuum system and all experiments being able to be carried out in the same vacuum system. The sample is avoided from contamination by the moisture, oxygen and so on.

XPS experiments were carried out using PHI ESCA 1600 shown in Fig. 2.3. XPS chamber consists of a vacuum system, a CHA, an ion gun, an UV source, a charge neutralization gun and a monochromatic and a conventional X-ray sources. The characteristic X-ray of Al Kα is used in the monochromatic X-ray source and the characteristic X-ray of Al Kα and Mg Kα in the conventional X-ray source. By using the monochromatic X-ray source and the charge neutralization gun it is possible to study on an insulator of core level, valence band and Auger transitions without sample changing. It allows a more comfortable reading of the spectra and a better interpretation of the specimen chemical nature. The ion gun is introduced in the apparatus with 30° for sample stage horizontally to yield a maximum sputtering rate. The sputtering with Ar^+ ion is used for the decontamination of sample surface and analysis of depth profile.

Figures 2.4 and 2.5 show the pictures of the TDS apparatus and sample stage. The TDS apparatus consists of a deuterium standard leak, a Quadrupole Mass Spectrometer (QMS), an ion gun, a vacuum system and a sample stage. More remarkable point of the TDS apparatus is variable sample temperature from ~125 K to ~1400 K by a cooling module and a PBN heater shown in Fig. 2.5. In the case of cooling the sample, the cooling module is filled with liquid nitrogen and then the sample was cooled via cupper wires extending from the cooling module (see Fig. 2.5). This way can potentially make a sample cool to several Kelvin using liquid helium as a coolant. In the case of heating the sample, the one's temperature can be elevated proportional to heating time by the PBN heater. The sample temperature is measured by a K-type thermocouple placed on the sample surface as shown in Fig. 2.5.

In high energy chemical reaction, particles with high energy (>several tens eV) can react each other without an activation energy as mentioned in Chap. 1.5.1. And then the thermalized ones react thermo chemically. Because these reactions are carried out consecutively during the ion implantations with the high energy it is very difficult to distinguish each other from ones. The thermo chemical reactions are not undergone at absolute zero, while the high energy chemical reaction is allowed to react. Hence the lower temperature implantation attends the

possibility for depression of the thermo chemical reactions during the implantation, however, the thermo chemical reactions is not completely depress at temperature in this study. This indicates that experiments with implantations at temperature from lower to higher are very useful to be spotted the high energy chemical reactions.

2.2 Theory

2.2.1 X-ray Photoelectron Spectroscopy (XPS) [4-10]

X-ray Photoelectron Spectroscopy known as XPS or Electron Spectroscopy for Chemical Analysis (ESCA) has been developed in mid-1960's by Professor K. Siegbahn and his research group. The most interesting thing of this technique is the ability to measure the variation of the electron binding energy resulting from its chemical environment. This type of spectrometry have been used as a key tool for the surface analysis because of two major features; (1) Quantitative analysis, and (2) Information on the chemical nature and state of the detected elements.

By absorbing a photon, an atom receives an energy equal to $h\nu$ and then the bound electron is emitted by the photoelectric effect. In usual X-ray sources Mg Kα (1253.6 eV) and Al Kα (1486.6 eV) are used to emit photoelectrons from an atom inner shell (see Fig. 2.6 and 2.7). Consequently, there will be some atoms with vacancies in their inner shells. To recover the vacancies, electrons in outer shells transfer to the vacancies by emitting the characteristic X-ray or undergoing an Auger transition (see Fig. 2.7).

The principle of the conservation of energy allows us to write the following energy balance equation, valid for the absorption of the photon energy of $h\nu$,

$$h\nu = E_{\text{Kinetic}} + E_{\text{Binding}} + \phi_{\text{Work function}} \tag{2-1}$$

where $h\nu$ is X-ray beam incident energy, E_{Kinetic} the kinetic energy of the emitted electron, E_{Binding} the binding energy of the atomic orbital, and $\phi_{\text{Work function}}$ the spectrometer work function. From Eq. (2-1), we can determine E_{Binding} by the measurement of E_{Kinetic}. The kinetic energy of the photoelectron is analyzed with Concentric Hemispherical Analyzer (CHA)

shown in Fig 2.8, in order to determine the binding energy in the element. The lens system focuses the emitted photoelectron until the pass energy (E_0) into CHA. The E_0 is the kinetic energy for the electron to pass though along the trajectory determined by r_0 and ΔV, as shown in Fig. 2.8. This analyzer consists of the two plates applied a potential. When the photoelectron is assumed to enter vertically the slit of CHA, it travels along the trajectory generated by the potential and the resolution of electron energy for CHA written as Eq. (2-2),

$$\Delta E_a = \omega E_0 / 2r_0 + \alpha^2 E_0 / 4 \qquad (2\text{-}2)$$

where ΔE_a is the resolution of CHA, ω the width of the slit, E_0 the pass energy, r_0 the radius of same potential and α the incidence angle of election at the entrance of CHA. From Eq. (2-2), it is needed to get the high resolution for $2r_0$ force to become larger, for ω and E_0 force to become smaller. However, when ω and E_0 force to become smaller, the intensity of spectrum become weak.

The FWHM, ΔE, of peak for XPS spectrum is considered to be due to (1) the X-ray line width, ΔE_p, (2) the energy resolution of fthe CHA, ΔE_a, and (3) the inherent electron bonding energy line width, ΔE_n and then ΔE is expressed by Eq. (2-3),

$$\Delta E = \left(\Delta E_p^2 + \Delta E_a^2 + \Delta E_n^2\right)^{1/2}. \qquad (2\text{-}3)$$

ΔE_p is 0.7 eV because C1s measurements in the present study were used Mg Kα characteristic X-ray. ΔE_a can be determined from Eq. (2-2). In the case of XPS at Shizuoka University, α is 7°, ω 0.8 mm, and r_0 139.7 mm. By submitting these values in Eq. (2-2), ΔE_a is determined to be 0.0066 eV. In general, ΔE_n is 0.23-0.80 eV in the case of $Z < 30$, where Z is the atomic number. [7]. In this study, HOPG was used as a sample. ΔE_n of the C1s level is of the order of 0.1 eV [11]. Hence, the FWHM of C1s peak should be 0.7-1.1 eV.

One of the most important things in XPS is Inelastic Mean Free Path (IMFP). When the photoelectron is emitted by X-ray sources, the kinetic energy is kept until the entering analyzer to detect as a photoelectron peak. However, the most of photoelectron lose the kinetic energy by the inelastic collision and then is converted into the background signal. The photoelectron, which does not lose the kinetic energy, is located near surface. Therefore, the distance needed

to keep the initial kinetic energy, that is, IMPF is equal to the Escape Depth (*ED*) of photoelectrons. However, the value determined experimentally is Attenuation Length (*AL*). The relationship between *ED* and AL is written as Eq. (2-4),

$$ED = AL\cos\theta \tag{2-4}$$

where θ is the angle between the analyzer and the vertical of sample.

Seah and Dench led to the equation for *AL* (λ_a) from various experimental data. Their equation is shown as follows,

$$\lambda_a = 538aE^{-2} + 0.41a^{3/2}E^{1/2}\ (\text{nm}) \qquad \text{for a single element target} \tag{2-5}$$

$$\lambda_a = 2170aE^{-2} + 0.72a^{3/2}E^{1/2}\ (\text{nm}) \qquad \text{for a compound target} \tag{2-6}$$

Where E is the photoelectron kinetic energy (eV), and a the thickness of the monoatomic layer. And a is represented as follows,

$$a = (10^{21}A/\rho nN_A)^{1/3} \tag{2-7}$$

where A is atomic weight, ρ the density (g cm^{-3}) of the target, n number of atoms in the target, and N_A Avogadro's number. By submitting Eq. (2-5) in Eq. (2-4), *ED* in the case of graphite is determined as shown in Fig. 2.9 (θ = 45°). And in the case of C1s binding energy, *ED* is plotted against several θ as shown in Fig.2.10. As shown in Fig. 2.9 and 2.10, *ED* in XPS measurements for C1s of graphite is maximum value to be ~1 nm. Therefore XPS technique is surface analysis one.

XPS have it own specific application domains for the surface analysis. This domain relates to physical parameters like the excitation energy and/or FWHM of excitation source energy. X-ray can excite inner shell electrons and are not very used for studying the fine structure of the valence band. Because the valence electron is excited to vacuum level directly, valence spectra correspond to the density of state. So it is often used comparison of theoretical calculations of the molecular orbital method.

2.2.2 Thermal Desorption Spectroscopy (TDS) [9, 12-15]

In studies of gas-surface interactions, Thermal Desorption Spectroscopy (TDS) or Thermal Programmed Desorption spectroscopy (TPD) are often used despite the fact that many other methods of surface analysis have been developed, and some of them are more sensitive and more precise. There are at least two reasons for TDS to be attractive; (1) the TDS technique is relatively simple and (2) the method can be applied even to electrically insulated sample without further difficulties.

One of the goals of TDS measurement is the determination of kinetic parameters such as desorption energy, order of kinetics, and pre-exponential factor. Thus, if the temperature-time relation for sample heating is suitably controlled the TDS spectra can be analyzed to yield information on various adsorption parameters. This information includes; (i) the number of the various desorbing phases and the population of individual phases, (ii) the activation energy of desorption of the various phases, and (iii) the order of the desorption reaction.

TDS spectra analysis is based on Redhead's work. Method of TDS spectra analysis starts from the Polanyi-Wigner desorption rate equation, which is one of the Arrhenius equation, written as Eq. (2-8),

$$N(t) = -d\sigma / dt = \nu_n \sigma^n \exp(-E / RT) \tag{2-8}$$

where n is the order of the desorption reaction, σ the surface coverage, ν_n the frequency factor, E the desorption activation energy, T the sample temperature, and R the gas constant. T is changed linearly with time written as Eq. (2-9),

$$T = T_0 + \beta t \tag{2-9}$$

where T_0 is the sample temperature without heating ($t = 0$), β the heating rate, that is, dT / dt. Here, it is assumed that E is independent of σ. The temperature (T_p) at which the desorption rate is a maximum is found in the desorption spectra, and T_p is given by the condition $d^2\sigma / dt^2 = 0$, which from Eq. (2-8) leads Eq. (2-10),

$$\frac{E}{RT_p^2} = \frac{\nu_n n \sigma^{(n-1)}}{\beta} \exp\left(-\frac{E}{RT_p}\right), \tag{2-10}$$

or rearranging as

$$\ln(T_p^2 / \beta) = (E / RT_p) + \ln(E / R\nu_n n) - (n-1)\ln(\sigma). \tag{2-11}$$

This equation indicates that the plot of $\ln(T_p^2 / \beta)$ vs. $(1/T_p)$ results in a straight line when the heating rate is varied with keeping σ, which means the amount of the implantation being kept constant.

Another rearrangement of Eq. (2-11) gives

$$\ln(\beta E / RT_p^2) + (E / RT_p) = \ln(\nu_n n) + (n-1)\ln(\sigma). \tag{2-12}$$

This equation indicates that n is determined from slope of the plot of $\ln(\beta E / RT_p^2) + (E / RT_p)$ vs. $\ln(\sigma)$ when E determined from Eq. (2-11) is substituted. Therefore, in the case of second-order reaction, T_p shift to lower temperature with increasing σ.

2.3 Sample

The sample used in the present study was highly oriented pyrolytic graphite crystal (HOPG) purchased from Pechiney Co. (taken over by SGL carbon group companies in 1992). The sample size was $10\times10\times1.5^t$ mm and its density was determined to be 2.3 g/cm^3. Figure 2.11 and 2.12 show the SEM image of cleavage face and figure for structure of HOPG [16, 17].

Figure 2.13(a) and (b) show XRD (X Ray Diffraction) pattern for an as-received sample. Each diffraction peak was identified with Ref. [18, 19]. Figure 2. 13(b) also shows diffraction peak resulted in PG (pyrolytic graphite) purchased from GE Advanced Ceramics Co. The diffraction peak of PG was very broad, while that of HOPG very sharp and indicated fine structures. The c_0 as shown in Fig. 2.12 was determined from Fig. 2.13 to be 0.336 nm for c_0 (002), 0.337 nm for c_0 (004) and 0.336 nm for c_0 (006) using Bragg's equation [20]. These results indicated the good agreement with 0.335 nm shown in Fig. 2.12 [16, 17]. The sample

used in this study is HOPG with high crystallinity, however its structure is not complete graphite structure because the splitting and shapes of (002) diffraction pattern would be resulted from irregular laminating layer [20, 21].

Fig. 2. 14(a) and (b) shows typical XPS spectra for a cleaved surface heated at 1400 K for 20 min in this study which were measured in (a) wide range and (b) narrow range using the monochromatic X-ray source. In the wide range scan, C1s, C_{KLL} of Auger electron, C_{VB} of valence band peaks and no peak attributed to contaminations were observed as shown in Fig. 2.14 (a). The C1s peak located at ~284.5 eV and plasmon peak due to π-π^* transition at ~292 eV as shown in Fig. 2.14(b). The π-π^* transition peak is one of the characteristics for graphite structure.

The results from XRD and XPS are confirmed that the sample used in this study is HOPG without any contaminations.

References

[1] Y. Morimoto, *et al.*, *Phys. Scr.*, **T103**, 117 (2003).

[2] G. Federici *et al.*, *J. Nucl. Mater.*, **266-269**, 14 (1999).

[3] Handbook of Hot Atom Chemistry, ed. by J.-P. Adloff, *et al.*, VCH Publishers, New York (1992).

[4] Partical Surface Analysis by Auger and X-ray Photoelectron Spectroscopy (Japanese edition), ed. by D. Briggs and M. P. Seah, AGNE Publishing Inc., Tokyo (1990), [in Japanese].

[5] X Sen Koudenshi Bunkouhou, ed. by The Surface Society of Japan, MARUZEN CO. LTD., Tokyo (1998) [in Japanese].

[6] K. Yosjihara and M. Yoshitake, Hyoumen Bunseki Nyumon, SHOKABO, Tokyo (1997), [in Japanese].

[7] L. C. Feldman and J. W. Mayer, Fundamentals of Surface and Thin Film Analysis (Japanese edition), KAIBUNDO Press, Tokyo (1989), [in Japanese].

[8] Hyoumen Bussei Sokutei, ed by A. Koma, MARUZEN CO. LTD., Tokyo (2001) [in Japanese].

[9] Kotai Hyoumen Bunseki I, ed. by T. Onishi, Y. Horiike and K. Yoshihara, KODANSHA, Tokyo (1995) [in Japanese].

[10] Handbook of X-ray Photoelectron Spectroscopy, ed. by J. Chastain and R. C. King, Jr., Physical Electronics Inc., Minesota (1995).

[11] Y. Gotoh and O. Okada, *J. Nucl. Sci. Technol.*, **21**, 205 (1984).

[12] K. Ashida, *et al.*, *J. Nucl. Mater.*, **128&129**, 792 (1984).

[13] E. Tomková, *Surf. Sci.*, **351**, 309 (1996).

[14] P. A. Redhead, *Vacuum*, **12**, 203 (1962).

[15] K. Okuno, *J. Plasma Fusion Res.*, **72**, 1376 (1996), [in Japanese].

[16] B. S. Elmen, *J. Appl. Phys.*, **56**, 2114 (1984).

[17] M. S. Dresselhaus and R. Kalish, Ion Implantation in Diamond, Graphite, and Related Materials, Springer-Verlag, Berlin (1992).

[18] Shin Tanso Zairyo Nyumon, ed. by The Carbon Society of Japan, SIPEC Co., Tokyo (1996) [in Japanese].

[19] Saisin Tanso Zairyo Zikken Gijutsu, ed The Carbon Society of Japan. SIPEC Co., Tokyo (2001) [in Japanese]

[20] M. Kato, Xsen Kaisetsu Bunseki, UCHIDA ROKAKUHO PUBLISHING CO., LTD., Tokyo (1990) [in Japanese].

[21] F. Schossberger, *Adv. X-ray Anal.*, 1, 73 (1957).

(1) Sample stage

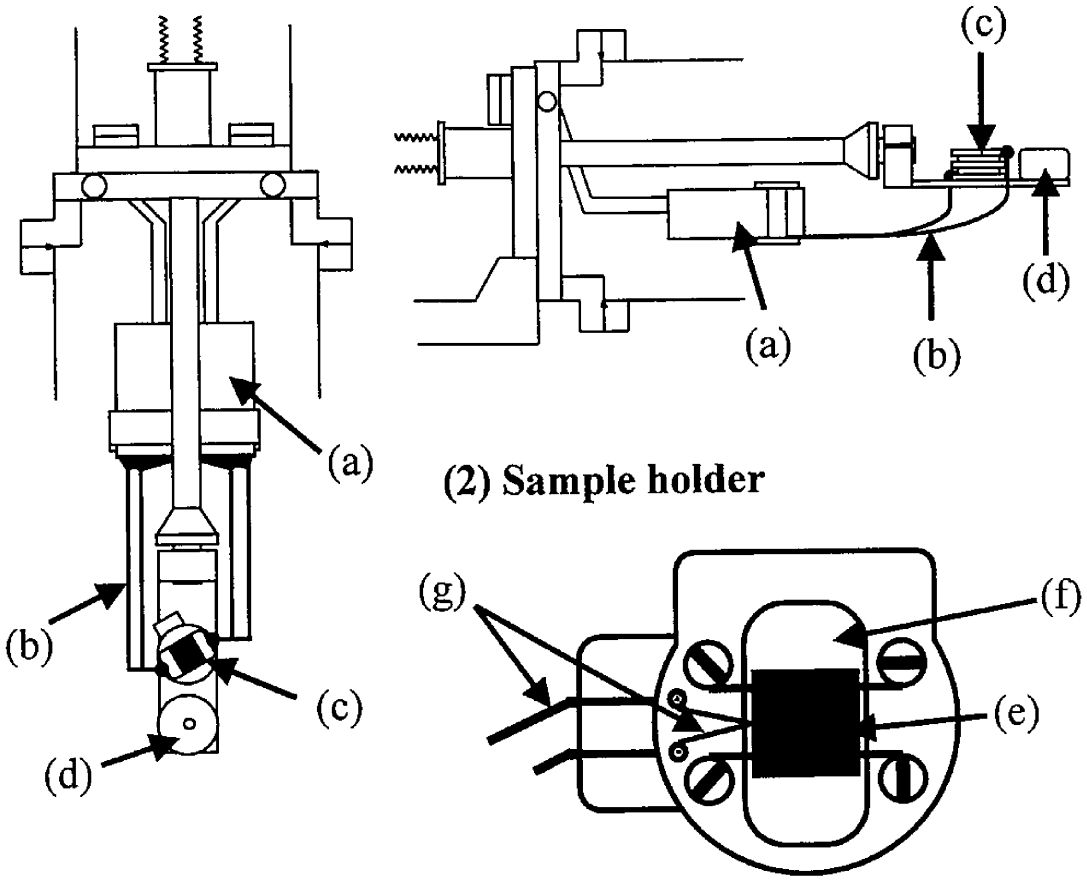

Fig. 2.1 Designs for (1) sample stage and (2) sample holder. Each character shows (a) Cooling module, (b) copper wires, (c) sample holder, (d)Faraday cup, (e) sample, (f) ceramics heater, (g) thermo couple.

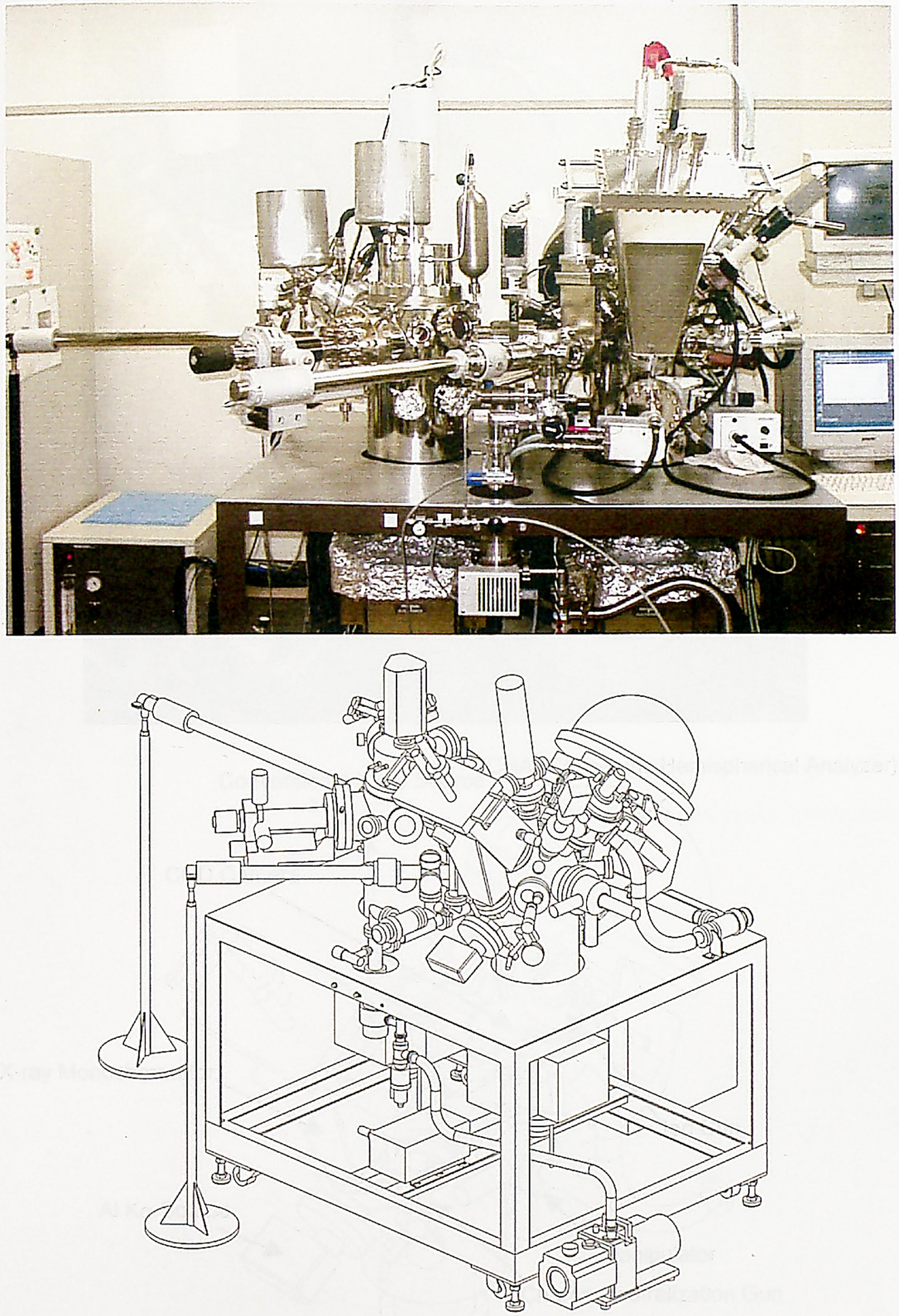

Fig. 2.2 Pictures of apparatus.

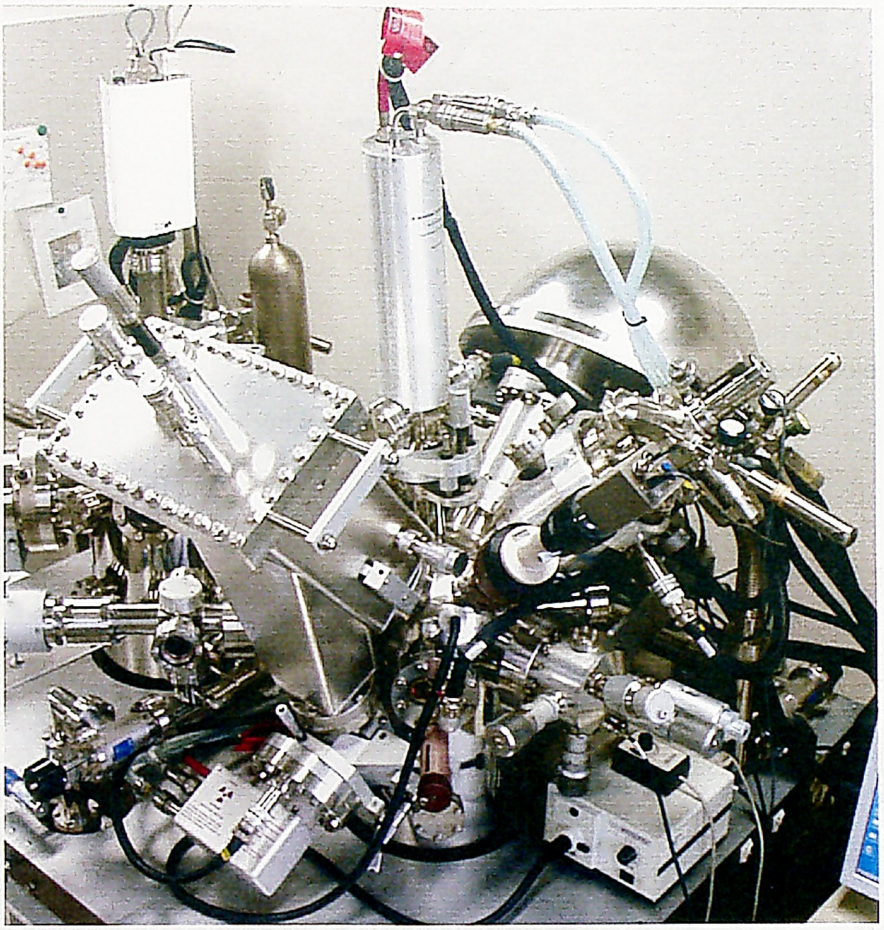

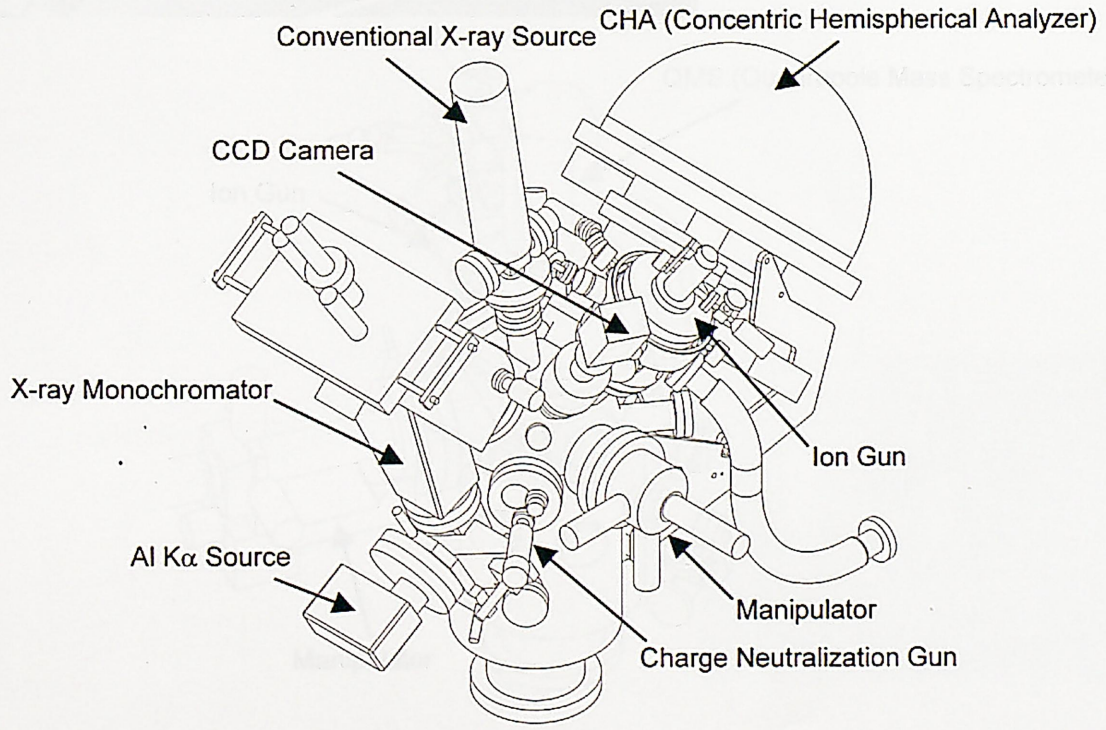

Fig. 2.3 XPS apparatus.

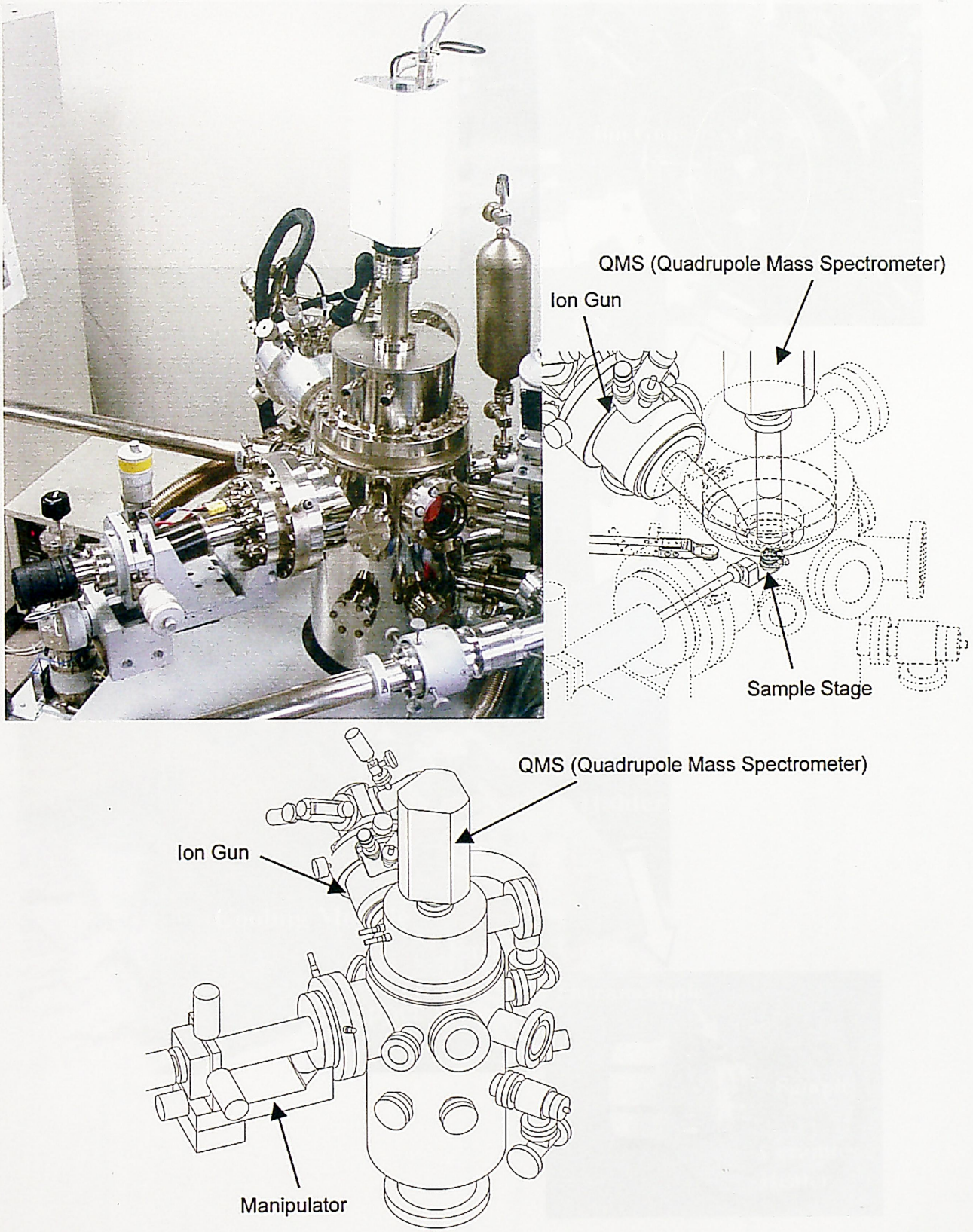

Fig. 2.4 TDS apparatus.

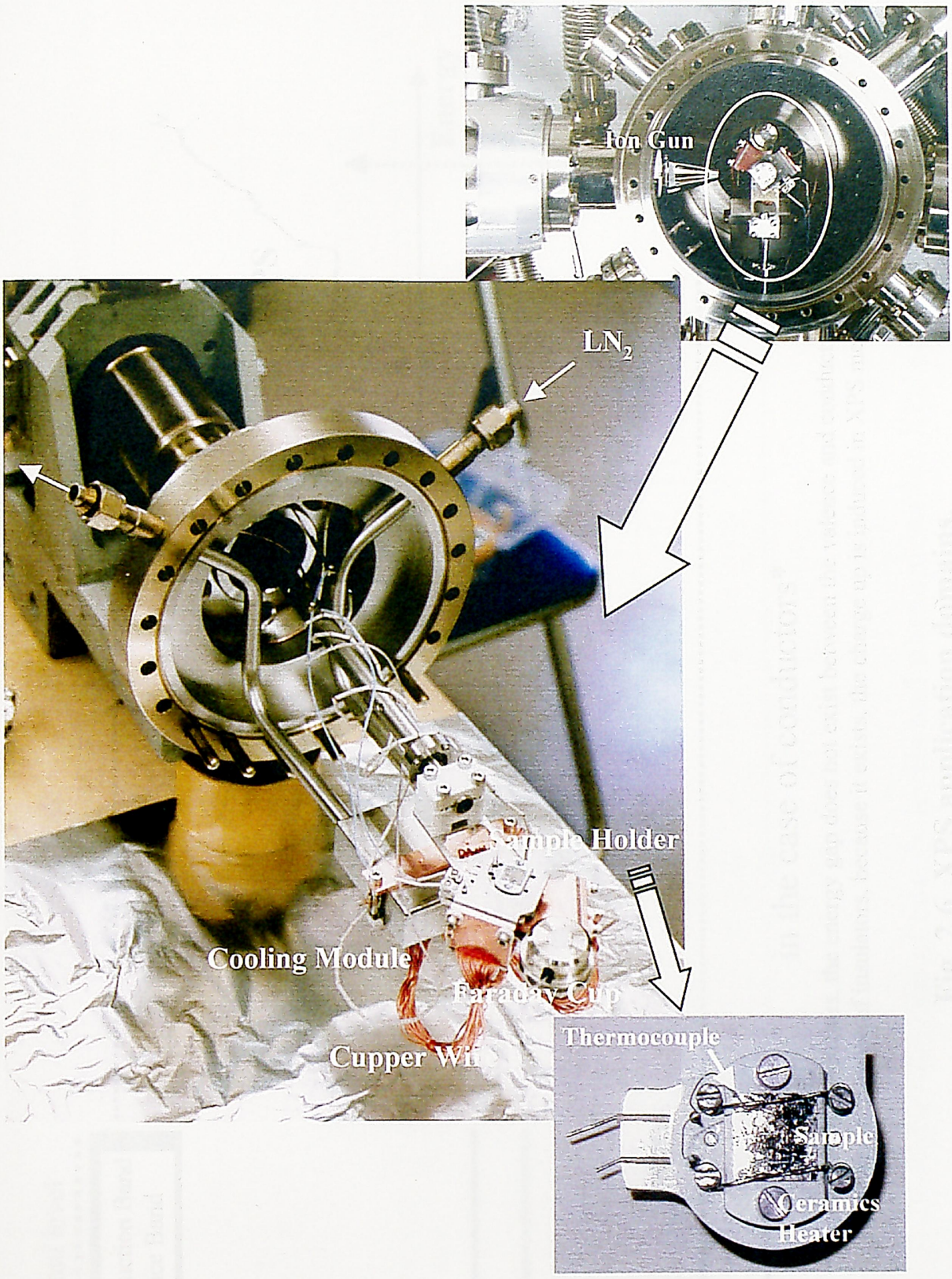

Fig. 2.5 Sample stage with TDS chamber and sample holder.

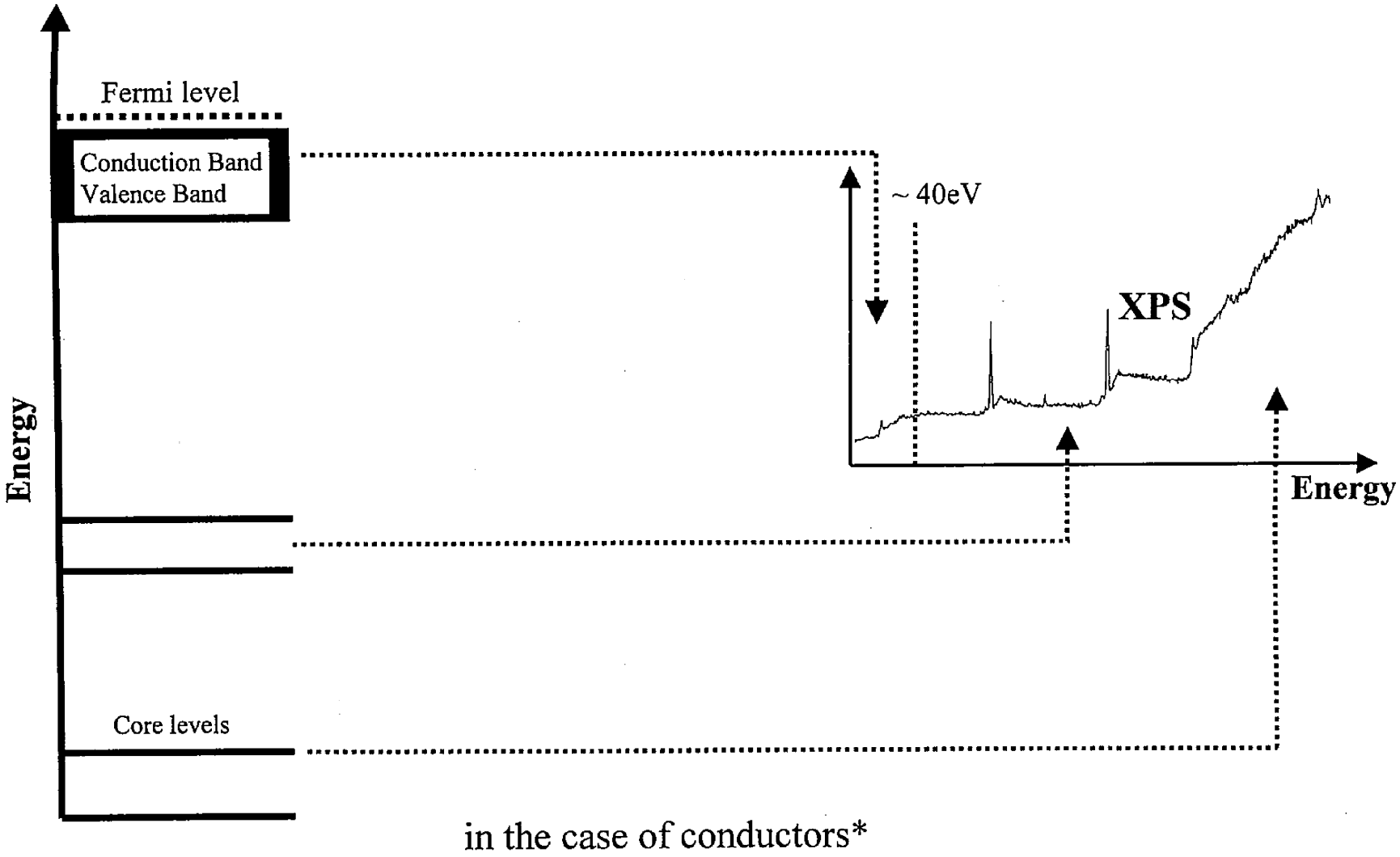

* In the case of conductors, the energy gap does not exist between the valence and conduction band. However, in the case of insulators, because it exists, the charge up is induced in XPS measurement.

Fig. 2.6 XPS application domains.

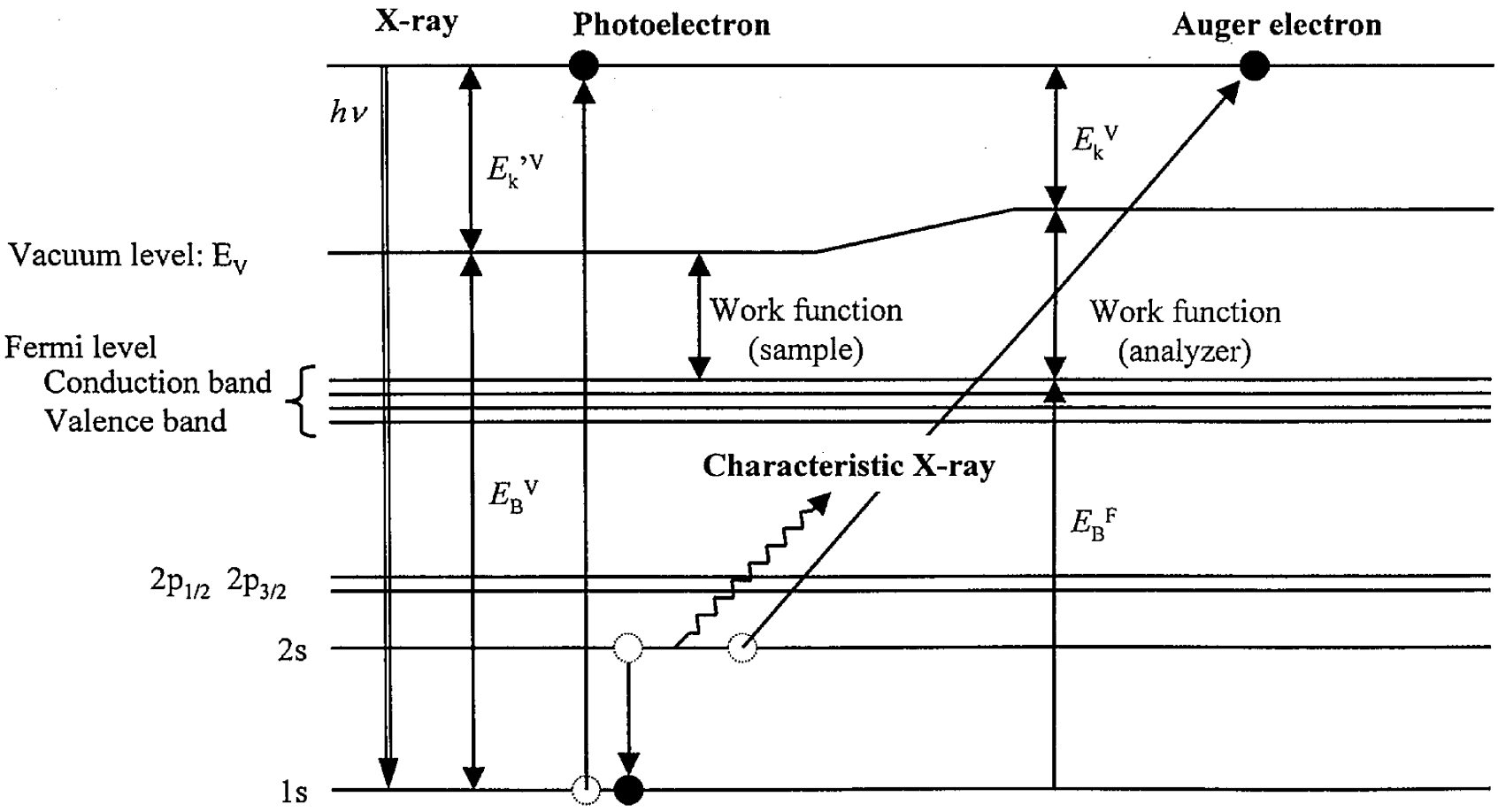

Fig. 2.7 Systematic diagram of energy levels and phenomena for XPS measurement.

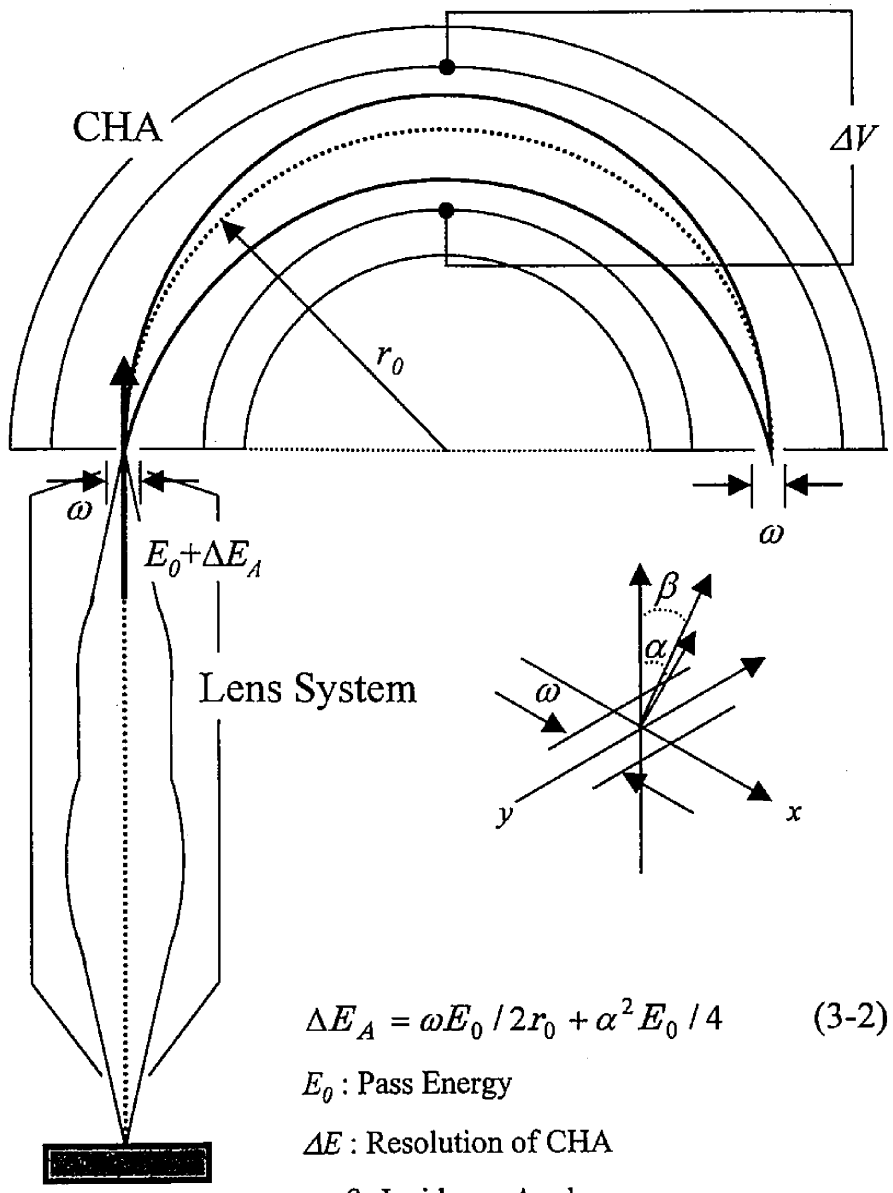

$$\Delta E_A = \omega E_0 / 2r_0 + \alpha^2 E_0 / 4 \qquad (3\text{-}2)$$

E_0 : Pass Energy

ΔE : Resolution of CHA

α, β : Incidence Angle

r_0 : Radius of Same Potential

ω : Width of Slit

V : Potential

Fig. 2.8 Concentric Hemispherical Analyzer (CHA).

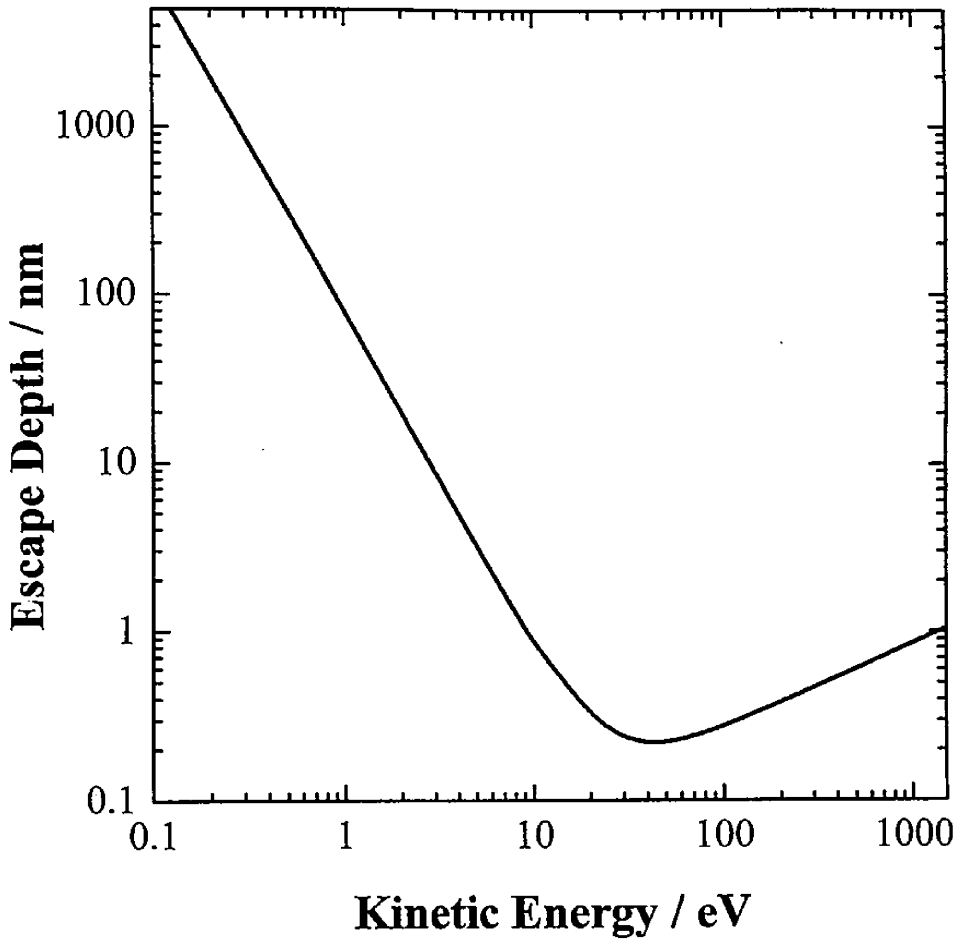

Fig. 2.9 Dependence on photoelectron energy on range of escape depth in graphite.

$$ED = AL \cos\theta \quad (2\text{-}3)$$

$$\lambda_a = 538\, aE^{-2} + 0.41\, a^{3/2} E^{1/2} \text{ (nm)} \quad (2\text{-}4)$$

$$a = (10^{21} A / \rho n N_A)^{1/3} \text{ (nm)} \quad (2\text{-}6)$$

θ : 45°
A : 12
ρ : 2.3 g cm^{-3}
n : 1
N_A : 6.02 × 10^{23} mol^{-1}

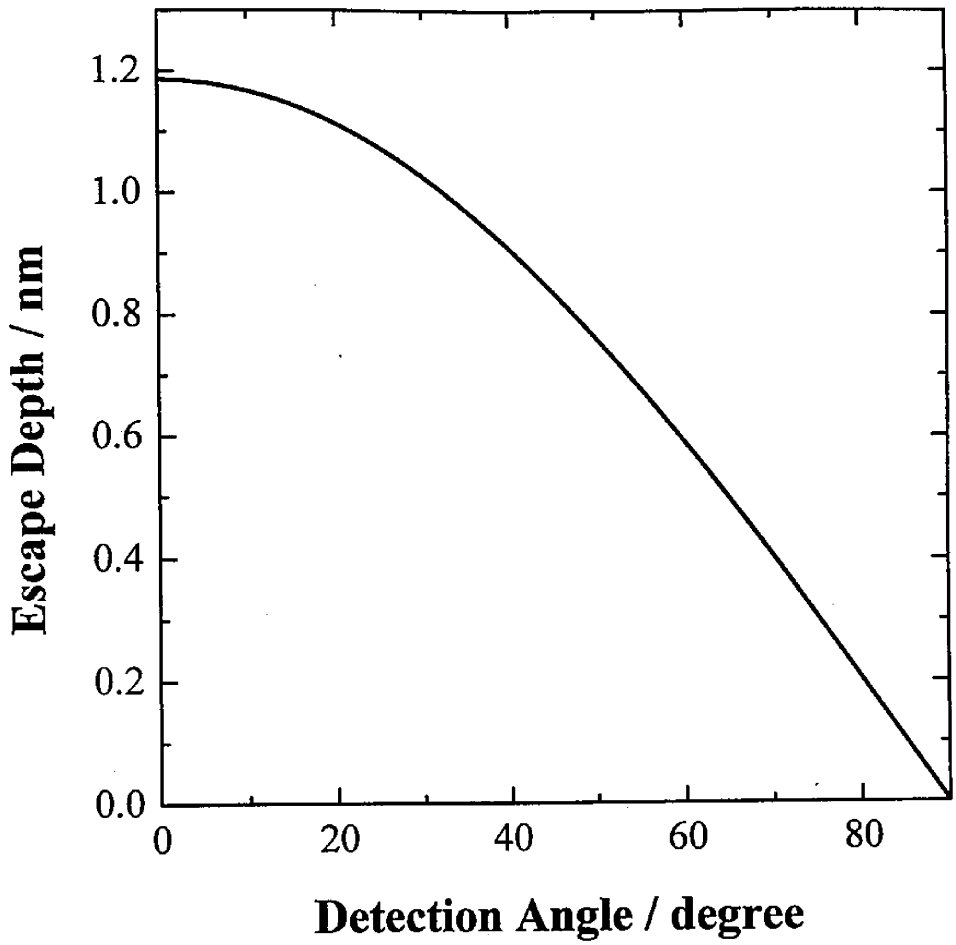

Fig. 2.10 Dependence on detection angle of escape depth in graphite.

$$h\upsilon = E_{\text{Kinetic}} + E_{\text{Binding}} + \phi_{\text{Work function}} \quad (2\text{-}1)$$

$$ED = AL\cos\theta \quad (2\text{-}3)$$

$$\lambda_a = 538aE^{-2} + 0.41a^{3/2}E^{1/2}\ (\text{nm}) \quad (2\text{-}4)$$

$$a = (10^{21}A/\rho nN_A)^{1/3}(\text{nm}) \quad (2\text{-}6)$$

E_{Binding} : 284.5 eV (C 1s)

$h\nu$: 1253.6 eV (Mg Kα)

$\phi_{\text{work function}}$: 4.37 eV

A : 12

ρ : 2.3 g cm^{-3}

n : 1

N_A : $6.02 \times 10^{23} mol^{-1}$

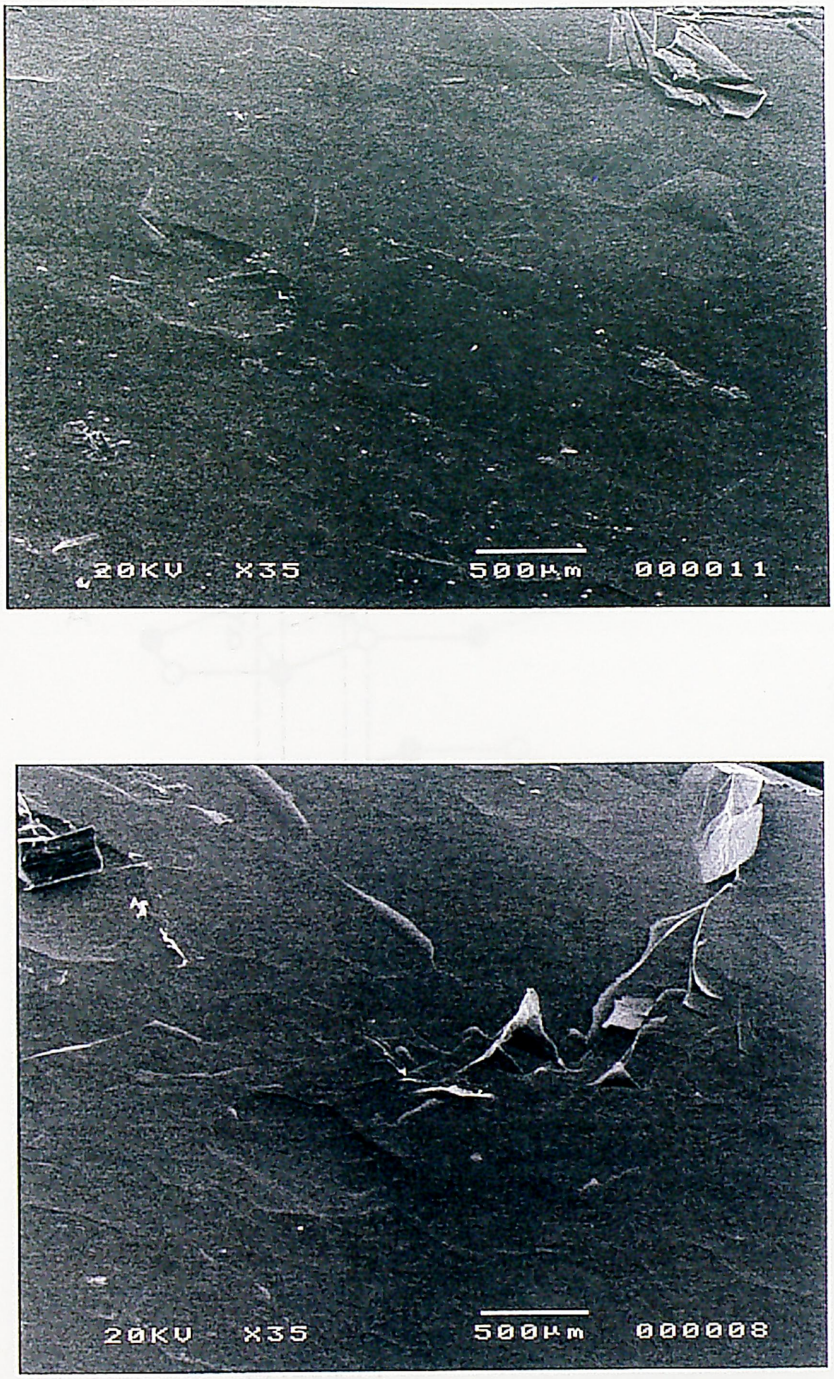

Fig. 2.11 SEM images of sample. Top is a surface of as-received sample. Bottom is a cleavage face of as-received sample.

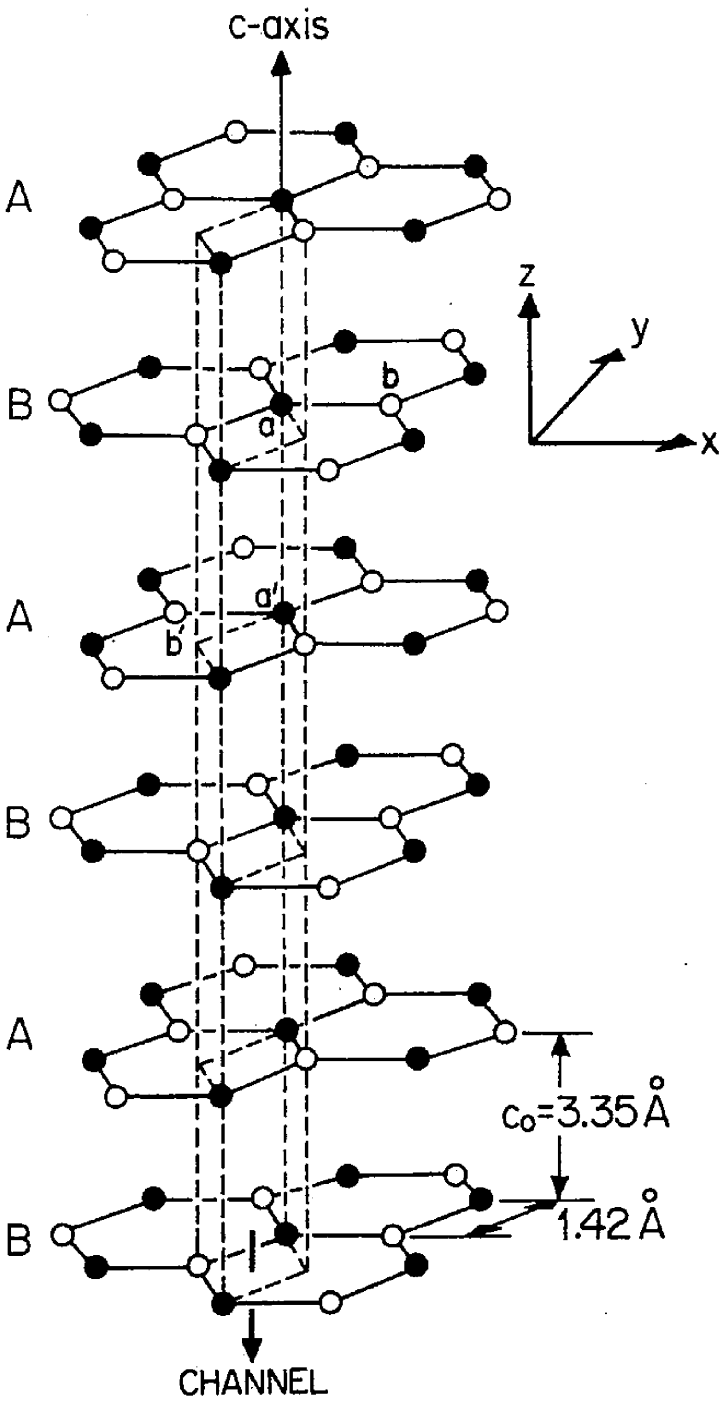

Fig. 2.12 Crystal structure of graphite.

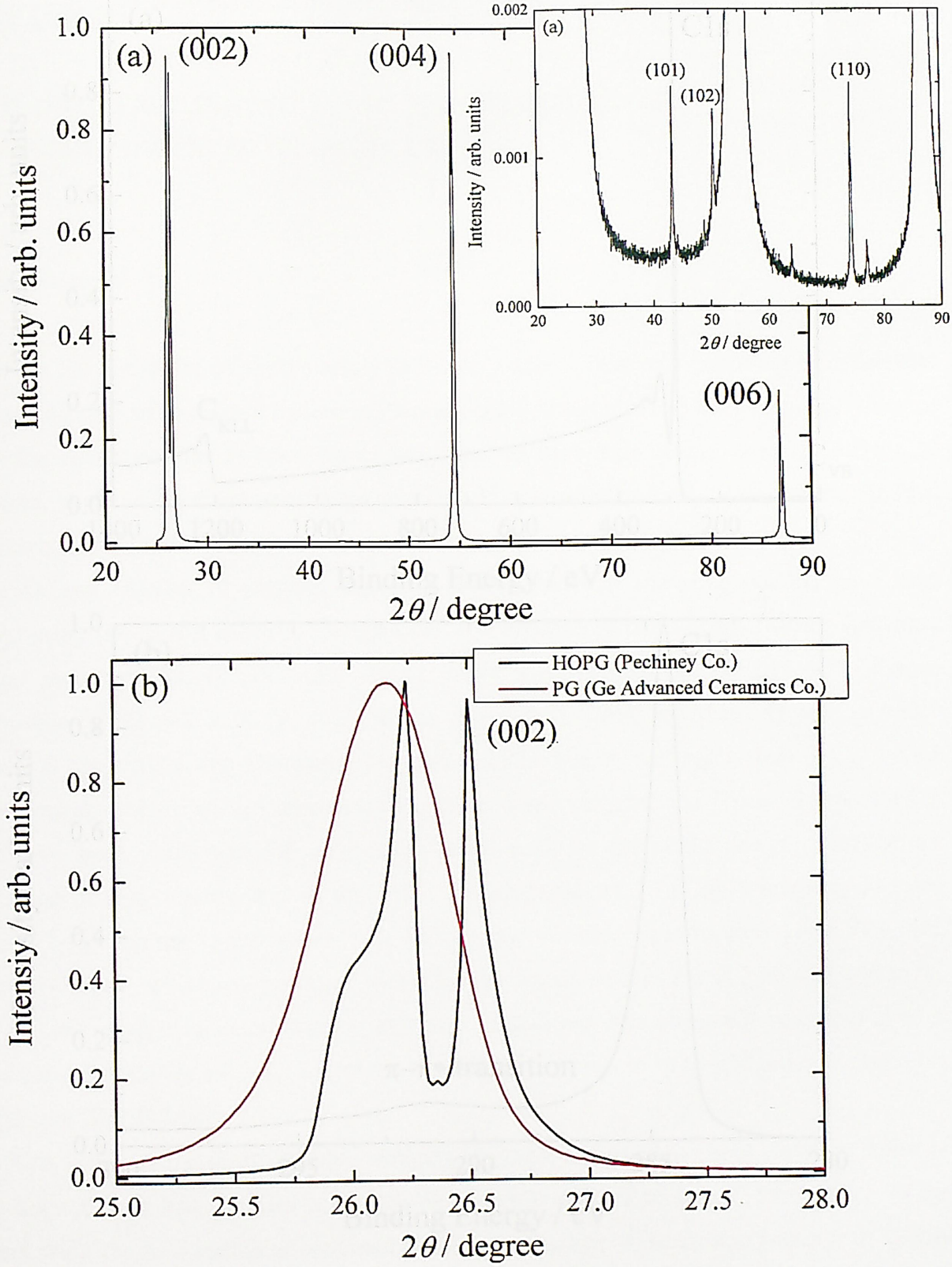

Fig. 2.13 XRD spectra for (a) HOPG used as sample in this study and (b) comparison with PG.

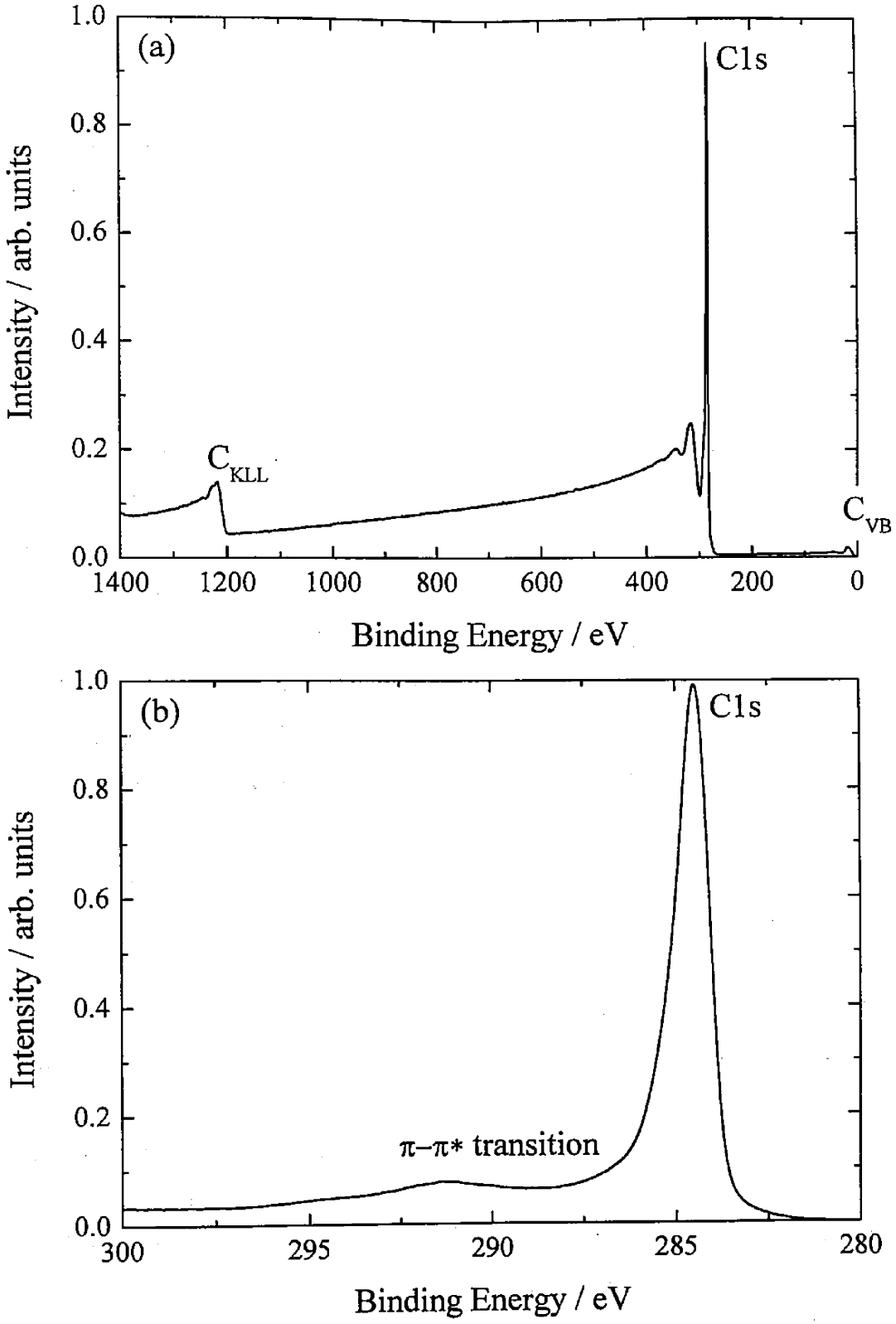

Fig. 2.14 Typical XPS spectra of (a) wide and (b) narrow range scans for cleaved face of graphite.

CHAPTER III

STUDY ON CHEMICAL STATE OF DEUTERIUM IMPLANTED INTO HIGHLY ORIENTED GRAPHITE CRYSTAL

3.1 Introduction

From the viewpoint of tritium safety in fusion reactors, it is very important to understand the trapping state of implanted tritium in Plasma Facing Materials (PFMs). Graphite is one of promising candidates for PFMs. As carbon is an element with strong chemical affinity to hydrogen, implanted hydrogen into graphite should be trapped chemically with carbon. In fact, hydrocarbons are produced in fusion reactors with carbon material PFMs [1].

Structural changes of graphite materials during hydrogen ions implantation have been studied using the in situ Electron Energy-Loss Spectroscopy (EELS) [2-4], Fourier-Transform Infrared spectroscopy (FT-IR) [5], Auger Electron Spectroscopy (AES) [6,7], Raman spectroscopy [7,8] and XPS [9, 10]. In the recent days, there are many reports in which graphite is convertible into Diamond-Like Carbon (DLC) or amorphous carbon (a-C)" by ion bombardment. Many studies on preparation method and physical and chemical properties of DLC have been performed for some applications such as electronic device, photothermal conversion of solar energy, and so on [11]. The properties of DLC were investigated using EELS [12-14], Raman spectroscopy [15], AES (Auger Electron Spectroscopy), and XPS [16]. In the DLC phase, which was produced by ion bombardment, such as argon, hydrogen and so on, both sp^2 and sp^3 hybridization states coexisted. In addition, this phenomenon occurs even at liquid nitrogen temperature [4]. However, the number of bonds in sp hybridization is negligible small in the DLC [17,18].

XPS is one of the most effective methods to obtain information about chemical states of elements and have been applied to studies on chemical state of carbon in DLC [16]. In the present study, the XPS technique was used for the investigation of the structure change of Highly Oriented Pyrolytic Graphite (HOPG) by deuterium ion implantation. The chemical states of carbon and existing state of deuterium implanted into graphite was investigated from the observation of dynamics of the structure change from graphite to DLC during deuterium and argon ion implantations by XPS.

3.2 Experimental

The sample used was HOPG mentioned in Chap. 2.2.2. An as-received HOPG was cleaved mechanically and the flesh cleavaged surface was used. This study employed in situ XPS measurements in situ during D_2^+ implantation. X-ray source used for all XPS measurements was the conventional source of Mg Kα and the monochromatic one of Al Ka.

Dependences of the chemical shift of C1s on the ion energy and fluence were investigated by procedures shown in Fig. 3.1. The common parameters of D_2^+ implantation were the implantation temperature of Room Temperature (RT), ion flux of 7.3×10^{16} D^+ m^{-2} s^{-1} measured with Faraday cup (0.25 mm ϕ), and incident angle at surface normal. D_2^+ ions were implanted into the sample using ion gun with energy ranging from 0.3 to 4.0 keV D_2^+ and fluence ranging from 0 to 7.3×10^{20} D^+ m^{-2}. The in situ XPS measurements were repeated during D_2^+ implantation.

The chemical shift should be induced by physical and chemical effects during the D_2^+ implantation. To estimate the physical effects for the chemical shift inert gas ion (Ar^+) implantation was carried out. The in situ XPS measurements were repeated during the Ar^+ implantation into HOPG as well as the first experiments. The D_2^+ implantation was performed in succession to the Ar^+ one and the in situ XPS measurements were repeated to confirm the chemical effect. Experimental procedures for both experiments were presented in Fig. 3.1. The common parameters of the implantations were the implantation temperature of RT, ion flux of 3.3×10^{17} Ar^+ m^{-2} s^{-1} for Ar^+ implantation, and 1.5×10^{17} D^+ m^{-2} s^{-1} for D_2^+ implantation and incident angle to surface normal. The Ar^+ and D_2^+ ions were implanted into the sample using the ion gun with energy of 5.0 keV Ar^+ and 1.0 keV D_2^+ and fluence ranging from 0 to 6.4×10^{20} Ar^+ m^{-2} and from 0 to 1.3×10^{21} D^+ m^{-2}.

3.3 Results and Discussion

3.3.1 Chemical Shifts and FWHM Changes of C1s peak during D_2^+ Implantation

Figure 3.2 shows change of C1s peak with increasing the fluence under (a) 0.4 and (b) 2.0 keV D_2^+ implantation. The shift of the C1s peak was observed in both spectra. The tendency

of the peak shift was almost the same; namely shifting to lower energy side (the negative shift) in low fluence region and to higher side (the positive shift) in high fluence region than the initial position. However, the magnitude of the shift for 0.4 keV D_2^+ implantation was not corresponding to that for 2.0 keV D_2^+ one. This shift is called chemical shift and reflects the change of chemical structure of graphite.

Figures 3.3 and 3.4 summarize the fluence dependence of (a) chemical shift and (b) Full Width at Half Maximum (FWHM) for the D_2^+ implantation with the energies of 0.3, 0.4, 0.5, 2.0 and 4.0 keV in the fluences below and above 7.3×10^{20} D^+ m^{-2}, respectively. All results shown in Fig. 3.3(a) indicated same tendency of chemical shift with increasing the deuterium fluence up to 7.3×10^{20} D^+ m^{-2} as mentioned above. The positive shift under the sub-keV D_2^+ implantation, however, showed same magnitude that under the keV D_2^+ implantation did not in this region. Above 7.3×10^{20} D^+ m^{-2}, however, the positive sift under the keV D_2^+ implantation became same magnitude as shown in Fig. 3.4(a). From Fig. 3.3(b), it was found that the FWHM increased with increasing the deuterium fluence up to 1.0×10^{20} D^+ m^{-2} and saturated. In the sub-keV D_2^+ the FWHM decreased in the region between 1.0 to 3.0×10^{20} D^+ m^{-2} and became to be constant. When the FWHM was constant above 3.0×10^{20} D^+ m^{-2}, the chemical shift showed constant values in the case of sub-keV (see Fig. 3.3(b)). In contrast, no decrease was observed in the FWHM change under the keV implantation even after the chemical shift was constant (see Fig. 3.4(b)).

One can also see the clear dependence of the chemical shift and FWHM change on the implantation energy, that is, the positive shift under the sub-keV implantation was larger and the FWHM change smaller than those under keV implantations. The depth of XPS measurements was calculated without the interlaminar distance as indicated in Figs. 2.4 and 2.5 in Chap. 2 to be ~0.8 nm. The correction value was estimated to be ~3 nm. Although the measurable depth of XPS is same (~3 nm) in this study, each ion range and vacancy distribution depends on implantation energies. Figures 3.5(a) and (b) showed the calculated results for the ion ranges and vacancy distributions at the fluences where the chemical shift and FWHM saturated. The ion range and vacancy distribution were calculated using TRIM code with displacement energy of 34 eV for carbon [19] and dissociation energy of 6.5 eV for graphite [20, 21], respectively. Both results represented that the maximum of vacancies distribution was attained in slightly shallower region than that of the ion distribution. In the XPS measurement range, the distributions of the deuterium implanted with sub-keV were clearly distinguished from those with keV. On the other hand, the distribution of vacancies was almost same in the implantation

with sub-keV and keV. These results expected that the results of XPS measurements during the sub-keV implantation could be different from those during keV one. In fact, the XPS result for the sub-keV implantation was distinguished from that for keV one. Therefore, the deuterium distribution plays an important role on the chemical structure change of the graphite.

For further investigation of the chemical shift by D_2^+ implantation, the inert ion, Ar^+ and subsequent D_2^+ implantation were performed. No chemical effects of implanted ion are expected for the structure change of HOPG during the Ar^+ pre-implantation, therefore only physical effect could be observed. Figures 3.6(a) and (b) summarize the results of chemical shift and FWHM under 5.0 keV Ar^+ and subsequent 1.0 keV D_2^+ implantations, respectively. The chemical shift was moved from negative to positive shifts in the region within 5.0×10^{19} Ar^+ m^{-2} and indicated negative one in the higher region than 1.0×10^{20} Ar^+m^{-2}. On the other hand, FWHM increased and became immediately constant value during the Ar^+ implantation. These results suggested that the graphite structure was distorted to a structure which was rearranged by the Ar^+ implantation. The rearrangement of the structure by the Ar^+ implantation should be induced by disordering of the graphite structure, such as displacements of carbon and relaxation of the disordered one. Both the effects should be at an equilibrium state in the constant region of the chemical shift and FWHM. Then subsequent D_2^+ implantation was induced the positive shift and decrease of FWHM as shown in Fig. 3.6(b). The D_2^+ implantation should be modified from the structure rearranged by Ar^+ to the relaxed one with C-D bonding. As the electronegativity of hydrogen proposed by Mulliken is larger than that of carbon, the C1s peak shifts toward to higher energy side. The physical effects by ion implantation is the rearrangement of the graphite structure and the chemical one is the formation of C-D bond during the D_2^+ implantation.

Figure 3.7 summarized the peak shift and FWHM changing resulted in the implantation where the peak shift was showed as a function of the FWHM changing. One can clearly see that the peak shifts by the sub-keV and the successional D_2^+ after Ar^+ implantation was distinguished from that by keV- and Ar^+ one. This result suggested that in the later implantations the structure disordering was only observed, on the other hand in the former ones not only the disordering but also chemical effect of deuterium were done. The positive shift resulted from the keV-implantation as shown in Fig. 3.3(a) was expected the formation of sp^3 carbon because the binding energy of C1s in diamond was higher than that in HOPG. That result also suggested that the implanted deuterium was retained in region of the ion range and bound with sp^3 carbon. Therefore the D_2^+ implantation allows to rearrange the graphite

structure as physical effect and to relax with forming C-D bond as chemical one.

3.3.2 Chemical Structure of HOPG after D_2^+ Implantation

Peak fitting results of C1s peak was summarized in Fig. 3.8 and Table 3.1. The C1s peak before Ar^+ implantation was assumed to consist of single sp^2 electron state and the C1s peak energy was determined to be 284.41 eV (Peak2) as shown in Fig.3.8(a). After Ar^+ implantation shown in Fig 3.8(b), the C1s peak was analyzed into three peaks, Peak2, higher and lower one than 284.41eV represented by Peak1 and Peak3, respectively. The binding energy and FWHM of each peak were determined to be 285.66 and 1.71 eV for Peak1, 284.41 and 1.31 eV for Peak2, and 283.63 and 1.11 eV for Peak3. Recently, it has been known that DLC can be induced even by Ar^+ implantation. Jascovich *et al.* investigated the sp^2/sp^3 ratio in amorphous and hydrogenated amorphous carbon and determined the C1s binding energy and FWHM for graphite, diamond, and various DLC [18,22] as shown in Table 3.1. Belton *et al.* also reported the C1s binding energy and FWHM during diamond growth [23] was identified as Table 3.1. In this study, Peak3 was attributed to an unstable state such as a dangling bond with sp^2 state from the result that the peak energy was lower than that of sp^2 state, called by electron localized state. Peak1 was also identified as sp^3 state referred by those literatures. These results were supported by the fact of sp^2/sp^3 ratio determined in this study coinciding with the literature value for DLC prepared by ion implantation [16]. After D_2^+ implantation a new peak was observed in the C1s peak of the sample pre-implanted by Ar^+, as indicated in Fig. 3.8(c). The peak named Peak4 located at 284.90 eV and extended with FWHM of 1.85 eV as shown in Table 3.1. These values are in excellent agreement with the literature values [22,24].

The each peak profile change was compared during Ar^+ pre- and D_2^+ implantations in Figs. 3.9(a) and (b). During Ar^+ implantation peak area ratios (such as Peak1/(Peak1+2+3)) of Peak1 and 3 were increasing and Peak2 decreasing. However the Peak1 turned to decreasing immediately. Then the ratios of all Peaks saturated in higher fluence than 1.0×10^{20} Ar^+ m^{-2}. These results suggest two processes during Ar^+ implantation that the chemical state attributed to Peak1, the electron localized state, is formed immediately and modified to those attributed to Peak2 and 3, sp^2 and sp^3 states. The former of these processes is defined to disordering and the later rearrangement of the disordered structure. In the constant region above 1.0×10^{20} Ar^+ m^{-2}, both the processes were equilibrated. The Peak4 increased rapidly up to ~3×10^{20} D^+ m^{-2} and above that fluence, became almost constant. On the other hand, the Peak1, 2 and 3 decreased

up to ~3×10^{20} D^+ m^{-2} and came almost constant. These results suggested that the disordering and rearrangement are induced by changing sp^2 state to the electron localized, sp^2 and sp^3 states during Ar^+ pre- and D_2^+ implantation, deuterium chemically anneals the damaged structure by forming the C-D bond.

3.4 Summary

The in-situ XPS measurements were carried out during Ar^+ and/or D_2^+ implantation with various energies for investigating chemical states of implanted deuterium in graphite.

The chemical shift and FWHM change are found to result from the formation of new electron states during D_2^+ implantation, which were determined to be the electron localized state and sp^3 C. The disordered structure was relaxed by the formation of C-D bond. They are also observed the dependence on the ion energy.

References

[1] For example, S. Higashijima, *et al.*, *J. Nucl. Mater.*, **290-293**, 623 (2001).

[2] K. N. Kushita, *et al.*, *J. Electron Microsc.*, **44**, 456 (1995).

[3] K. N. Kushita and K. Hojou, *Ultramicroscopy*, **35**, 289, (1991).

[4] K. N. Kushita, *et al.*, *J. Nucl. Mater.*, **191-194**, 351 (1992).

[5] Y. Gotoh and S. Kajiura, *J. Nucl. Mater.*, **266-269**, 1051 (1999).

[6] N. Kangai and T. Tanabe, *J. Nucl. Mater.*, **220-222**, 776 (1995).

[7] N. Kangai, *et al.*, *J. Nucl. Mater.*, **212-215**, 1234 (1994).

[8] T. Tanabe, *et al.*, *Fusion Eng. Des.*, **29**, 428 (1995).

[9] Y. Gotoh and O. Okada, *J. Nucl. Sci. Technol.*, **21**, 205 (1984).

[10] Y. Gotoh, *Fusion Technol.*, **6**, 424 (1984).

[11] A. H. Lettington, *Phil. Trans. R. Soc. Lond.*, **A342**, 287 (1993).

[12] J. Biener, *et al.*, *Surf. Sci.*, **307-309**, 228 (1993).

[13] K. W. R. Gilikes, *et al.*, *J. Non-Cryst. Solids*, **164-166**, 1107 (1993).

[14] F. Xiong, *et al.*, *J. Mater. Res.*, **8**, 2265 (1993).

[15] X. He, *et al.*, *Vacuum*, **45**, 977 (1994).

[16] S. T. Jackson and R.G. Nuzzo, *Appl. Surf. Sci.*, **90**, 195 (1995).

[17] B. Dishler *et al.*, *Solid State Commun.*, **48**, 105 (1983).

[18] J. C. Lascovich, *et al.*, *Appl. Surf. Sci.*, **47**, 17 (1991).

[19] S. J. Carroll, *et al.*, *Phys. Rev. Lett.*, **81**, 3715 (1998).

[20] A. Miyahara and T. Tanabe, *J. Nucl. Mater.*, **155-157**, 49 (1988).

[21] JANAF Thermochemical Tables and NBS Technical Note.

[22] J. C. Lascovich and S. Scaglione, *Appl. Surf. Sci.*, **78**, 17 (1994).

[23] Handbook of X-ray Photoelectron Spectroscopy, ed. by J. Chastain and R. C. King, Jr., Physical Electronics Inc., Minesota (1995).

[24] D. N. Beleton and S. J. Schmieg, *J. Vac. Sci. Technol.*, **A8**, 2353 (1990).

Table 3.1 The each peak energy, FWHM, and area ratio of the fitted C1s peak after ions implantation.

Implanted ion		Peak1	Peak2	Peak3	Peak4	sp^3 / %	sp^2 / %
5.0 keV Ar^+	BE / eV	285.66	284.41	283.63			
	FWHM / eV	1.71	1.31	1.11			
	Area ratio / %	25.0	62.4	12.6		25.0	75.0
	Literatures / eV	285.35 [18]	284.36 [18, 19] 284.50 [23]			27.6 [16]	72.4[16]
1.0 keV D_2^+	BE / eV	285.66	284.41	283.63	284.90		
	FWHM / eV	1.71	1.31	1.11	1.85		
	Area ratio / %	12.2	31.7	0.4	55.7		
	Literatures / eV	285.35 [8]	284.36 [18,19] 284.50 [23]		284.8, 284.6 [19] 285.3 [21]		

BE expresses the binding energy, and FWHM the full width at half maximum.

[18, 19] : the results of XPS measurements for the ion bombarded diamond, a-C:H, and as received graphite

[16] : the results of XPS measurements for the a-C sample implanted Ar^+ with energy of 3 keV Ar^+

[21] : the results of XPS measurements for diamond growth on Pt foil by vacuum deposition

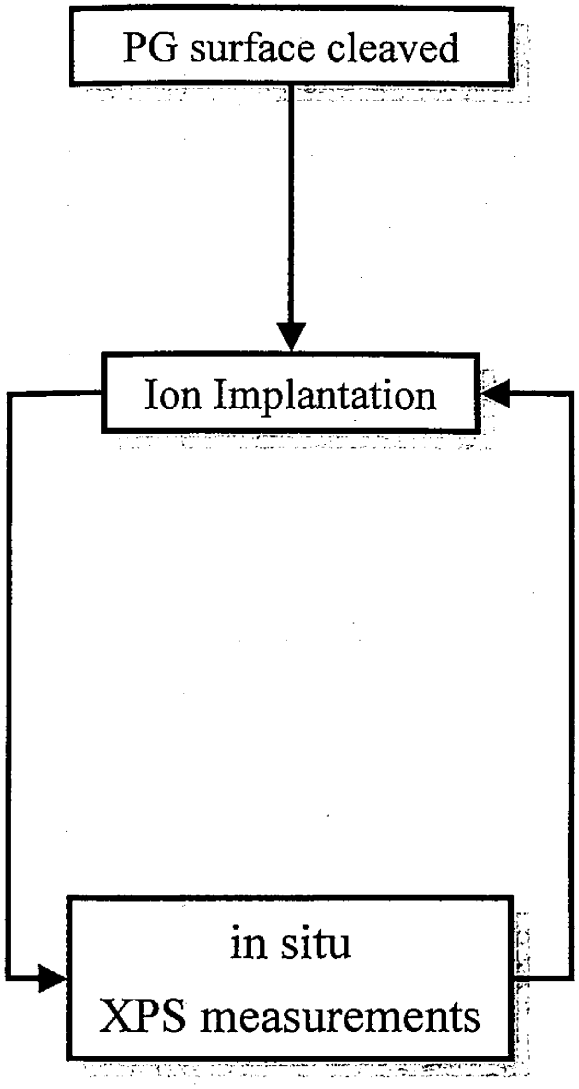

Implantation Conditions :

1) D_2^+ implantation

- Temperature : R. T.
- Energy : 0.3, 0.4, 0.5, 2.0, 4.0 keV D_2^+
- Flux : 7.3×10^{16} D^+ m^{-2} s^{-1}
- Fluence : $0 - 7.3 \times 10^{2}$ D^+ m^{-2}

2-1) Ar^+ implantation

- Temperature : R. T.
- Energy : 5.0 keV Ar^+
- Flux : 3.3×10^{17} Ar^+ m^{-2} s^{-1}
- Fluence : $0 - 6.4 \times 10^{20}$ Ar^+ m^{-2}

2-2) D_2^+ implantation

- Temperature : R. T.
- Energy : 1.0 keV D_2^+
- Flux : 1.5×10^{17} D^+ m^{-2} s^{-1}
- Fluence : $0 - 1.5 \times 10^{21}$ D^+ m^{-2}

Fig. 3.1 Flowchart of XPS experiments.

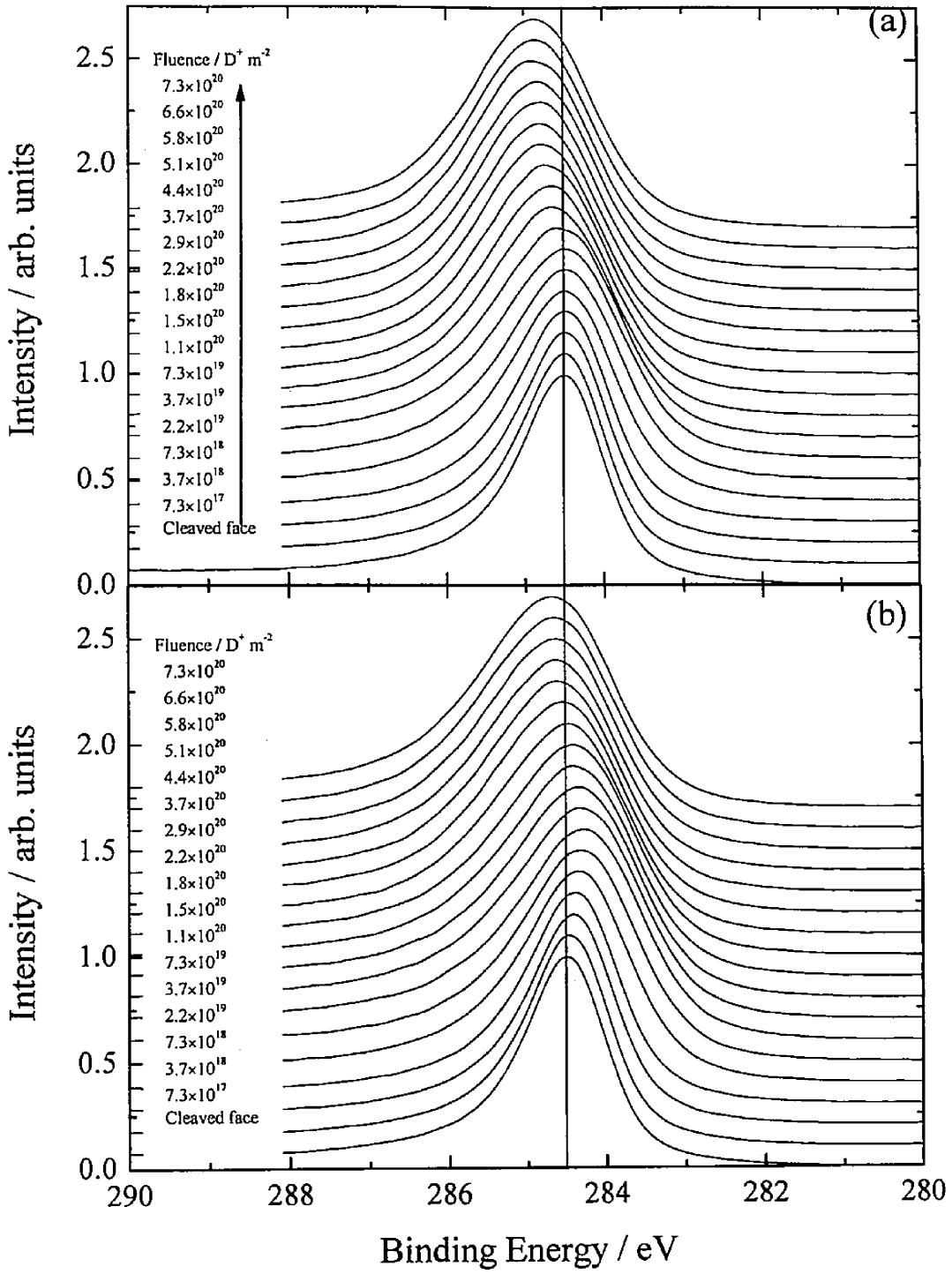

Fig. 3.2 Profile change of C1s peak with increasing fluence under (a) 0.4 and (b) 2.0keV D_2^+ implantations.

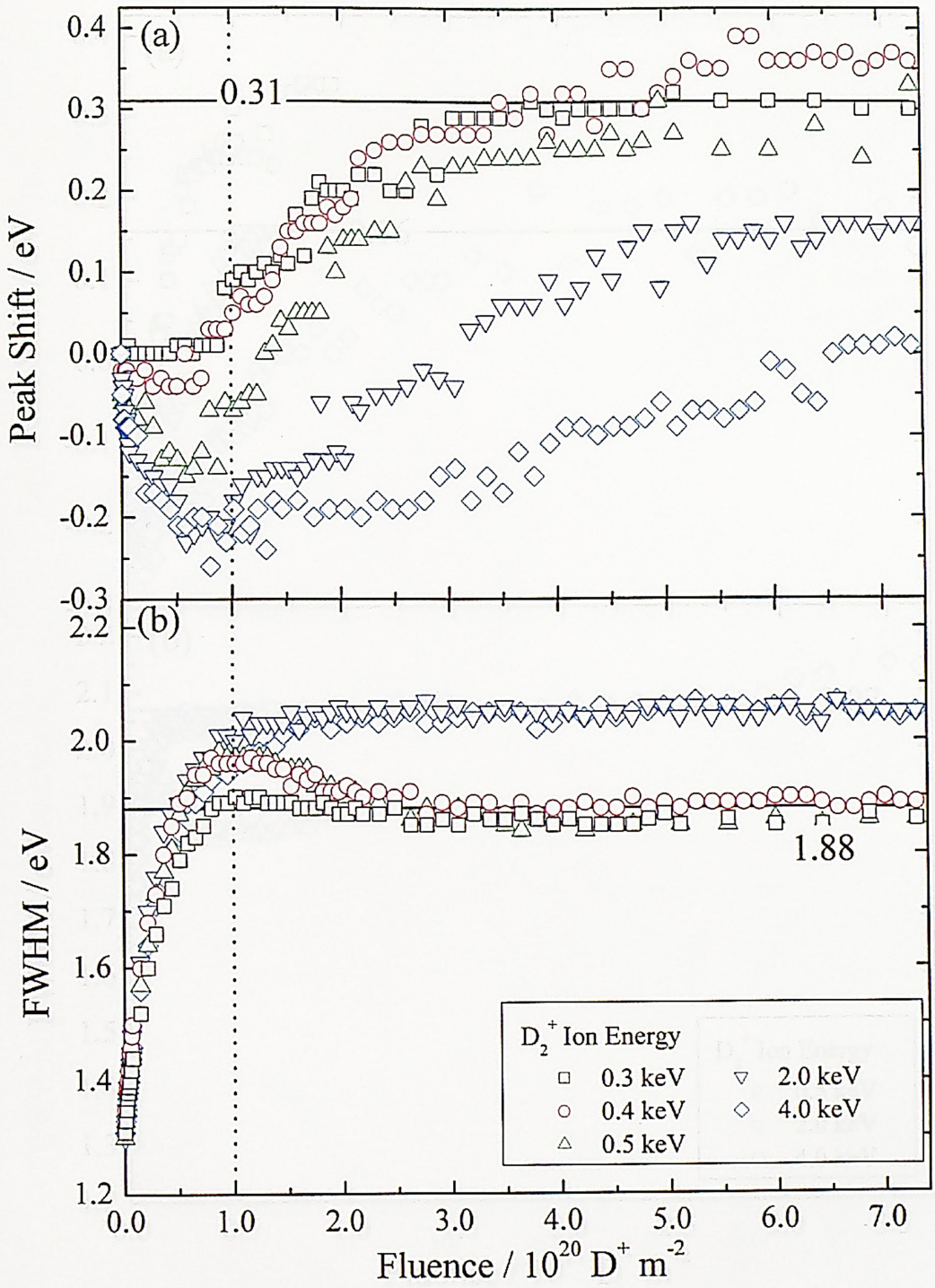

Fig. 3.3 Fluence dependence of (a) chemical shift and (b) FWHM for C1s peak under D_2^+ implantation with various energies.

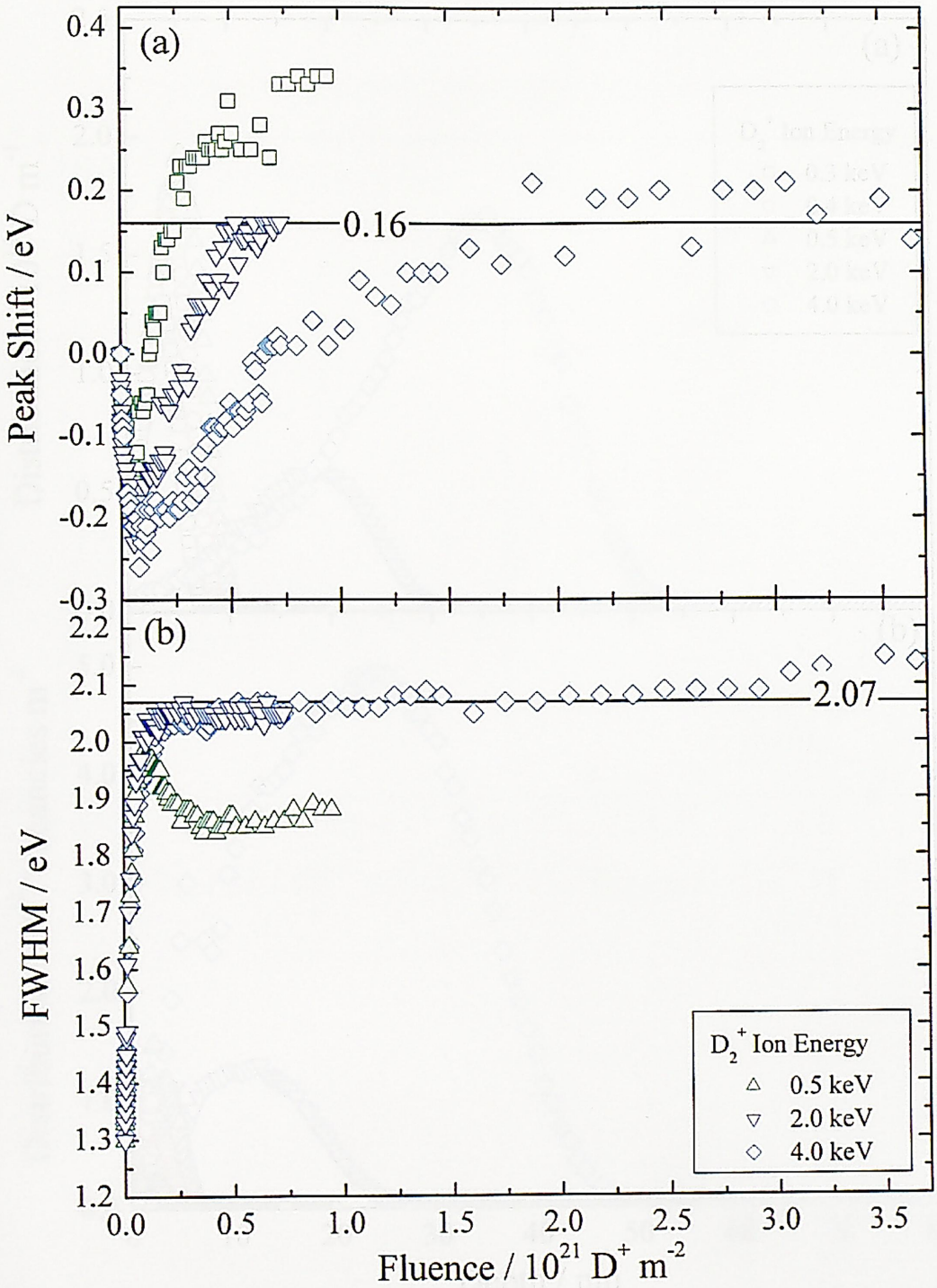

Fig. 3.4 Fluence dependence of (a) chemical shift and (b) FWHM for C1s peak under D_2^+ implantation with 0.5, 2.0 and 4.0 keV D_2^+.

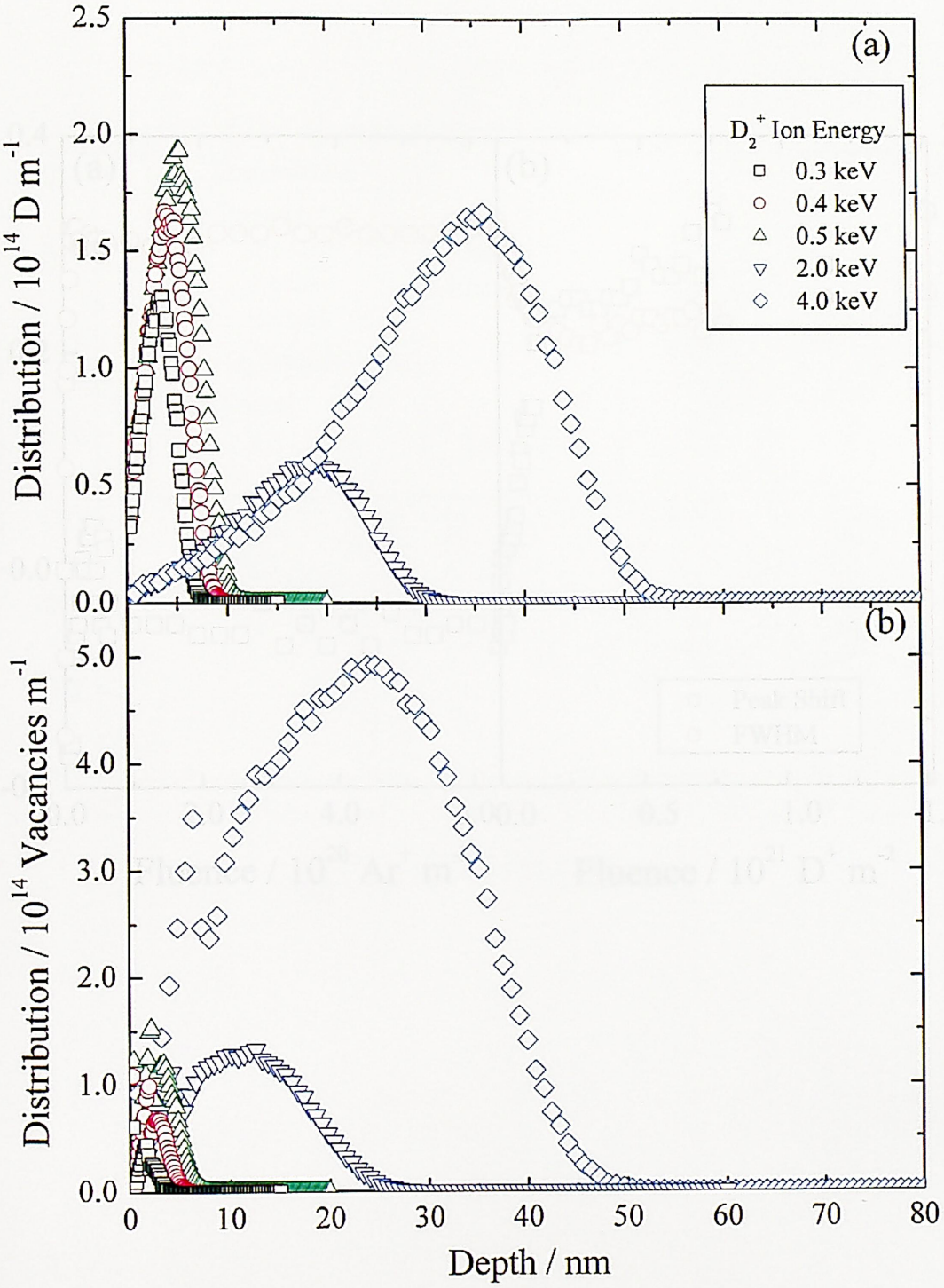

Fig. 3.5 TRIM calculation results of (a) the ion distribution and (b) the vacancy distribution at saturation fluence.

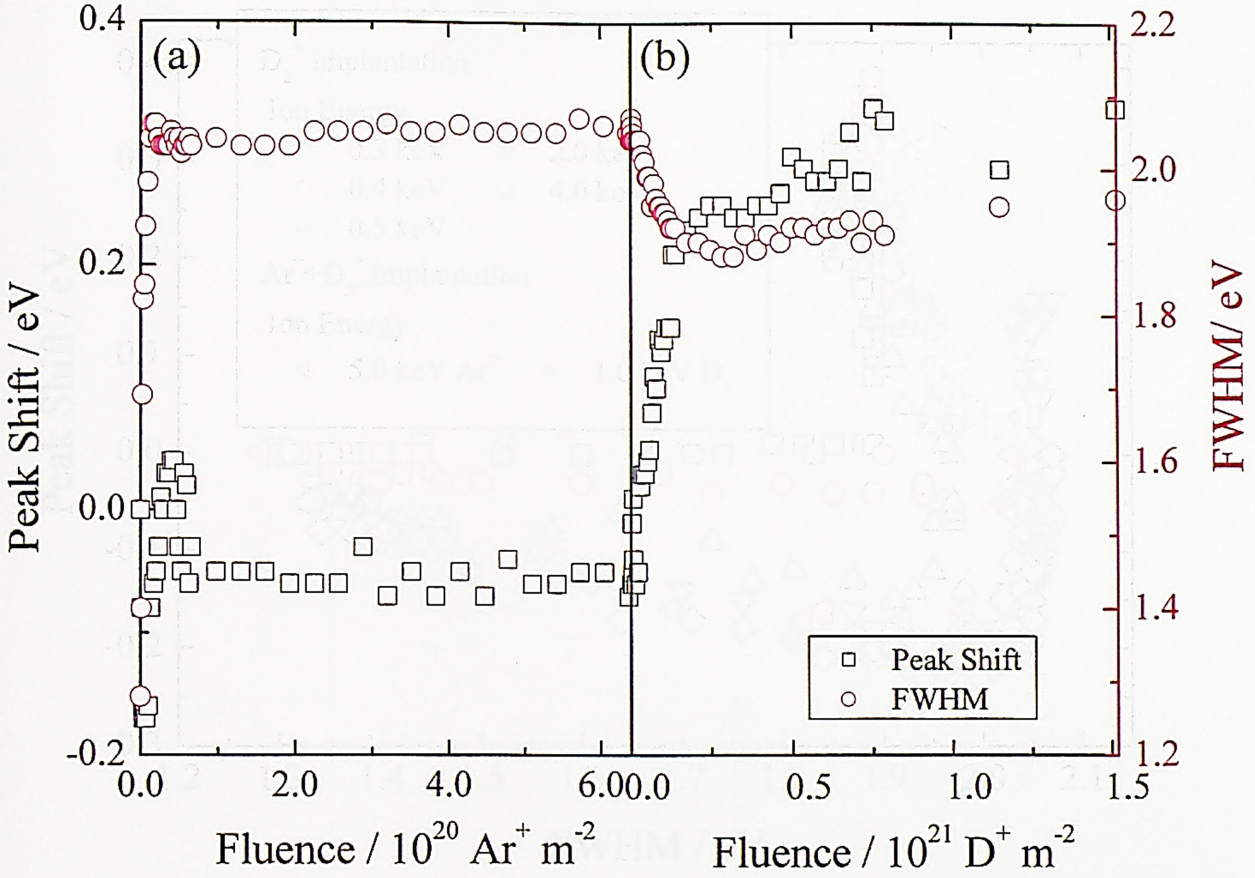

Fig. 3.6 Fluence dependence of C1s chemical shift and FWHM under (a) Ar^+ and (b) D_2^+ implantation.

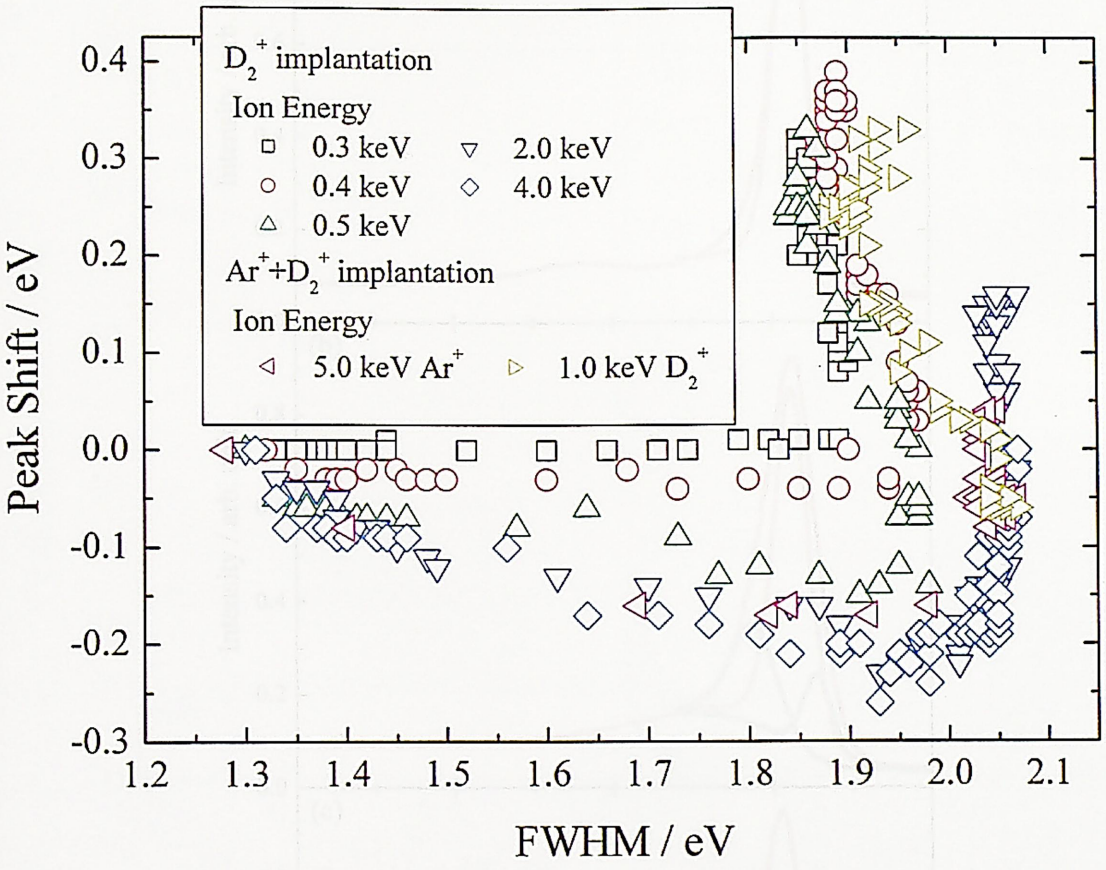

Fig. 3.7 Summary of peak shift and FWHM changing observed in this study.

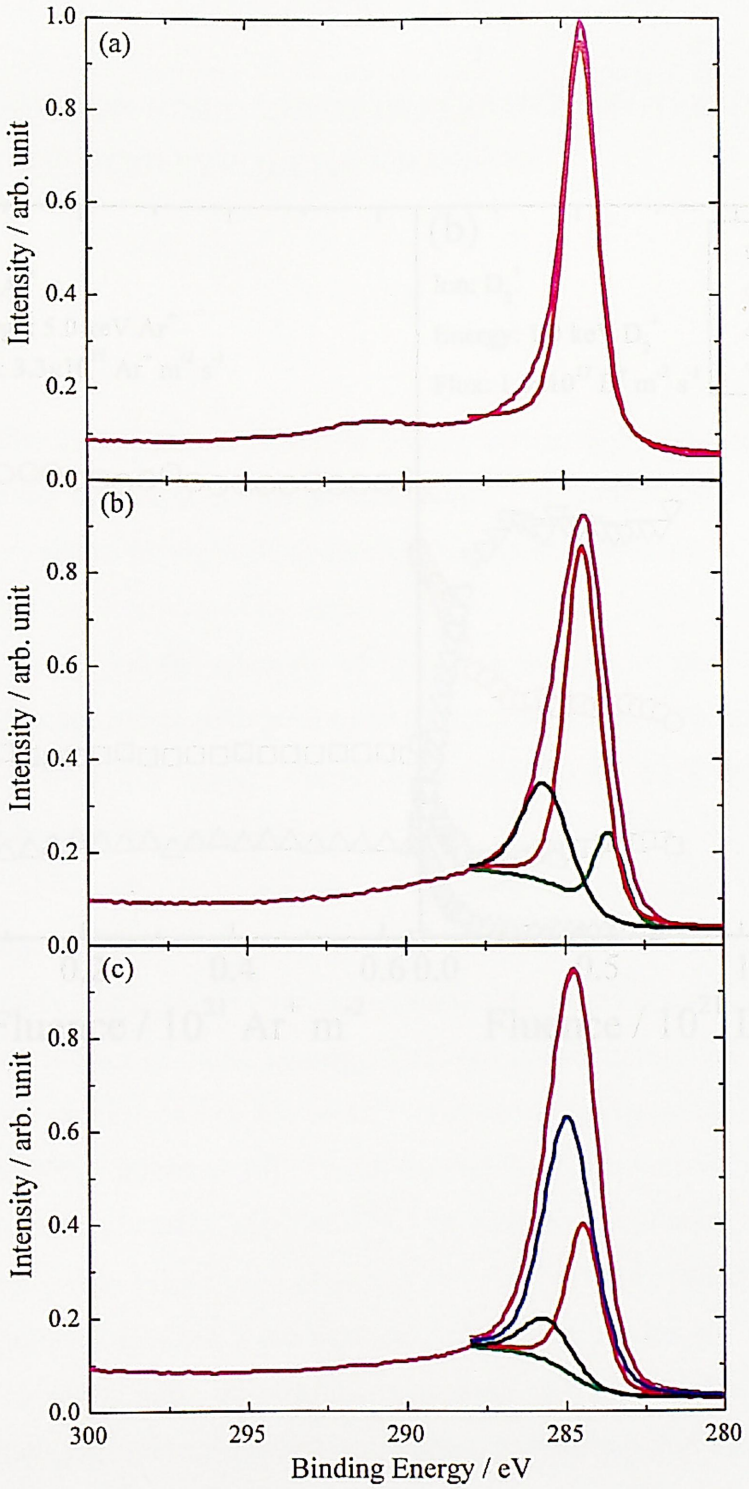

Fig. 3.8 Peak fitting result of C1s spectrum for (a) as-received sample, (b) after Ar^+ implantation and (c) Ar^+ and D_2^+ implantations.

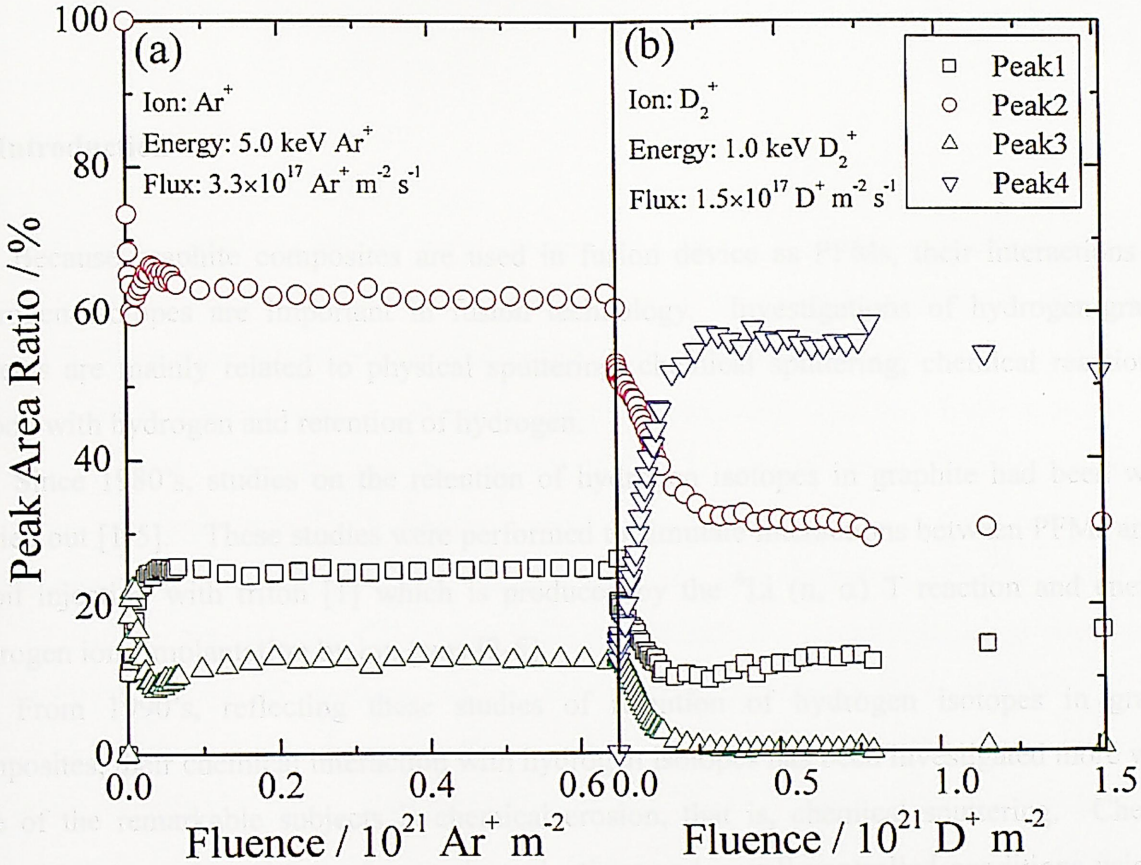

Fig. 3.9 Fluence dependence of C1s peak area ratio under (a) Ar^+ and (b) D_2^+ implantation.

CHAPTER IV

STUDY ON DESORPTION BEHAVIOR OF IMPLANTED DEUTERIUM FROM HIGHLY ORIENTED PYROLYTIC GRAPHITE

4.1 Introduction

Because graphite composites are used in fusion device as PFMs, their interactions with hydrogen isotopes are important in fusion technology. Investigations of hydrogen-graphite systems are mainly related to physical sputtering, chemical sputtering, chemical reactions of carbon with hydrogen and retention of hydrogen.

Since 1980's, studies on the retention of hydrogen isotopes in graphite had been widely carried out [1-5]. These studies were performed to simulate interactions between PFMs and the recoil injection with triton [1] which is produced by the ^{6}Li (n, α) T reaction and energetic hydrogen ions implantation by ion guns [2-5].

From 1990's, reflecting these studies of retention of hydrogen isotopes in graphite composites, their chemical interaction with hydrogen isotopes has been investigated more widely. One of the remarkable subjects is chemical erosion, that is, chemical sputtering. Chemical erosion has been the subject of many investigations under well-controlled conditions using ion beams in the energy range from 10 eV to keV and fluxes between 10^{18} and 10^{20} m^{-2} s^{-1} as reviewed at the 12th PSI Conference [6]. From the results of many investigations, the chemical erosion process has been gradually clarified [7]. In addition, simulation models and codes of the chemical erosion process have been proposed [8-11]. As this phenomenon is the inherent problem of the graphite composites, it has been studied in the most detail.

From the fusion safety point of view, the most necessary pieces of information are on the tritium retention, chemical interactions between carbon and tritium and the migration of tritium in the graphite composites contributing to tritium inventory. At present, in order to suppress chemical erosion, the boronization [12-16] or siliconization [17] has been conducted in form of coating on the graphite wall of fusion devices and the inventory properties have been investigated [18]. However, the simulated energy range is keV order in Ref. [1-5, 12-18], and the retention and chemical interaction of hydrogen isotopes in materials was discussed under the fitted ion energy.

In this study, sub-keV deuterium ion was implanted into Highly Oriented Pyrolytic Graphite (HOPG) for investigating the desorption behavior and the retention. The behavior was analyzed kinetically and the retention was estimated with TDS for various implantation conditions.

4.2 Experimental

The sample used was HOPG crystal mentioned Chap. 2.2.2. An as-received sample was cleaved mechanically and the new cleavage surface was degassed at 1400 K for 20 min. A flow chart of TDS experiments were indicated in Fig. 4.1. The desorbed species during the sample heating were monitored with Quadrupole Mass Spectrometer (QMS). Release behavior of deuterium (m/e=4) and hydrocarbons (m/e=16, 18, 20, 32, and 36) from HOPG implanted with D_2^+ were measured with QMS during heating. In the case of CH_4, the cracking pattern coefficients are 17.1 for CH_2, and 85.6 for CH_3, when the peak intensity of CH_4 is normalized to 100. The observed CD_2 and CD_3 peaks included not only the directly desorbed ones but also the fragment species of cracking CD_4. A relative factor between D_2 and CD_x of QMS intensities is also needed to determine the released amount of CD_x using the standard leak of D_2. The relative sensitivity factor is determined to be D_2/CD_4 =0.25 using the calibrated gas, which is D_2/Ar or CH_4/Ar mixture gases. The net amount of CD_3 and CD_4 species originated from D_2^+ implantation was estimated with the cracking pattern coefficients and the relative sensitivity factor. For the estimation for the net amount of CD_2 was not determined because of the unknown the cracking pattern coefficient for cracking CD_3.

To estimate the change of the desorption behavior of implanted deuterium in the sample, 1.0 keV D_2^+ was implanted into HOPG sample under various temperatures. Common parameters of the implantations were the flux of 1.0×10^{18} D^+ m^{-2} s^{-1} and the fluence of 6.4×10^{21} D^+ m^{-2}. After the implantation, all TDS measurements were performed with the heating rate of 0.5 K s^{-1}.

To determine kinetic parameters of the desorption behavior of implanted deuterium, 1.0 keV D_2^+ ion was implanted into the graphite sample with the ion flux of 1.0×10^{18} D^+ m^{-2} s^{-1}, fluences in the range from 6.4×10^{19} D^+ m^{-2} to 6.4×10^{21} D^+ m^{-2} at 173 K. After the implantations, the chamber was evacuated to remove residual gases for ~2 hours, and the implanted sample was heated up to ~ 1400 K with heating rate in the range from 0.083 to 1.0 K s^{-1}.

In both experiments, the implantations were carried out with the ion beam raster size of 3×3

mm^2 and the incident angle of 90°. The obtained TDS spectra were analyzed by the Redhead equation [19], and the peak top temperature and peak area were determined from the analyzed spectra.

4.3 Results and Discussion

4.3.1 TDS spectra after D_2^+ Implantation under Various Conditions

In this study, only D_2 and CD_x release behavior were discussed, because the C_2D_x release was negligible small. The desorption of CD_3 and CD_4 indicated that not only sp^2 hybridization state but also sp^3 one could be generated in HOPG. This was also supported by many other reports [2-11]. In these reports, coexisting sp^3 and sp^2 graphite is called Diamond Like Carbon (DLC) or amorphous carbon (a-C) [7-11, 20, 21].

Figures 4.2 (a) and (b) respectively indicate D_2 and CD_4 peaks of TDS spectra after 1.0 keV D_2^+ implantation with various implantation temperature. A higher temperature part of the D_2 peaks changed with increasing the implantation temperatures. On the other hand, the CD_4 peaks were in symmetry. Therefore the D_2 peak was consisted of two peaks and the CD_4 peak was a single peak. Those suggests that the D_2 desorption behavior consisted of two and the CD_x desorption behavior one process.

Figures 4.3 (a) and (b) indicate that D_2 and CD_4 peaks of TDS spectra after 1.0 keV D_2^+ implantation at 173 K with various fluences. In Fig. 4.3 (a), a new peak was observed in the temperature region between ~200 and ~300 K. Although the peak appeared in TDS spectra after the implantation at 173 K, it was not always observed. To discuss about it the more detail experiments are needed. On the other hand, the peak temperature of a main peak in D_2 and CD_4 spectra shifted to the lower temperature side with increasing the fluence. According to the Redhead's equation [19], when the peak temperature decreases with increasing the ion fluence, the release process could be a second-order reaction. This suggested that the rate determining step is a re-combination reaction of detrapped D_2 and CD_3 in the desorption processes of D_2 and CD_4 from HOPG.

As shown in Fig 4.4 (a), the D_2 TDS spectra were separated to two peaks (Peak1 and Peak2) by fitting with the Redhead equation for second order reactions [19]. It is well known that continuous implantation of hydrogen into graphite at room temperature builds up a hydrogen

saturated layer [22-25], in which hydrogen is chemically trapped to carbon atoms [5, 26, 27]. The desorption resulted in Peak1 and Peak2 should be induced by detrapping from the site chemically trapped by carbon atoms. On the other hand, PeakCD_x shown in Fig. 4.4 (b) appeared in the same temperature region of Peak1. The CD_x desorption would be correlated with D_2 one.

4.3.2 Desorption Process of Implanted Deuterium and Thermal Annealing of Disordered Structure in HOPG

As described in Chap. 2.1.2, the activation energy of the D_2 and CD_x desorption process can be determined by Eq. (2-11). Figure 4.5 shows the plots of $\ln(T_p^2/RT)$ vs $(1/T_p)$ for the desorption spectra of D_2 and CD_x with varying the heating rate from 0.083 to 1.0 K s^{-1}after the deuterium implantation of 6.4×10^{20} D^+ m^{-2} at 173 K. The activation energies were determined for the desorptions after the implantation at various temperatures in the same manner that at 173 K. The desorption activation energies are listed in Table 4.1.

As mentioned in Chap. 2.1.2, the reaction order can be determined by Eq. (2-12). The plots of $\ln(\beta E/RT_p^2)+E/RT_p$ vs $\ln\sigma$ are shown in Fig. 4.6 for each peak of the TDS spectra, where E was used the value determined above. In these measurements, σ, which is the amounts of implanted deuterium in HOPG, was estimated from each peak area of the TDS spectra. The reaction order determined in this study is summarized in Table 4.2. The reaction order was determined to be n=2 for both of D_2 and CD_x desorption processes.

Rates of all desorption processes were limited by recombination processes. In general a desorption process of atoms implanted into a sample is consisted of detrapping, diffusion and a recombination reaction. In addition, the disordered structure by the ion implantation was annealed by heating during the implantation. The activation energy could include not only the desorption process but also the thermal annealing process of the disordered structure. In fact, the activation energies listed in Table 4.1 showed temperature dependency. Figure 4.7 summarizes change of the activation energies under various implantation temperatures. The activation energies of D_2 desorption resulted in Peak1 and Peak2 were decreased with increasing the implantation temperature and came to each constant value. The difference between the maximum and steady values in both Peak1 and Peak2 was ~2 eV. In the implantation at lower temperature, the thermal annealing could be depressed more than in that at higher one. Niwase *et al.* and Tanabe *et al.* used Raman spectroscopy to study the ion irradiated HOPG and showed

the presence of stable and unstable defects [28-30]. The unstable defects annealed easily below 573 K are due to a vacancy clustering process which keep a chemical structure of carbon with sp^2 state [31, 32]. The activation energy of this process was determined to be 1.8±0.3 eV [31]. Therefore in the implantation at lower temperatures the activation energy of the D_2 desorption processes resulted in the Peak1 and Peak2 could include that of the thermal annealing due to clustering of vacancies formed by the implantation. During the implantation at higher temperatures the vacancy clustering can occur with disordering of the structure in the same time. Thus the net activation energy of the D_2 release was determined to be the value obtained for the implantation above 573 K.

The deuterium implanted into a diamond polycrystalline was also trapped by sp^3 carbon [33]. The desorption behavior of D_2 from HOPG implanted with 1.0 keV D_2^+ was compared with that from diamond polycrystalline implanted with 0.5 keV D_2^+ [33] in Fig. 4.8. One can see that the result of HOPG was corresponding to that of diamond. This result implied that the disordered structure of HOPG was almost same as that of diamond. The implanted deuterium in HOPG should be trapped at a similar trapping site in diamond. Therefore, the implanted deuterium was trapped by sp^3 carbon in HOPG and desorbed from there. For the activation energy of D_2 desorption for the Peak1 and Peak2 were determined to be 2.36±0.24 eV and 1.43±0.09 eV after the implantation at 573 K, respectively. In the TDS spectrum, the release peak appeared at higher temperature with increasing the activation energy [19]. This is applied to the desorption from trapping sites which are independent each other. In the present work, the activation energies determined did not obey that. Thus the desorption resulted in Peak2 depended on that resulted in Peak1 so that the annealing process of the disordered structure was a successive reaction with the desorption of deuterium detrapped by two ways.

The literature's value [8, 9, 11] and each desorption activation energy determined are also listed in the Table 4.1. Wittmann *et al.* reported that the thermal decomposition energy of sp^3 to sp^x, which is radical C center, was determined to be 2.7 eV for the parameter in thier chemical sputtering model as shown in Table 4.2 and Fig. 4.9 [8-11]. The required energy for annealing from the sp^x state to complete sp^2 state was estimated to be 1.7 eV [8, 9, 11]. These activation energies were corresponding to that in this study. The annealing process from sp^3 to sp^2 state in their model, however, was directly progressed as a main process [9, 11]. In this study, the disordered structure after the implantation were annealed as the successive reaction with rearrangement from sp^3 to sp^2 via sp^x state carbon. Therefore, for desorption process via Peak1, the rate-determining step was the recombination of deuterium after detrapping from the carbon

of sp^3 state. The Peak2 desorption behavior was attributed to annealing of sp^x state to sp^2 state. The rate-determining step was the recombination of deuterium after detrapping from sp^3 state C, which was the neighboring sp^x state C.

For PeakCD_4, there were the fluence dependence of peak temperature of TDS spectra and desorption amounts. In addition, there was the threshold fluence for CD_4 desorption. Those subjected that the CD_4 desorption depended on CD_3 concentration produced during the deuterium implantation. The thermal decomposition energy of methyl groups from sp^3 state carbon was determined to be 2.4 eV and one from sp^3 state carbon neighboring sp^x state carbon 1.5 eV. The recombination reaction of CD_3 and D was the rate-determining step. The reaction depended on CD_3 concentration. The CD_3 desorption process should be same as the CD_4 desorption. The activation energy determined in this study assumed a constant value, because of a large deviation.

4.4 Summary

TDS measurements were carried out for HOPG implanted deuterium in order to investigate of the desorption behavior of deuterium from it. From experimental results, the implanted deuterium desorbed with D_2 and hydrocarbons.

The desorption behavior of D_2 consisted of two processes because two peaks, Peak1 and Peak2, were observed. Both D_2 desorption processes were determined to be second order reactions and their activation energies were estimated after the implantation at various temperatures. The D_2 desorption processes were limited by the recombination reaction after detrapping from the sp^3 (Peak1) and sp^3 neighbored with sp^x state C (Peak2).

The desorption behavior of CD_x consisted of single process because one peak, PeakCD_x, was observed. The desorption process was determined to be the recombination of CD_{x-1} and D after detrapping from sp^3 state C.

During TDS experiment, the disordered structure in HOPG was also annealed from sp^3 to sp^2 via sp^x state by detrapping D. On the other hand, the vacancy formed by the implantation clustered to keep the chemical structure of sp^2 state whose carbon did not trapped D.

References

[1] R. A. Causey, *et al.*, *Carbon*, **17**, 323 (1978).

[2] E. Vietzke, *et al.*, *J. Nucl. Mater.*, **111&112**, 763 (1982).

[3] K. Ashida, *et al.*, *J. Nucl. Mater.*, **111&112**, 769 (1982).

[4] W. Möller, *et al.*, *Nucl. Instrum. Methods Phys. Res.*, **B19/20**, 826 (1987).

[5] K. Ashida, *et al.*, *J. Nucl. Mater.*, **128&129**, 792 (1984).

[6] J. W. Davis and A. A. Haasz, *J. Nucl. Mater.*, **241-243**, 37 (1997).

[7] Y. Ueda, *J. Plasma Fusion Res.*, **75**, 384 (1999), [in Japanese].

[8] A. Horn, *et al.*, *Chem. Phys. Lett.*, **231**, 193 (1994).

[9] M. Wittmann and J. Küppers, *J. Nucl. Mater.*, **227**, 186 (1996).

[10] J. Roth and C. Garacía-Rosales, *Nucl. Fusion*, **36**, 1647 (1996).

[11] B. V. Mech, *et al.*, *J. Appl. Phys.*, **84**, 1655 (1998).

[12] M. Saidoh, *et al.*, *Fusion Eng. Des.*, **22**, 271 (1993).

[13] M. Saidoh, *et al.*, *Jpn. J. Appl. Phys.*, **32**, 3276 (1993).

[14] Y. Hirooka, *et al.*, *J. Nucl. Mater.*, **176&177**, 473 (1990).

[15] J. Winter, *et al.*, *J. Nucl. Mater.*, **162-164**, 713 (1989).

[16] J. Winter, *et al.*, *J. Nucl. Mater.*, **176&177**, 14 (1990).

[17] U. Samm, *et al.*, *J. Nucl. Mater.*, **220-222**, 25 (1995).

[18] Y. Yamauchi, *et al.*, *Fusion Eng. Des.*, **39-40**, 427 (1998).

[19] P. A. Radhead, *Vacuum*, **12**, 203 (1962).

[20] B. Dishler *et al.*, *Solid State Commun.*, **48**, 105 (1983).

[21] J. C. Lascovich, *et al.*, *Appl. Surf. Sci.*, **47**, 17 (1991).

[22] G. Staudenmaier, *et al.*, *J. Nucl. Mater.*, **84**, 149 (1979).

[23] S. A. Cohen and G. M. McCracken, *J. Nucl. Mater.*, **84**, 149 (1979).

[24] W. R. Wampler and C. W. Magee, *J. Nucl. Mater.*, **103&104**, 509 (1981).

[25] B. L. Doyle, *et al.*, *J. Nucl. Mater.*, **93&94**, 551 (1980).

[26] R. B. Wright, *et al.*, *J. Nucl. Mater.*, **63**, 415 (1976).

[27] K. Ashida, *et al.*, *J. Nucl. Mater.*, **137**, 792 (1984).

[28] K. Niwase *et al.*, *J. Nucl. Mater.*, **191-194**, 335 (1992).

[29] T. Tanabe *et al.*, *Fusion Eng. Des.*, **29**, 428 (1995).

[30] T. Tanabe, *Phys. Scr.*, **T64**, 7 (1996).

[31] E. Asari, *et al.*, *Phys. Rev.*, **B 47**, 11143 (1993).

[32] T. Tanabe and S. Muto, *Phys. Scr.*, **T81**, 104 (1999).

[33] M. Sasaki, Master thesis, Shizuoka University, Japan (2004).

Table 4.1 Desorption activation energy determined in the present study and literatures.

	Present study			
	Peak1 / eV	Peak2 / eV	$PeakCD_4$ / eV	$PeakCD_3$ / eV
173 K	4.41±0.91	3.56±1.67	2.98±0.07	2.97±0.17
273 K	2.98±0.36	2.42±0.30	2.66±0.50	2.66±0.50
473 K	2.10±0.01	1.40±0.40	5.11±3.81	4.12±0.75
573 K	2.36±0.24	1.43±0.09	3.69±0.88	3.44±0.65
673 K	2.09±0.06	1.17±0.10	3.75	4.92
	Literatures			
2.7 eV	Thermal decomposition of sp^3 centers to sp^x [7-9]*1			
1.7 eV	H induced actived H release [9]*2			
2.4 eV	Thermally activated methyl release [9]*3			
1.5 eV	H induced actived methyl release [9]*4			

Table 4.2 Desorption reaction order determined in present study.

	Peak 1	Peak 2	Peak CD_4	PeakCD_3
n-1	0.8±0.19	0.9±0.18	0.7±0.29	1.3±0.34
n	1.8±0.19	1.9±0.18	1.7±0.29	2.3±0.34

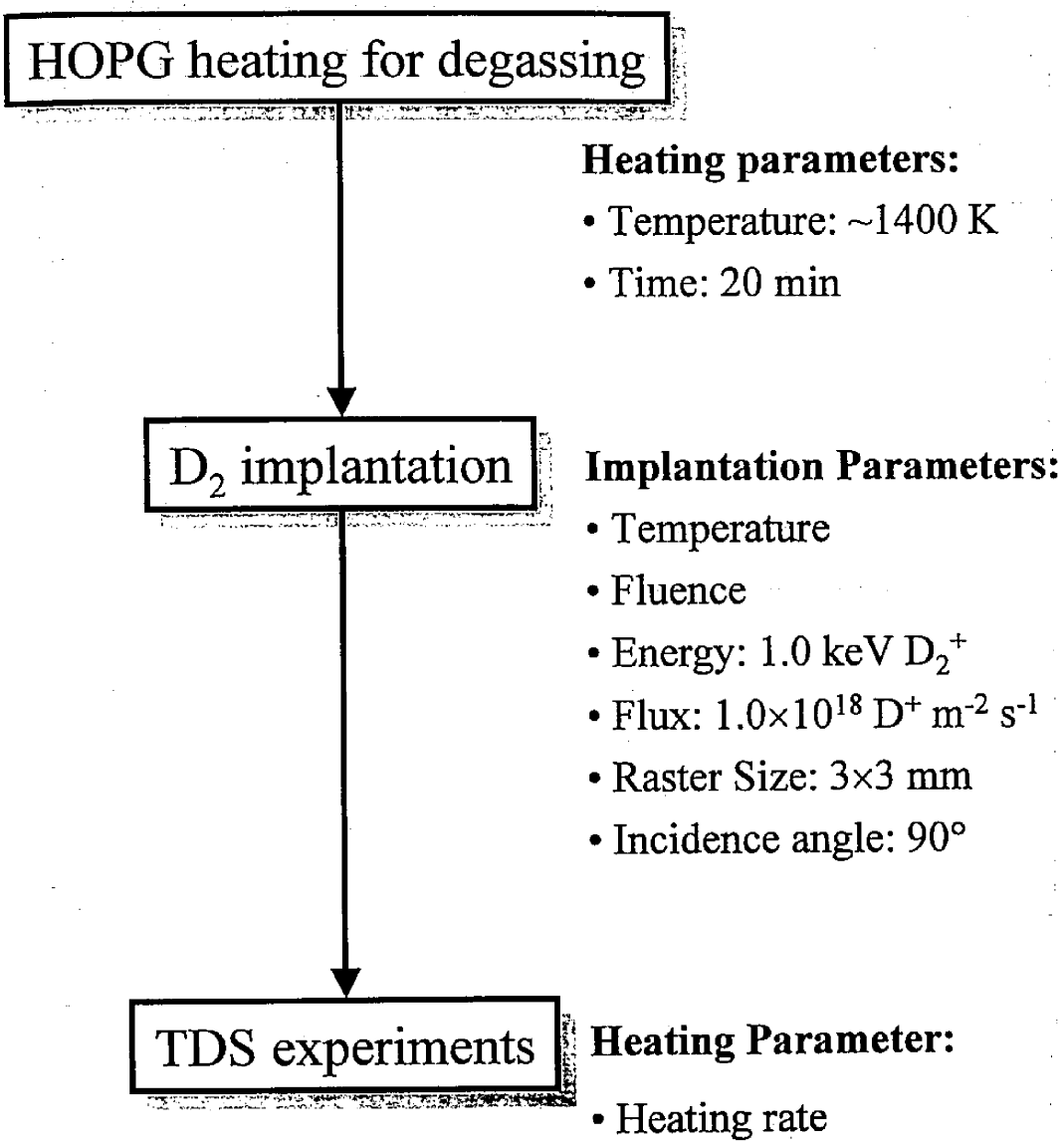

Fig. 4.1 Flowchart of TDS experiments.

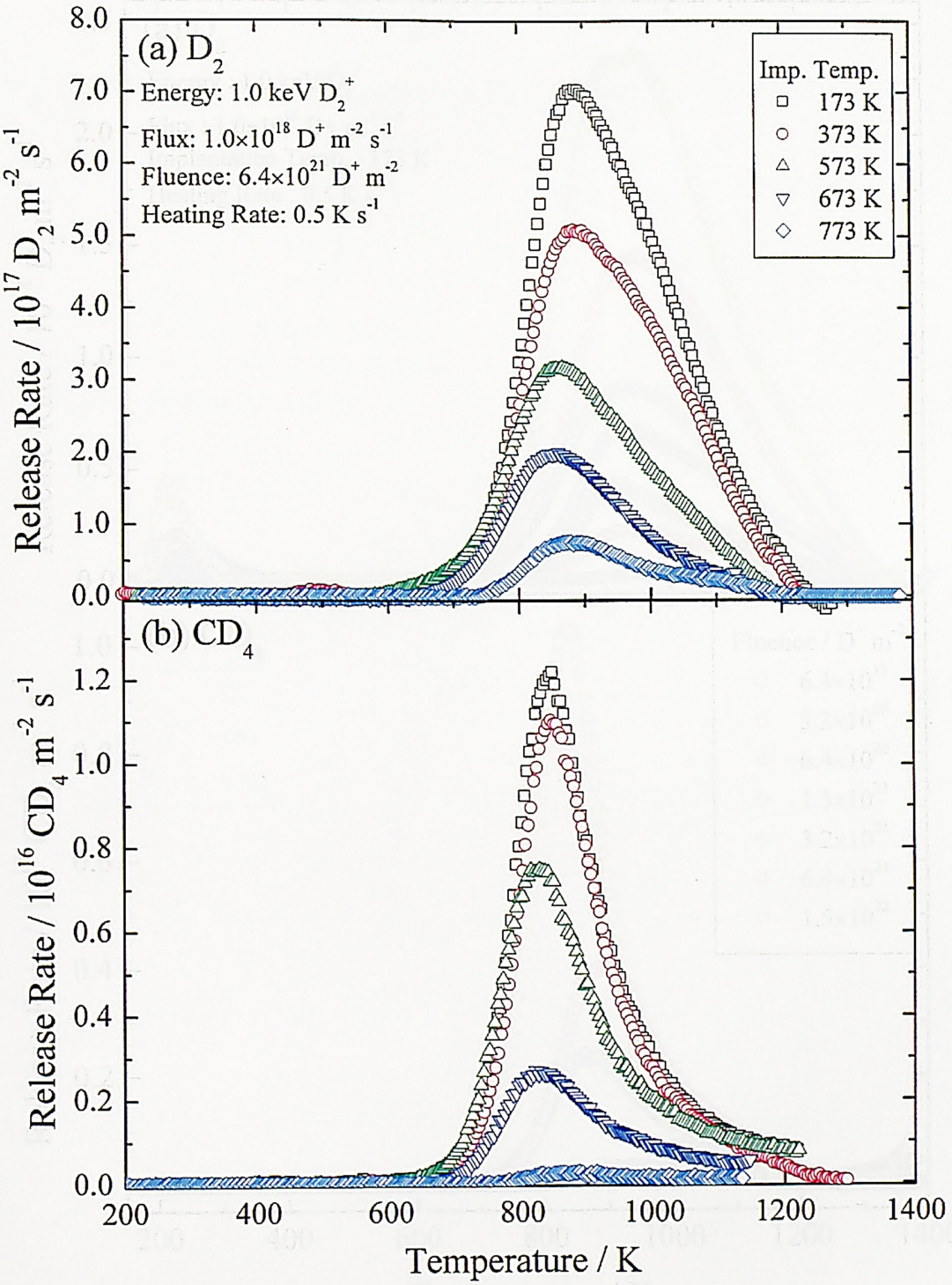

Fig. 4.2 TDS spectra of (a) D_2 and (b) CD_4 released from HOPG implanted by 1.0 keV D_2^+ under various temperature.

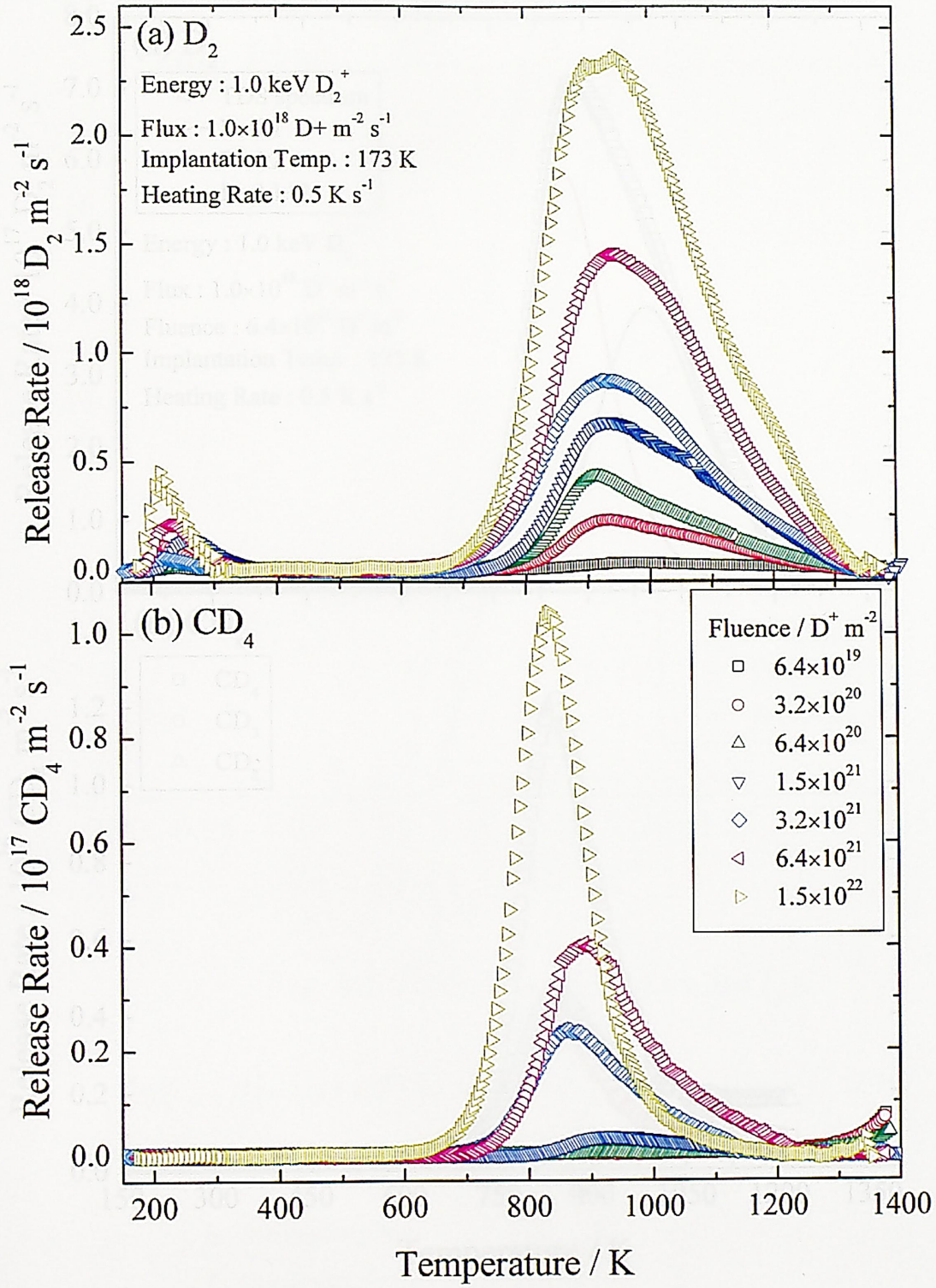

Fig. 4.3 TDS spectra of (a) D_2 and (b) CD_4 released from HOPG implanted by 1.0 keV D_2^+ under various fluence.

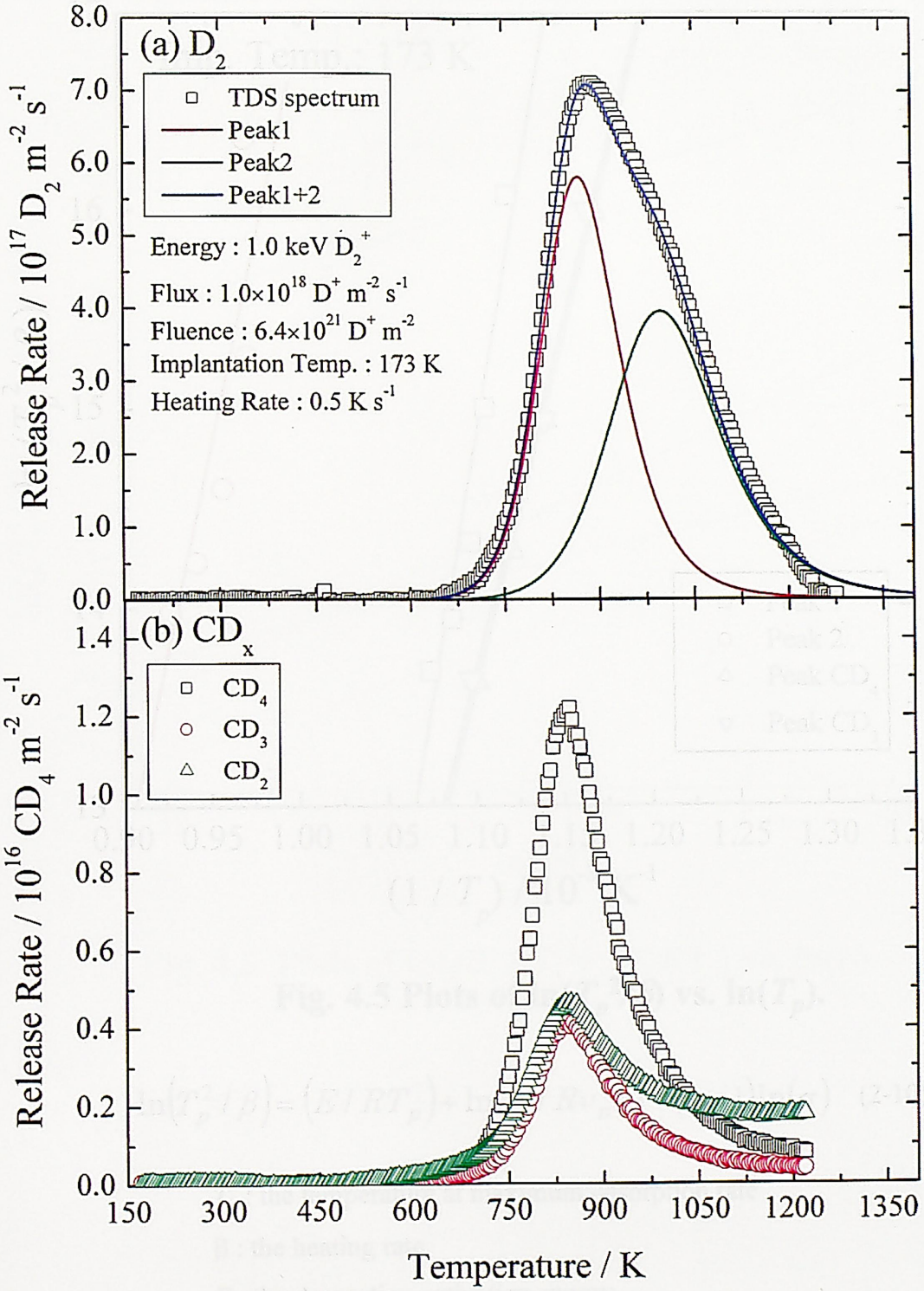

Fig. 4.4 TDS spectra of (a) D_2 and (b) CD_x and fitting results of D_2 TDS spectrum.

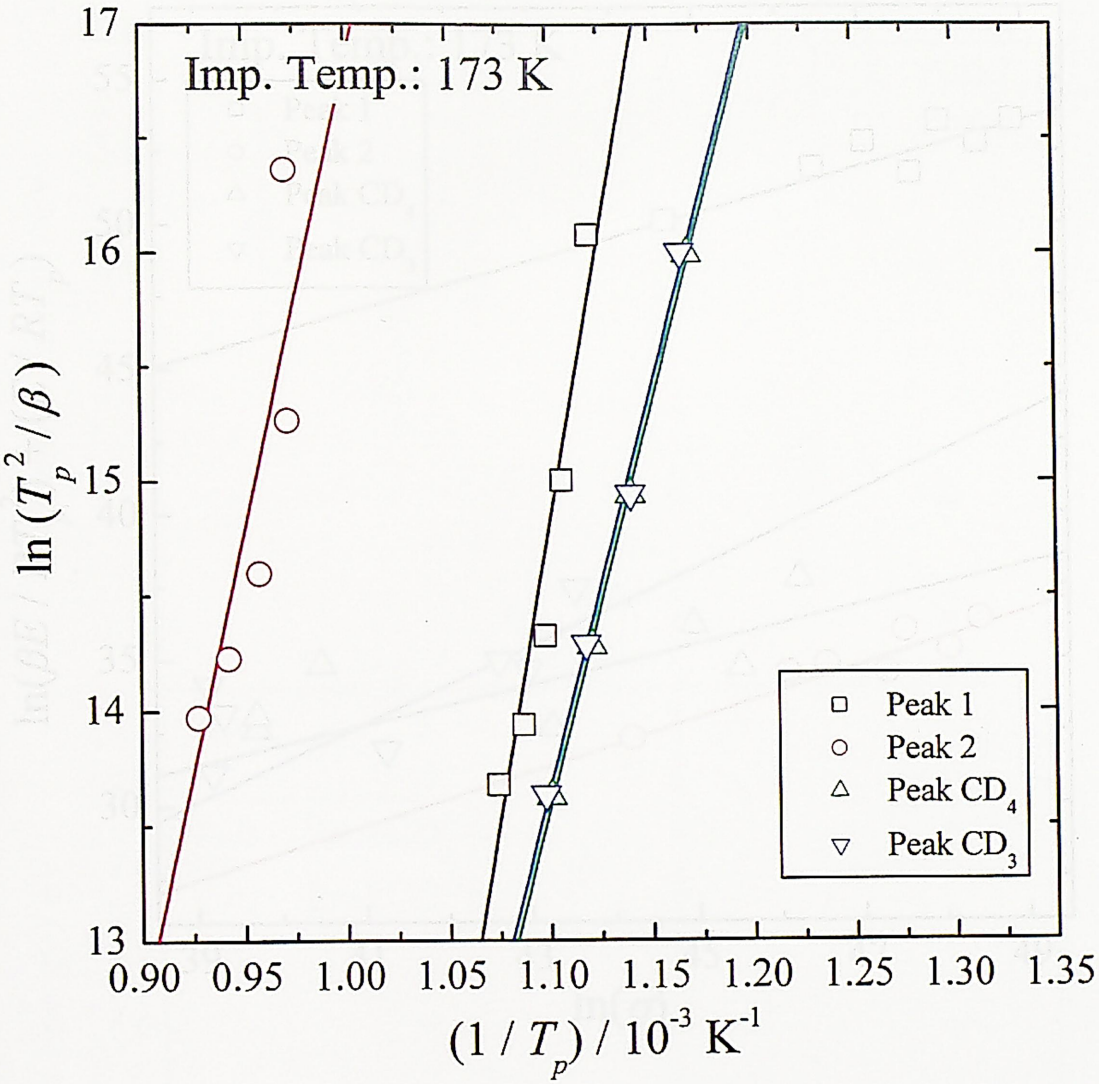

Fig. 4.5 Plots of $\ln(T_p^2/\beta)$ vs. $\ln(T_p)$.

$$\ln\left(T_p^2/\beta\right)=\left(E/RT_p\right)+\ln\left(E/R\nu_n n\right)-\left(n-1\right)\ln\left(\sigma\right) \quad (2\text{-}10)$$

T_p : the temperature at maximum desorption rate

β : the heating rate

E : the desorption activation energy

R : the gas constant

ν_n : the frequency factor

n : the order of the desorption reaction

σ: the surface coverage

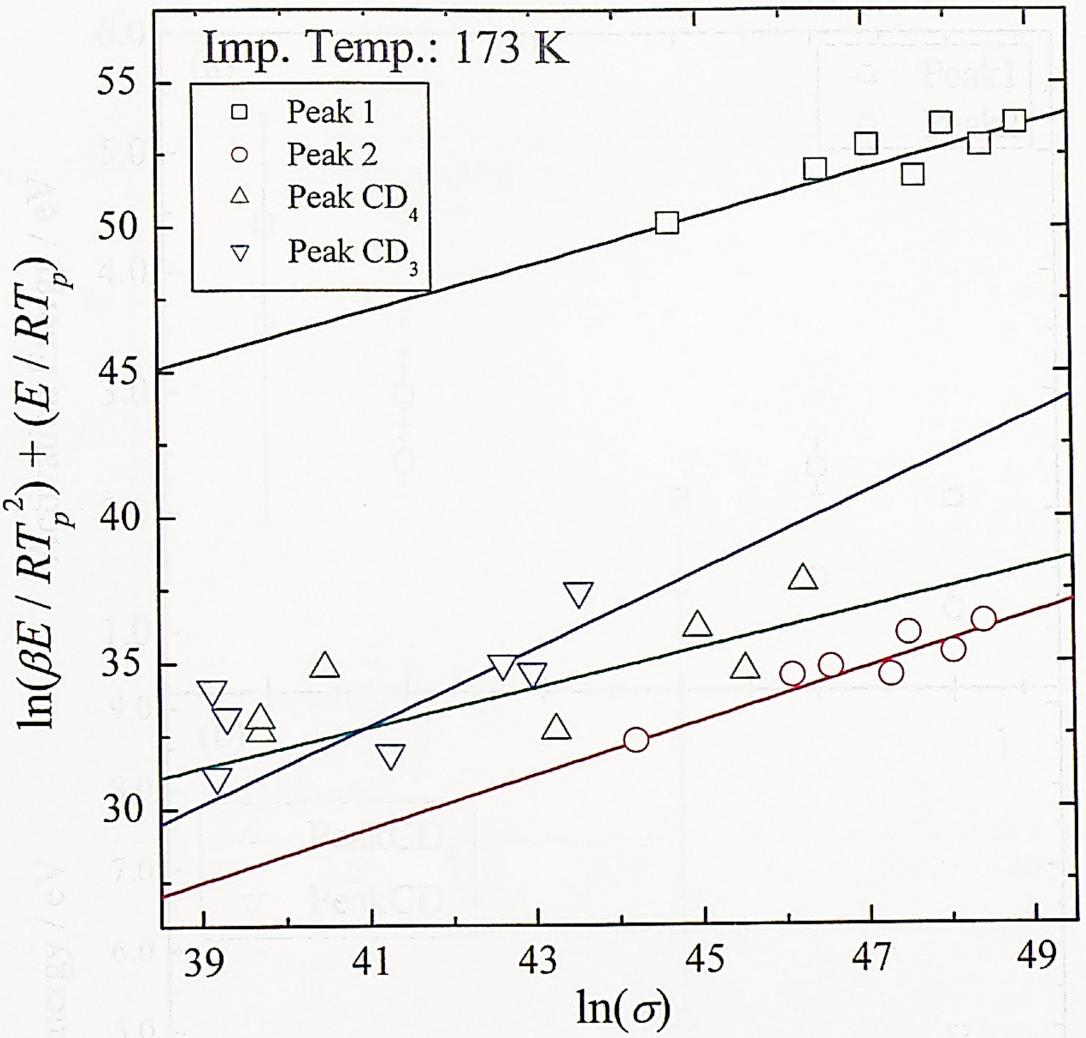

Fig. 4.6 Plots of $\ln(\beta E/RT_p^2)+(E/RT_p)$ vs. $\ln(\sigma)$.

$$\ln(\beta E / RT_p^2) + (E / RT_p) = \ln(\nu_n n) + (n-1)\ln(\sigma) \qquad (2\text{-}12)$$

T_p : the temperature at maximum desorption rate

β : the heating rate

E : the desorption activation energy

R : the gas constant

ν_n : the frequency factor

n : the order of the desorption reaction

σ: the surface coverage

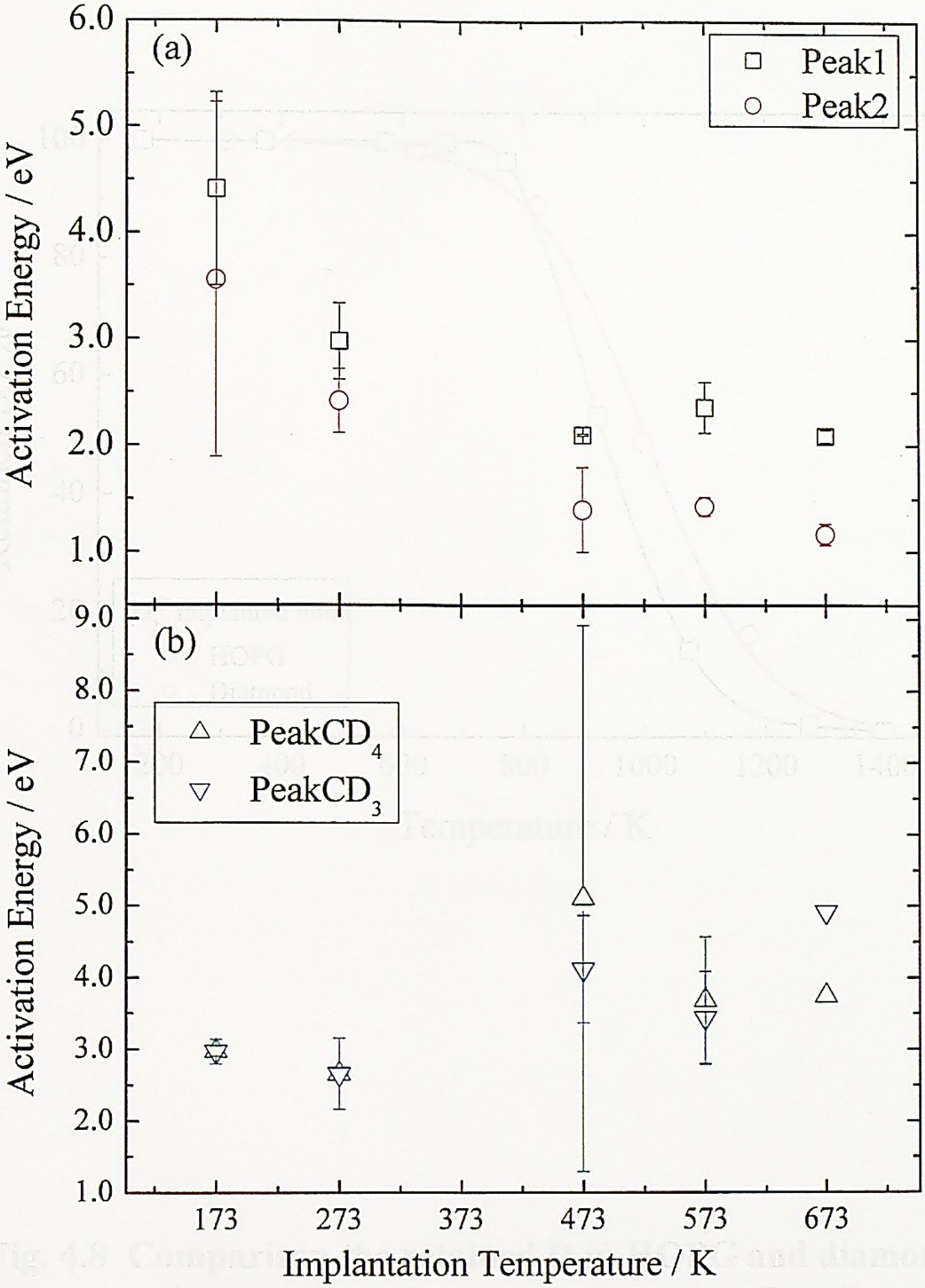

Fig. 4.7 Implantation temperature dependence of activation energy for (a) D_2 and (b) CD_x desorption from HOPG.

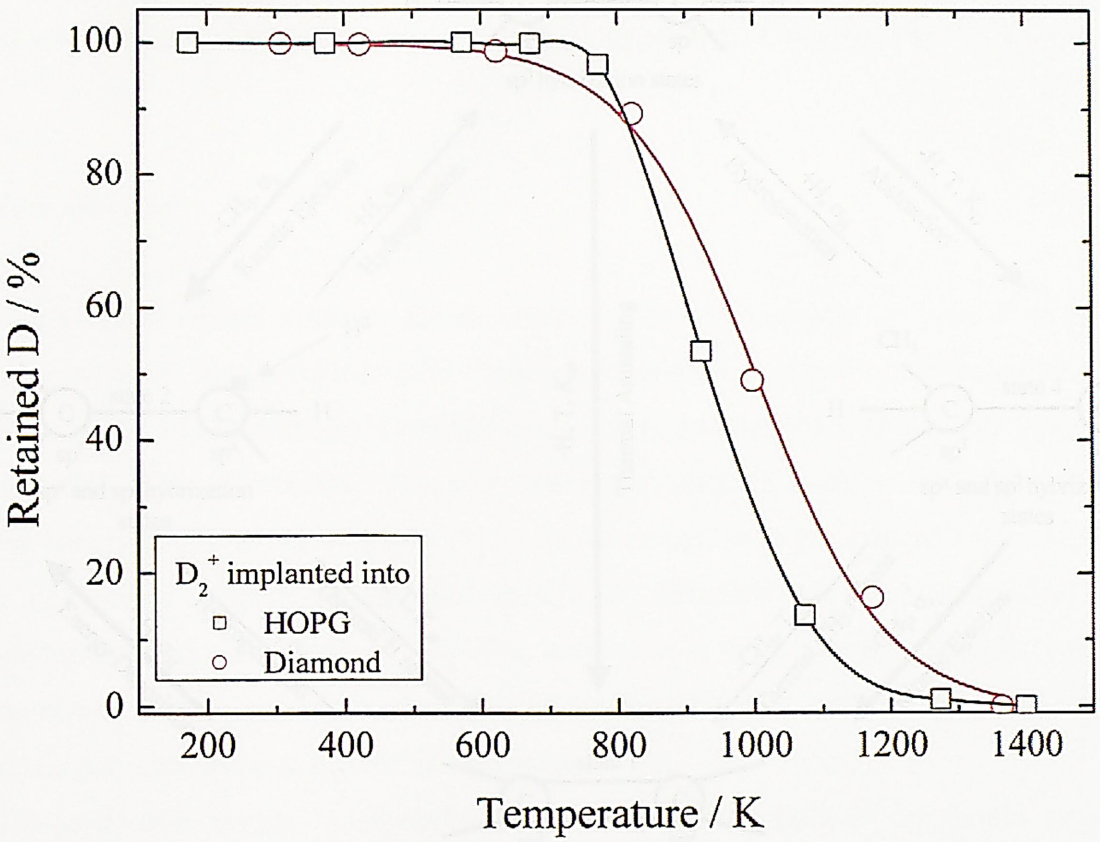

Fig. 4.8 Comparison the retained D in HOPG and diamond polycrystalline after the implantation. For diamond, the release rate was measured by heating at each temperature for 10 min. For HOPG, TDS spectrum was measured with heating rate of 0.5 K s-1 after the implantation at 173 K.

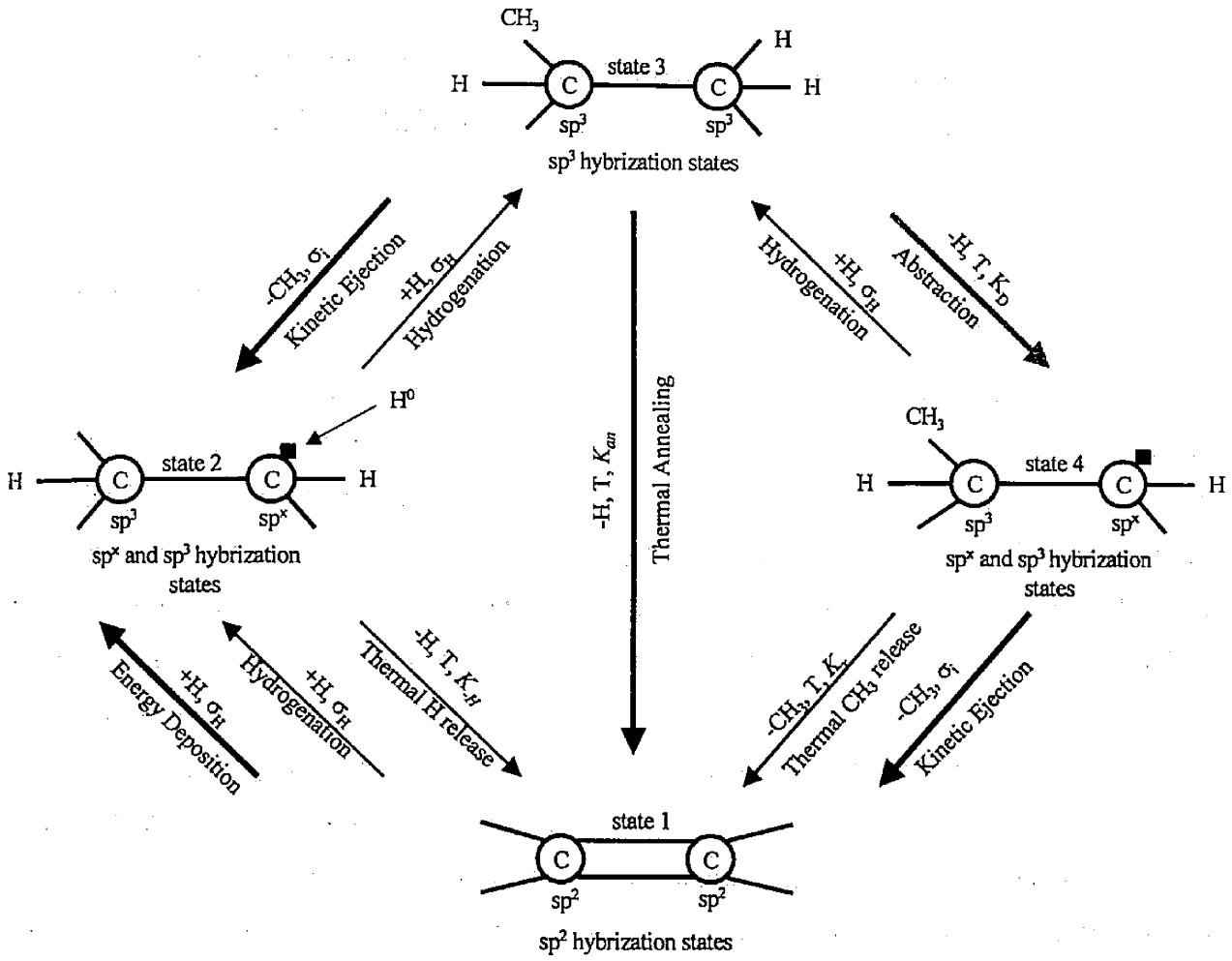

Fig. 4.9 Schematic diagram of the model for hydrogenation due to hydrogen impact on graphite [8-11].

CHAPTER V

STUDY ON TEMPERATURE DEPENDENCE OF TRAPPING FOR DEUTERIUM IMPLANTED INTO HIGHLY ORIENTED PYROLYTIC GRAPHITE

5.1 Introduction

To evaluate tritium safety in fusion reactors, it is very important in case of an accident to know how tritium implanted into PFMs behaves chemically at operating temperatures. Tritium behavior in the PFMs could be governed by chemical interactions with damage induced by ion implantation. The PFMs are exposed by energetic particles, such as deuterium and tritium, whose energy could be below 1 keV [1]. The chemical reactions induced by ion implantation with high-energy (< keV), are assumed specifically different from thermal chemical reactions. To understand special chemical reactions known as a high energy chemical reaction [2], phenomenon during ion implantation should be distinguished between reactions induced by energetic particles and that by thermalized particles.

Experimental results obtained by lower temperature implantation should provide new information about the reaction between the PFMs and energetic hydrogen isotopes, because the implantation at lower temperature could be expected to depress annealing of structure disordered by the implantation as shown in Chap. 4.3.2. In addition it was reported that graphite structure is disordered by hydrogen and/or electron irradiation around liquid nitrogen temperature [3-6]. The graphite become to Diamond Like Carbon (DLC) in which the carbon atoms are connected to each other by random network of sp^3 bonding [4, 6]. On the other hand, it was also demonstrated that hexagonal atomic ring in the graphite structure is reconstructed to non-hexagonal atomic rings [3]. This could indicate the existence of intermediate states carbon atoms between sp^2 and sp^3 bonding in DLC. Anyway, the structure change is induced by the implantation at lower temperature. Implantation temperature is one of most important parameters for rearrangements of disordered structure, formation of bonding and so on.

In the present study, the temperature dependence of chemical behavior of deuterium in HOPG is focused and investigated to reveal the reactions by the implantation, from view point of the non-equilibrium chemistry; that is high energy chemistry.

5.2 Experimental

The sample used was HOPG crystal mentioned in Chap. 2.2.2. An as-received sample was cleaved mechanically and the new cleavage surface was degassed at 1400 K for 20 min.

To investigate implantation temperature dependence of retained deuterium and graphite structure, the deuterium ions were implanted into HOPG with an energy of 1.0 keV D_2^+, a flux of 1.0×10^{18} D^+ m^{-2} s^{-1}, and a fluence of 6.4×10^{21} D^+ m^{-2} at various temperatures in the region from 173 to 773 K. After D_2^+ implantation at each temperature, HOPG was cooled down to 173 K and TDS experiments were carried out by heating the sample up to 1400 K with heating rate of 0.5 K s^{-1}, and XPS spectra were measured by cooled down to RT. Post heating experiments were performed; (1) with the implantation at 573 K and annealing at 573 K for 155 min and (2) with implantation at 302 K and annealing at 573 K for 103 min as same as a time of the implantation before TDS experiment.

To investigate flux dependence of retained deuterium, the deuterium ions were implanted into HOPG with an energy of 1.5 keV D_2^+ and various fluxes in the region between 5.0×10^{17} and 5×10^{18} D^+ m^{-2} s^{-1} for 60 min at various temperatures in the region from 173 to 773 K. After D_2^+ implantation at each temperature, TDS experiments were carried out by heating the sample up to 1400 K with heating rate of 0.5 K s^{-1}.

All ion implantations were carried out in an area of 3×3 mm^2 of the samples and the incident angle of surface normal. The released species during the sample heating was monitored with QMS described in Chap. 4.2.

5.3 Results and Discussion

5.3.1 Deuterium Retention in HOPG

Figure 5.2 summarizes changes of the retention of deuterium implanted into HOPG at various temperatures. The figure is also indicated results by Doyle *et al.* who reported that the saturated concentration of hydrogen in pyrolytic graphite decreased with increasing the implantation temperature [7]. One can see that the present results agreed with their report except the part with temperatures lower than Room Temperature (RT). Möller *et al.* reported an increase of retained amount of implanted deuterium into graphite polycrystalline with decreasing

temperature below RT [8]. This corresponded with the present results. Deuterium implanted into HOPG, thus, was saturated at each implantation temperature in this study. An increasing of the retained amount with decreasing temperature even lower temperature is clearly established in contradiction to the assumption of a fixed maximum concentration below RT [9, 10] and to the estimation of the tritium inventory in a plasma-facing area using 0.4 of H/C ratio [11,12]. On the other hand, the amount of retained D which was released by forming CD_x was very small (<several % for total). The formation of CD_x depended on the deuterium fluence as indicated in Fig. 5.3. In Fig. 5.3, the retention of D released by forming CD_x was increased from a threshold fluence (6.4×10^{20} D^+ m^{-2} in this study) up to saturation where gradient for the increase of amounts of CD_x and D_2 was changed. It was suggested that the implanted deuterium was trapped by carbon, and further implantation induced deuterium trapping to carbon which already retained the deuterium. In the present study, the retention of deuterium which desorbed by forming D_2 was focused below.

Figure 5.4 shows retained amount of deuterium implanted into HOPG as a function of temperature for samples implanted and for those annealing with a heating rate of 0.5 K s^{-1}, that is TDS, after the implantation at 173 K. Comparing the release amount during thermal annealing to the retained deuterium after implantation at elevated temperature, it was noted that the saturated amounts in HOPG was decreased with the temperature elevating. Further plotted in Fig. 5.4 are retained amounts of deuterium in HOPG annealed at 573 K for 155 and 103 min after the implantation at 573 and 302 K, respectively. One can see that no-release of deuterium trapped in HOPG was observed because the retention after thermal annealing at 573 K was not decreased comparing with that after implantation at various temperatures. These results indicated that the deuterium trapped by carbon in HOPG after the implantation was released at a threshold temperature which was at ~700 K estimated from TDS spectrum as shown in Fig. 5.1. TDS spectra attributed to thermal release during thermal annealing of the trapping site and that was suggested the thermal release of trapped deuterium should not be induced during the implantation in the temperature region from 173 to 700 K. Therefore there were possibilities that the deuterium trapped by carbon was released by the implantation, namely ion-induced release, could be progressed.

It was reported by Möller *et al.* and Scherzer *et al.* that the ion-induced release process occurred during the implantation [5, 13]. They reported that after implantation to saturation at low temperature, the reemission was found during additional irradiation at the temperature where the thermal release is not yet observed [5, 13]. Any collisional processes in the graphite could

detrap deuterium atoms retained by carbon and detrapped deuterium could recombine at the depth of their origin and migrate to the surface as molecules. This process will be progressed by the energy transfer from the energetic deuterium implanted into HOPG and the activation energy is not concerned. Therefore the high energy chemical reaction occurred on a reemission of deuterium during the implantation. However, the more experimental data such as the implantation with various energies and/or fluxes is needed to discuss the ion-induced reaction. Figure 5.5, which is one of the results for discussion of the ion-induced reaction, shows the retention of implanted deuterium to fluence ratio after the implantation with various fluxes at various temperatures. That ratio was almost 100% after the implantation with the lowest flux (5.0×10^{17} D^+ m^{-2} s^{-1}) and decreased with increasing the flux. This result suggested that the deuterium was retained up to an amount which was threshold to occur of the ion-induced release as the first step and the retained deuterium was desorbed by the energetic deuterium successional coming during the implantation as the second step. After the ion-induced desorption the trapping site without deuterium could be annealed easier and the formation of a new trapping site resulted in the temperature dependence of the retention of the deuterium.

5.3.2 Thermal Annealing during D_2^+ Implantation at Elevated Temperature

Disordering of the structure is induced by the implantation and depends on the energy of ions. Decrease of the retention can resulted in annealing of trapping sites, that is, the annealing of the structure disordered and/or the ion-induced release of the deuterium trapped by carbon.

Figure 5.6 shows XPS spectra of (a) C1s and (b) π-π^* transition after the implantation at various temperatures. Although the π-π^* transition peak associated with the electron transition between the HOMO-LUMO gap was not observed after the implantation at 173 K, the peak was found to be clear after that at 573 K. This result suggested that graphite structure began to be ordered during the implantation at 573 K. The energy loss of the π-π^* transition peak, which is a gap between energies of C1s and π-π^* transition peak, determined to be 7.01, 5.88 and 6.77 eV for HOPG cleaved and heating at 1400 K, and implanted deuterium at 573 and 773 K respectively. For example, the π-π^* transition peak is also found in XPS spectra of glassy carbon and fullerene (C_{60}), however, their energy loss is smaller than that of HOPG [14]. In addition C1s peak after the implantation at 573 K was observed at lower energy side than that of the cleaved face after heating shown in Fig. 5.6. These results indicated that the structure disordered by the implantation was rearranged to the graphite structure by thermal annealing

which could have not only hexagonal but also non-hexagonal atomic rings such as pentagonal and/or polygonal ones. And many defects were still retained in the structure disordered by the implantation at 573 K in beginning of the annealing.

A process during thermal annealing of the disordered structure could be due to the vacancy clustering because of described above and the activation energies as determined in Chap. 4.3.2. Nevertheless, the sp^2 to sp^3 transition of carbon atoms by ions implantation in Chap. 3.3.2 should allow for the thermal annealing of the disordered structure. This is a reason why the activation energy of sp^3 to sp^2 transition in a diamond disordered by 0.5 keV Ar^+ implantation was determined to be 1.8 eV, which is almost corresponding to the present result (~2.0 eV), and the disordered diamond structure is annealed by carbon atoms bonding in a graphitic network [15, 16]. It is found using Electron Energy Loss Spectroscopy (EELS) that the disordered structure is similar to Diamond Like Carbon (DLC) structure induced by 0.5 keV Ar^+ implantation to HOPG [15]. Therefore the sp^3 carbon without deuterium produced by the implantation in the present study could be converted to sp^2 one during the implantation. Unfortunately, although those two possibilities was not identified, it was confirmed that the thermal annealing of the disordered structure was occurred in HOPG during the implantation and that was one of the causes for reducing the retention of deuterium.

5.4 Summary

The amount of retained D after the implantation at various temperatures was investigated and was found decreasing of with increasing the implantation temperature. An increasing of the saturated retention with decreasing temperature even lower temperature is clearly established in contradiction to the assumption of fixed maximum concentration below room temperature [9, 10] and to the estimation of the tritium inventory in a plasma-facing area using 0.4 of H/C ratio [11,12].

As the thermal release of deuterium trapped with carbon forming C-D bond was not observed below 773 K it was suggested that the ion-induced release occurred during the implantation. The ion-induced release occurred by any collisional processes in the graphite and progressed by which the deuterium trapped by carbon could recombine to deuterium successional coming and migrate to the surface as molecules. This process is high energy chemical reaction because the activation energy is not concerned. After the ion-induced

desorption the trapping site without deuterium could be annealed easier and that was one of the causes for reducing the retention of deuterium.

References

[1] J.-P. Adloff, P. P. Gaspar, M. Imamura, A. G. Maddoch, T. Matsuura, H. Sano and K. Yoshihara (Eds), Handbook of Hot Atom Chemistry, VCH Publishers, New York 1992, p.647.

[2] K. Yoshihara, Hotto atomu kagaku, Kibo shoten, Kooriyama (1978), [in Japanese].

[3] M. Takeuchi, *et al.*, *J. Nucl. Mater.*, **271&272**, 280 (1999).

[4] K. N. Kushita, *et al.*, *J. Electron Microsc.*, **44**, 456 (1995).

[5] K. N. Kushita and K. Hojou, *Ultramicroscopy*, **35**, 289, (1991).

[6] K. N. Kushita, *et al.*, *J. Nucl. Mater.*, **191-194**, 351 (1992).

[7] B. L. Doyle, *et al.*, *J. Nucl. Mater.*, **103&104**, 513 (1981).

[8] W. Möller, *et al.*, *Nucl. Instrum. Methods Phys. Res.*, **B19/20,** 826 (1987).

[9] D. K. Brice, *et al.*, *J. Nucl. Mater.*, **111-112**, 598 (1982).

[10] W. Möller and B. M. U. Scherzer, *J. Appl. Phys.*, **64**, 4860 (1988).

[11] R. A. Causey, *et al.*, *Fusion Eng. Des.*, **61-62**, 525 (2002).

[12] R. A. Causey, *J. Nucl. Mater.*, **300**, 91 (2002).

[13] B. M. U. Scherzer, *et al.*, *J. Nucl. Mater.*, **162-167**, 1013 (1989).

[14] J. A. Leiro, *et al.*, *J. Electron Spectrosc. Relat. Phenom.*, **128**, 205 (2003).

[15] A. Hoffman, *et al.*, *Diamond Relat. Mater.*, **5**, 76 (1996).

[16] Y. V. Betenko, *et al.*, *J. Appl. Phys.*, **88**, 4380 (2000).

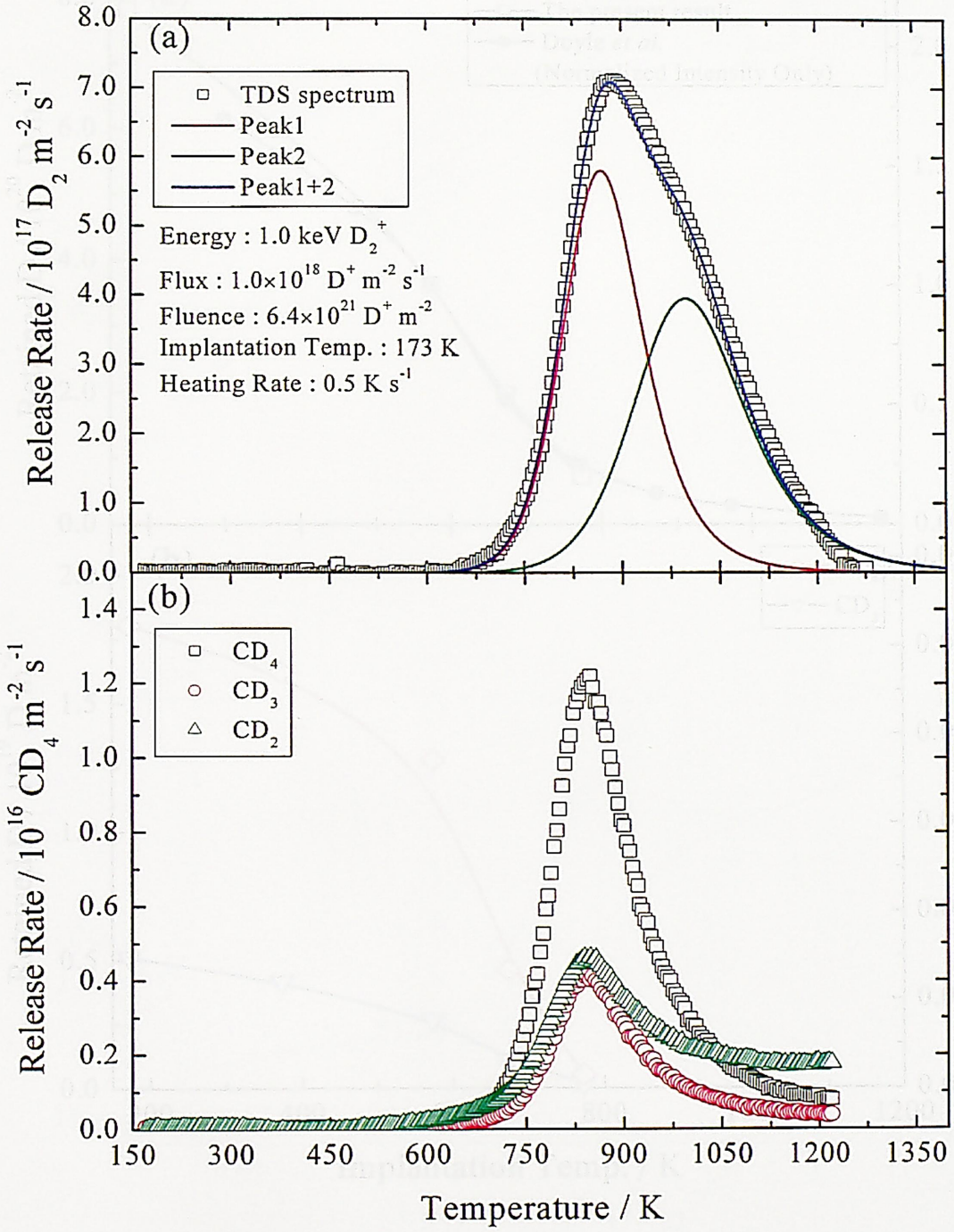

Fig. 5.1 TDS spectra of (a) D_2 and (b) CD_x and fitting results of D_2 TDS spectrum.

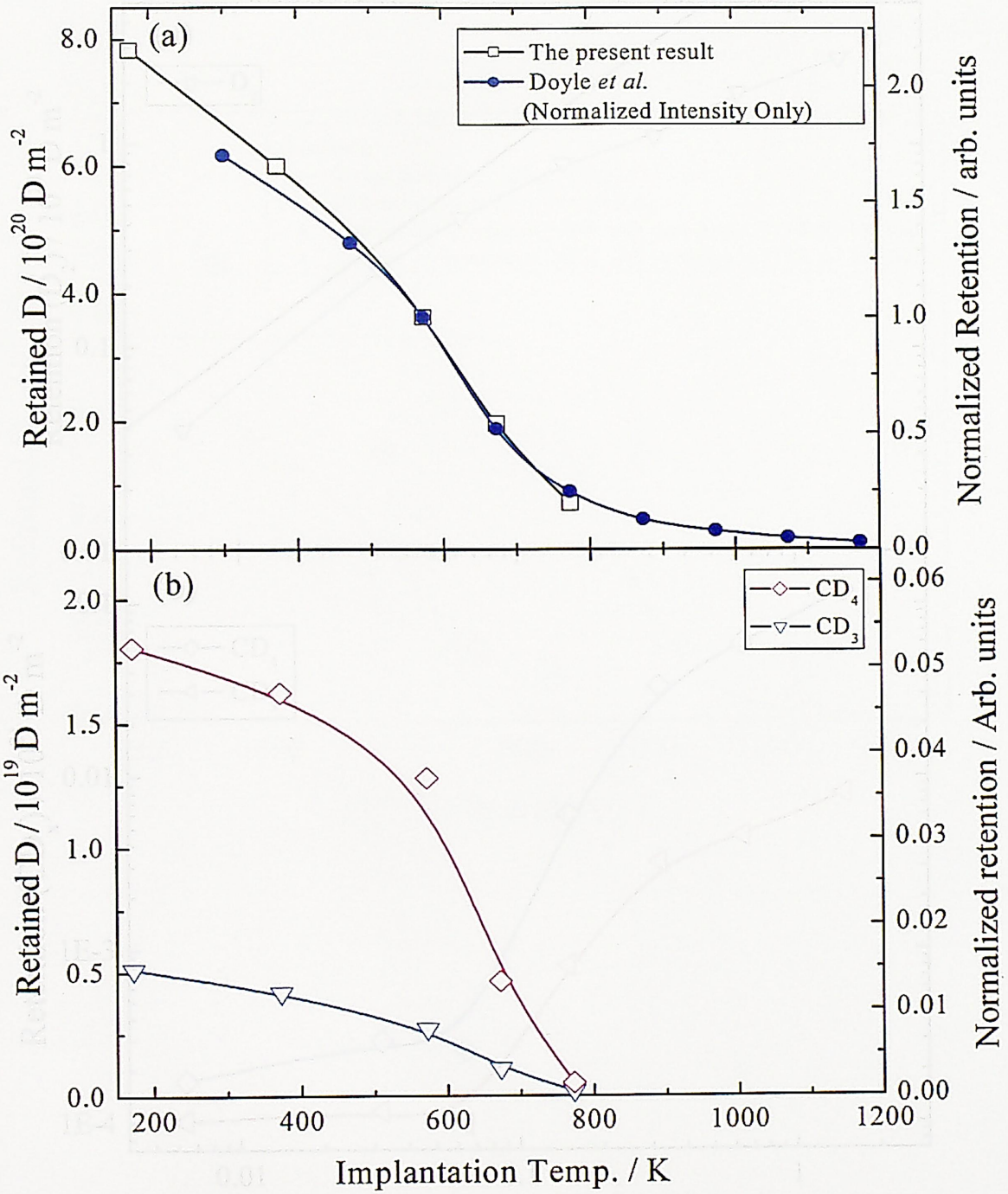

Fig. 5.2 Implantation temperature dependence of (a) total and (b) CD_x retention after the implantation. Retention amount estimated from each peak area was normalized by total one after D_2^+ implantation at 573 K.

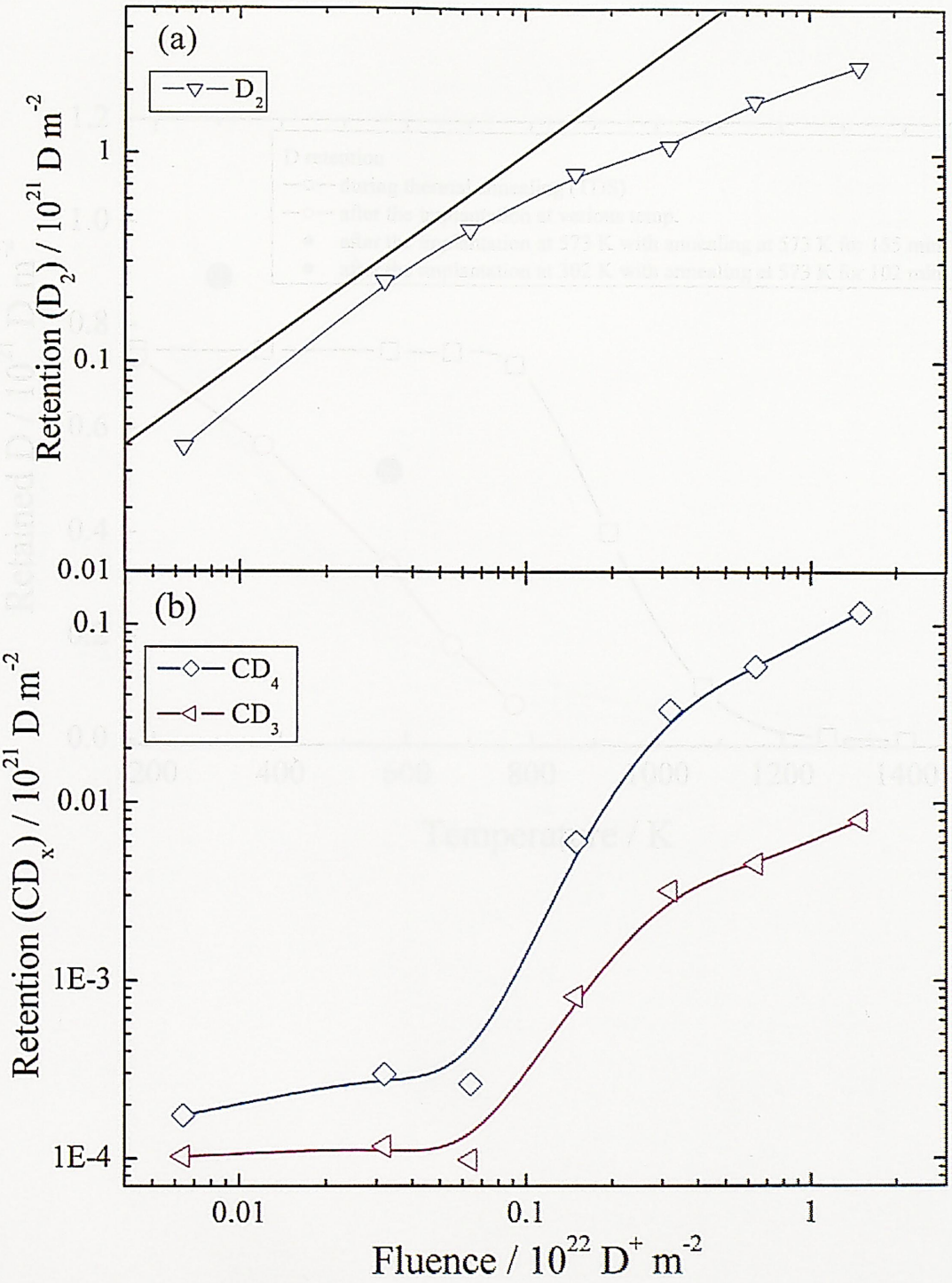

Fig. 5.3 Amount of retained deuterium forming (a) D_2 and (b) CD_x during thermal desorption from HOPG after the implantation with with various fluence.

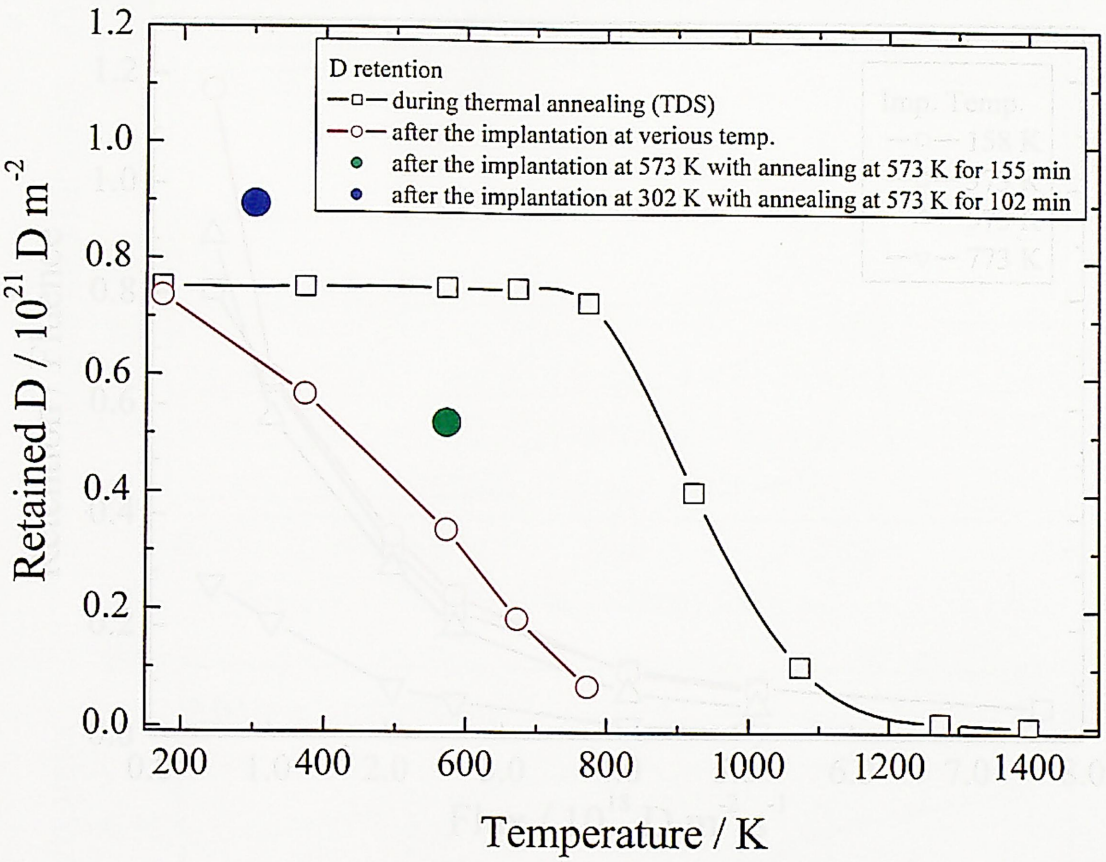

Fig. 5.4 Retained amounts of deuterium implanted into carbon as a function of temperature.

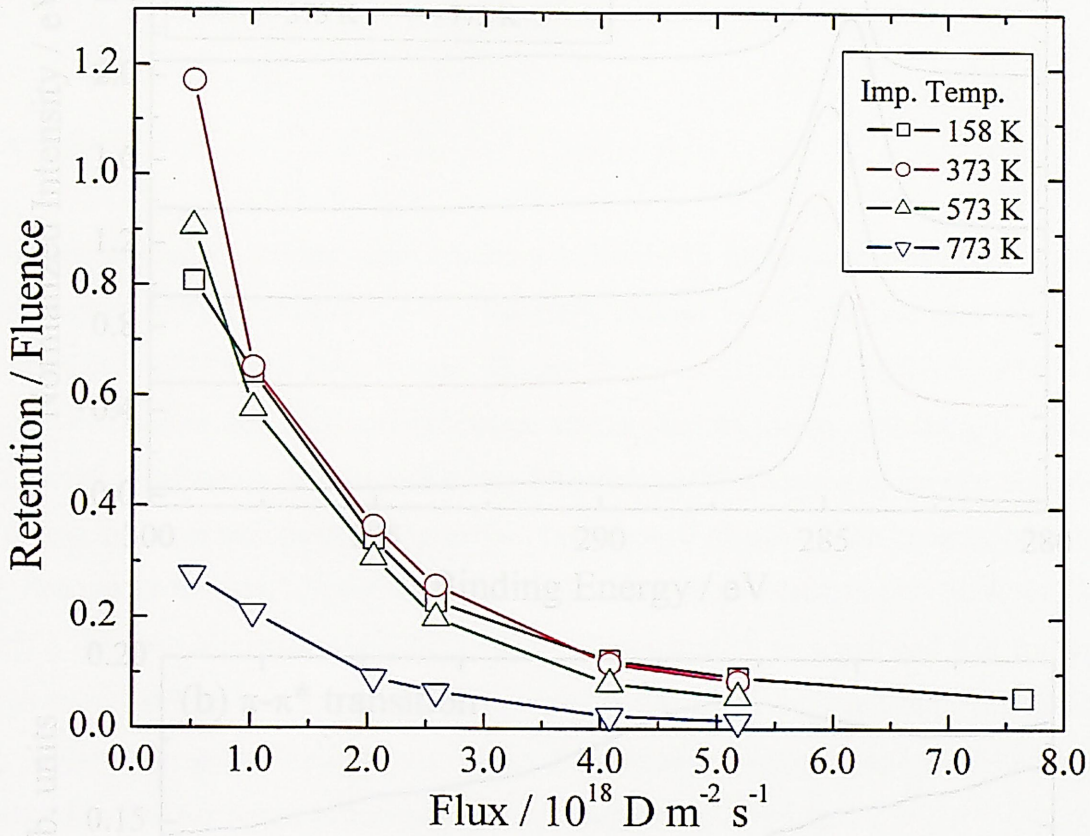

Fig. 5.5 Retention of implanted deuterium to fluence ratio after the implantation with various fluxes at various temperatures.

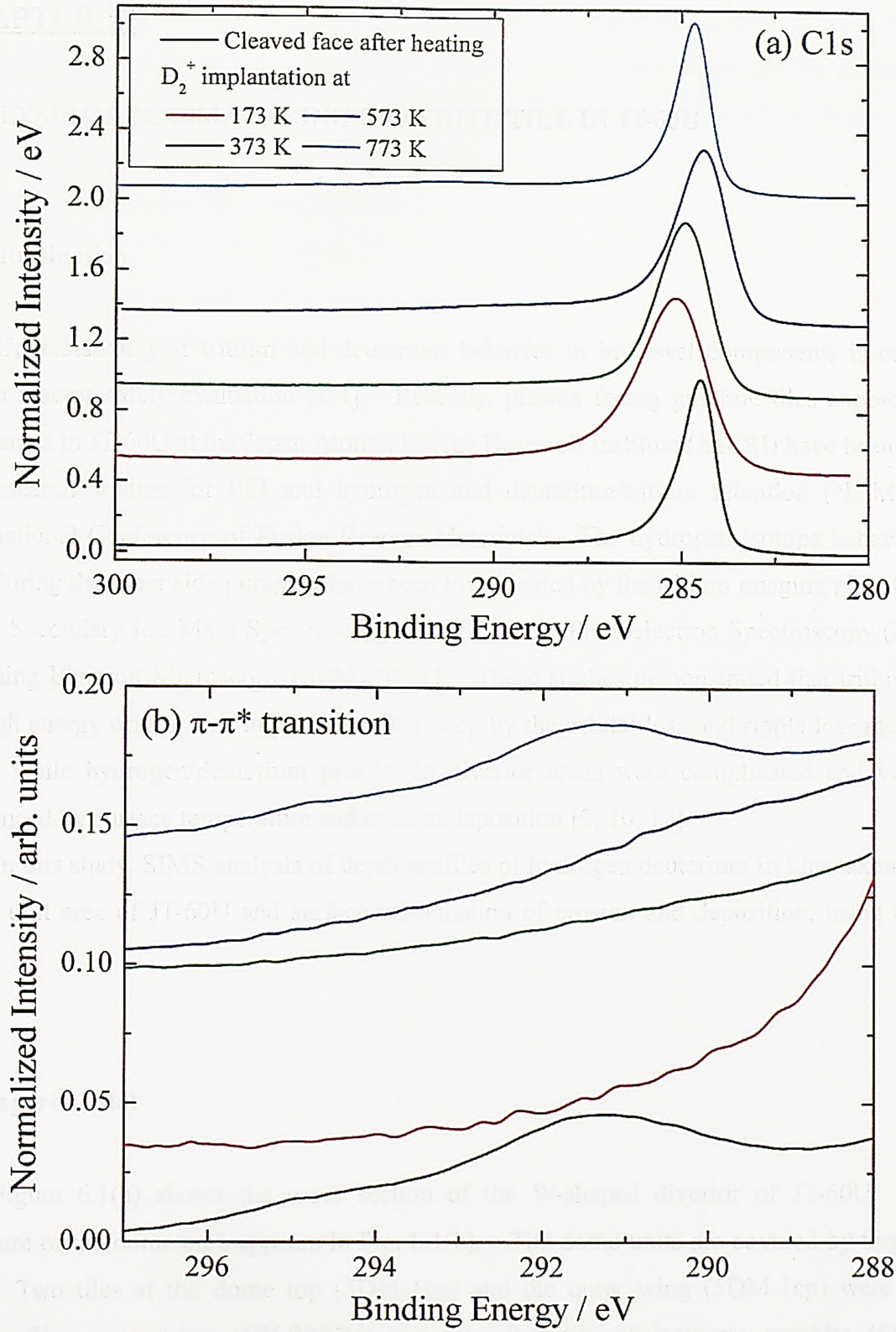

Fig. 5.6 XPS spectra of (a) C1s and (b) π-π* transition after D_2^+ implantation at various temperature.

CHAPTER VI

ANALYSIS OF PLASMA FACING GRAPHITE TILE IN JT-60U

6.1 Introduction

Understanding of tritium and deuterium behavior in in-vessel components is critical for fusion reactor safety evaluation [1-4]. Recently, plasma facing graphite tiles exposed to DD discharges in JT-60U at the Japan Atomic Energy Research Institute (JAERI) have been available for research studies for PSI and hydrogen and deuterium/tritium retention (N. Miya, 11th International Conference of Fusion Reactor Materials). The hydrogen isotope behavior in the tiles during the inner side pumping have been investigated by the tritium imaging plate technique [5-8], Secondary Ion Mass Spectroscopy (SIMS), X-ray Photoelectron Spectroscopy (XPS) and Scanning Electron Microscopy (SEM) [9-11]. These studies demonstrated that tritium, due to its high energy origin, was implanted rather deep by the orbital loss and ripple loss mechanisms [5-8], while hydrogen/deuterium profiles in divertor areas were complicated and very much influenced by surface temperature and erosion/deposition [9, 10, 12].

In this study, SIMS analysis of depth profiles of hydrogen/deuterium in tiles taken from the dome unit area of JT-60U and surface examination of erosion and deposition, using SEM and XPS.

6.2 Experimental

Figure 6.1(a) shows the cross section of the W-shaped divertor of JT-60U. Detailed structure of the dome area appears in Fig. 6.1(b). The dome units are covered by three carbon tiles. Two tiles at the dome top (5DM-1bp) and the outer wing (5DM-1cp) were made of carbon fiber composites (CX-2002U) and the other tile of isotropic graphite (5DM-1aq). Sample disks (about 10×10×1 mm^3) were cut from these tiles and numbered as indicated in the figure.

All tiles were subjected to total of 6700 DD discharges, 4300 for inner side pumping and the remainder for both side pumping. 350 HH discharges were also performed after the DD

discharges to remove tritium accumulated in the tiles. Boronization was performed three times during this discharge period. The temperature of the tiles was measured by thermocouples embedded 6 mm beneath the surface as indicated in Fig. 6.1(a) and was 650 K at the maximum (Ave.: 600 K). However, surface temperature of the tiles would be much higher.

The depth profile of hydrogen isotopes retained in the samples were analyzed by SIMS (ULVAC-PHI ADEPT1010 Dynamic SIMS System), using cesium ion (Cs^+) as the primary ion with an energy of 5.0 keV and a beam current of 100 nA at 45° to the surface normal. The beam size was about 32 μm and the rastering area was set at 400×400 μm^2. Depth profiling with a profilometer showed the sputtering rate to be around 1 μm h^{-1}.

The XPS measurements were also performed for surface characterization (ULVAC-PHI ESCA5500MC system), using a Mg Kα 400W X-ray source and a concentric hemispherical analyzer. The depth profile was also analyzed by Ar ion (Ar^+) sputtering with an ion energy of 4.0 keV and a raster size 1×1 mm^2 at 30°orientation to the surface normal. For XPS, the sputtering rate was nearly 10 nm min^{-1}, measured by the profilometer. To remove surface contamination, 6min (corresponding to 60-70 nm) of Ar^+ sputtering was required for most cases. Nevertheless, charging of the sample during XPS analysis made the estimation of true chemical shifts very difficult [12]. Therefore, the chemical shifts were estimated by referring to the O1s peak assumed to originate from the carbonyl group at 531.4 eV [13]

6.3 Results

Figure 6.2 shows SEM images of the sample surfaces. On the inner divertor-facing side, no re-deposition layers were observed. The surface kept the original surface structure typical of IG-430U graphite as seen in Fig. 6.2(a) for the sample 5DM-1aq5. Figure 6.2(b) for the dome top area (5DM-1bp2), which directly faced on the plasma, also shows no re-deposition. The outer divertor-facing surface (5DM-1cp2), in contrast, shows a rather smooth structure covered with open pores (Fig. 6.2(c)), indicating the existence of a re-deposited layer. A measurements of the thickness showed that most of the surface area of the outer wing tile (5DM-1cp) was covered by re-deposition layers and the maximum of 10 μm thick layers appeared near the bottom edge. On the outer divertor-facing side of the dome top tile (5DM-1bp3), the re-deposition showing lamellar layers were also found, but the thickness was less than that of the outer dome wing (5DM-1cp).

Figure 6.3 compares depth profiles of H and D determined by SIMS for (a) the inner divertor-facing surface (5DM-1aq5), (b) the dome top (5DM-1bp2) and (c) the outer divertor-facing surface (5DM-1cp3). Since SIMS analysis does not give absolute amounts, signal intensities of negative ions of H and D were normalized to that of C for comparison.

At the inner divertor-facing surface (5DM-1aq5) with the eroded area, deuterium retention was quite low, and almost nothing was retained in deeper area, while in the outer divertor-facing surface (5DM-1cp3), in the re-deposited area, deuterium was retained with nearly constant amount. On the dome top area (5DM-1bp2), where there was no appreciable erosion nor re-deposition, the deuterium retention was highest but clearly decreased with depth.

Hydrogen profiles were nearly the same for all samples, and the highest retention appeared at or very near the surface and sharply decreased to certain levels irrespective of the samples. Considering that hydrogen discharges were performed after the deuterium discharges and before ventilation to remove the accumulated tritium produced in D-D reactions, we conclude that deuterium retained near surfaces was replaced by hydrogen. Thus H+D profiles shown in Fig. 6.3 must correspond to deuterium retention during the deuterium discharges. As seen in Fig. 6.3, the highest retention was observed at the re-deposited area and the least at the eroded area.

Figure 6.4 compares the integrated retention of H and D within the thickness of 1.7 μm obtained by integration of $H/^{12}C$ and $D/^{12}C$ SIMS signal ratios for all samples. One can see that the H+D retention in the inner divertor-facing side was smaller than that in the outer divertor-facing side. This indicates that the retention of hydrogen isotopes on the re-deposited area is larger than that on the eroded area. The H retention in all samples was almost the same. This indicated that the hydrogen retention saturated at a certain levels irrespective of erosion or re-deposition surface.

In XPS measurements, B1s, C1s and O1s peaks were observed. Figure 6.5 (a) and (b) show XPS spectra respectively for B1s and C1s observed after removal of the surface contaminants, i.e. Ar^+ sputtering for 6 min (corresponding to 60-70 nm). Before surface cleaning the B1s peaks for all samples showed single peaked structure, boron oxide at ~192 eV. After the surface cleaning, the B1s peaks split into two peaks as shown in Fig. 6.5(a) indicating the existence of a carbon-related peak at ~188 eV. [14]. The atomic concentration of boron in the outer divertor-facing surface (~4%) was almost twice that in the inner divertor-facing surface. In contrast to boron, the atomic concentrations of oxygen in all samples was almost constant (~6%). Because there was little boron oxide, most of oxygen is probably bonded to carbon, forming some carbonyl groups.

The peak energy of C1s for all tiles was a little lower than that for cleaved surfaces of pyrolytic graphite (PG) and the outer divertor-facing surface shows slightly higher peak energy than that of the inner divertor-facing surface as shown in Fig. 6.5(b). The XPS spectra of all samples showed that peak shapes were asymmetric with larger shoulders at the lower energy side compared to PG. In XPS studies for hydrogen implanted graphite [15], it is known that the C1s peak energy first shifts toward the low-energy side due to damage formation induced by the implantation, and then turns upward with increasing hydrogen fluence.

6.4 Discussion

In the divertor area in most of tokamaks, the inner divertor is deposition-dominated and the outer divertor erosion-dominated [7]. However, observations in the dome area of JT-60U are opposite, i.e. the outer divertor-facing dome wing was re-deposition dominated and the inner divertor-facing one erosion-dominated. Nevertheless H+D profiles show the higher retention on the re-deposited area, and the least on the eroded area, similar to other tokamaks. In addition, H+D profile of the eroded tile shows a sharp decay very near the surface, probably owing to the retreating surface by erosion. The H profiles are very similar for all tiles and penetrate rather deep with nearly constant concentration, suggesting pore diffusion. This indicates that mechanisms of hydrogen uptake or exchange to deuterium are similar for all dome tiles, or the re-deposition layers one the dome tile shows similar characteristics to hydrogen retention as the eroded surface.

It was shown that the depth profiles of hydrogen isotopes were quite different for erosion dominated outer divertor tiles and re-deposition dominated inner divertor tiles [9]. In particular, retention of H and D in the deposited surface layers on the inner divertor tile was quite small, even smaller than that in the erosion dominated outer divertor tile. Most probably, the poor adhesion or porous nature of the deposited layers on the inner divertor of JT-60U inhibited plasma heat load to conduction to the substrate, resulting in temperature increases in the surface deposited layers. Actually, the depth profiles and retention of hydrogen isotopes for both divertors are inversely correlated to the heat load.

In contrast, the dome area is not likely to carry a very high heat flux, and the temperature increment during shots must be smaller than that of the divertor tiles. Hence, hydrogen retention was higher at the re-deposited layers as observed in most tokamaks.

Recent NRA and TDS analysis shows the absolute (H+D)/C ration in those tiles were less than 0.05 [16, 17], which is much less than those observed in other tokamaks, giving another indication that tiles were subjected to higher temperatures. In depth profiling of C1s in XPS, lower energy shifts were found out with increasing depth shown in Fig. 6.6. This seems to correspond to reduction of retained H+D in depth. However, taken such small amounts of hydrogen retention compared to boron+oxygen (about 10%) into account, these low energy shifts could be due to the removals of B and O. In other words, hydrogen retention in the samples was too small to give clear influence on XPS measurements.

6.5 Summary

To reveal the hydrogen isotope behavior in the graphite tiles used for the dome unit with two side pumping in JT-60U, depth profiles of hydrogen and deuterium retained in carbon tiles were analyzed by SIMS and the chemical states of C1s, B1s and O1s were evaluated by XPS. The existence of the re-deposition layers was examined by SEM.

It was found that the inner divertor-facing side of the dome unit was erosion dominated, while the outer divertor-facing side was covered by the re-deposited layers. This is opposite to the observations in most tokamaks. Nevertheless, deuterium retention in the re-deposited layer on the outer divertor-facing side was the highest, and was least at the eroded inner divertor-facing side as often observed for high hydrogen retention in re-deposited layers. The chemical shift of C1s XPS peak clearly correlated with hydrogen retention, but its FWHM did not, indicating the nature of tile surfaces. The characteristics of the deposited layers for hydrogen seems to depend quite on its temperature history, which controls the hydrogen retention.

In all tiles, deuterium on the top surface was completely replaced by hydrogen indicating that hydrogen discharges employed for detritiation seems to work well to exchange most of deuterium retained by forming C-D bonds in near-surface areas irrespective of the tile positions. However, deuterium deeply retained was not effectively replaced by hydrogen discharges, particularly for the dome top tiles which retained large amounts of deuterium.

References

[1] G. Federici, *et al.*, *J. Nucl. Mater.*, **266-269**, 14 (1999).

[2] G. Janeschitz, ITER JCT and HTs, *J. Nucl. Mater.*, **290-293**, 1 (2001).

[3] J. P. Coad, *et al.*, *J. Nucl. Mater.*, **290-293**, 224 (2001).

[4] C. Stan-Sion, *et al.*, *J. Nucl. Mater.*, **290-293**, 491 (2001).

[5] T. Tanabe, *et al.*, *Fusion Sci. Technol.*, **41**, 877 (2002).

[6] K. Sugiyama, *et al.*, *Phys. Scr.*, **T103**, 58 (2003).

[7] T. Tanabe, *et al.*, *J. Nucl. Mater.*, **313-316**, 478 (2003).

[8] K. Masaki, *et al.*, *J. Nucl. Mater.*, **313-316**, 514 (2003).

[9] Y. Hirohata, *et al.*, *Phys. Scr.*, **T103**, 15 (2002).

[10] Y. Oya, *et al.*, *J. Nucl. Mater.*, **313-316**, 211 (2003).

[11] Y. Gotoh, *et al.*, *J. Nucl. Mater.*, **313-316**, 370 (2003).

[12] Y. Oya, *et al.*, *Phys. Scr.*, in press (2004).

[13] S. Gardner, *et al.*, *Carbon*, **587-595**, 587 (1995).

[14] W. Cermignani, *et al.*, *Carbon*, **33**, 367 (1995).

[15] Y. Gotoh, *Fusion Technol.*, **6**, 424 (1984).

[16] T. Hayashi, *et al.*, private communications.

[17] T. Shibahara, *et al.*, private communications.

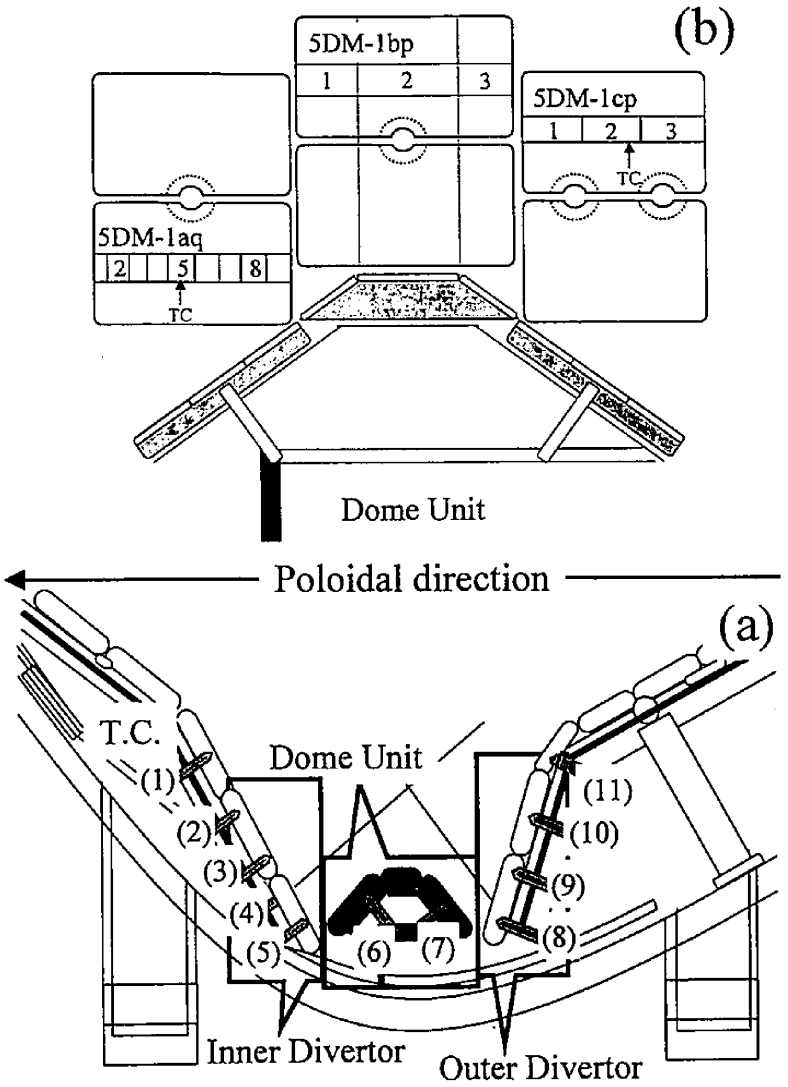

Fig. 6.1 (a) Cross section of the W-shaped divertor of JT-60U and (b) detailed structure of carbon tiles in the dome area and the area of samples examined.

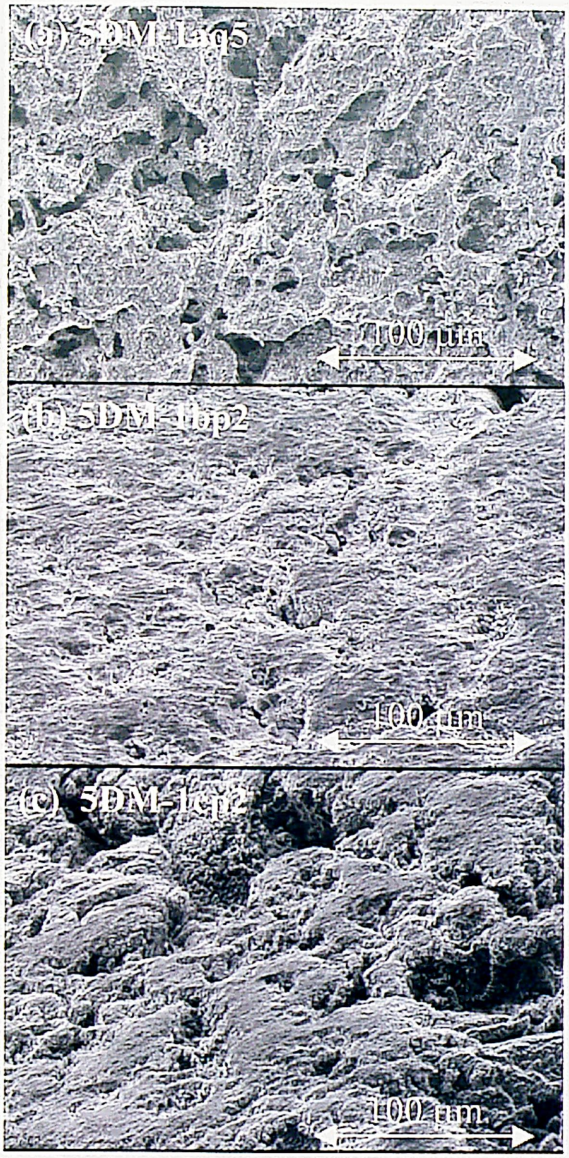

Fig. 6.2 SEM images observed for (a) 5DM-1aq5 (the inner divertor-facing side), (b) 5DM-1bp2 (the dome top area) and (c) 5DM-1cp2 (the outer divertor-facing side).

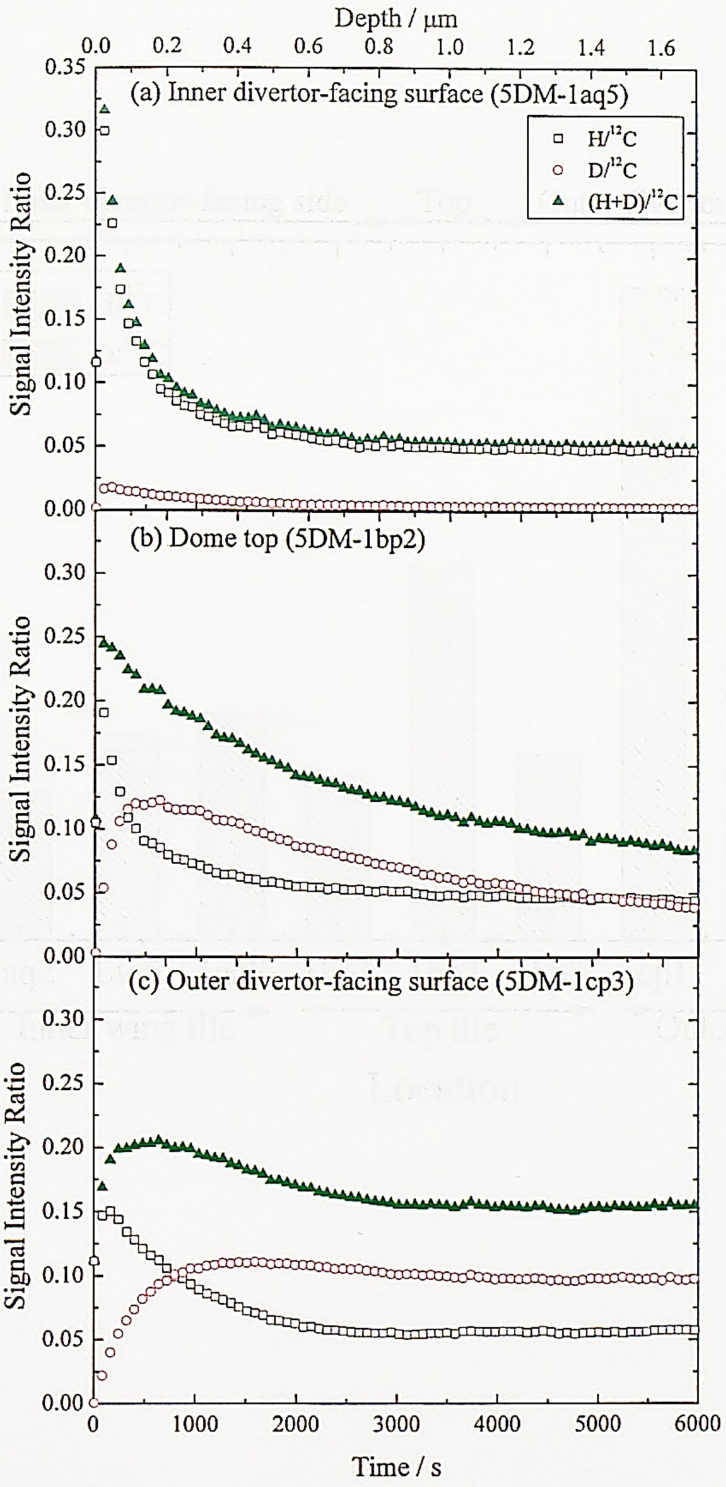

Fig. 6.3 Depth profiles of $H/^{12}C$, $D/^{12}C$, and $(H+D)/^{12}C$ signal intensity ratios determined by SIMS for (a) the inner divertor-facing surface (5DM-1aq5) with the eroded area, (b) the dome top (5DM-1bp2) where there was no appreciable erosion nor re-deposition and (c) the outer divertor-facing surface (5DM-1cp3) in the re-deposited area.

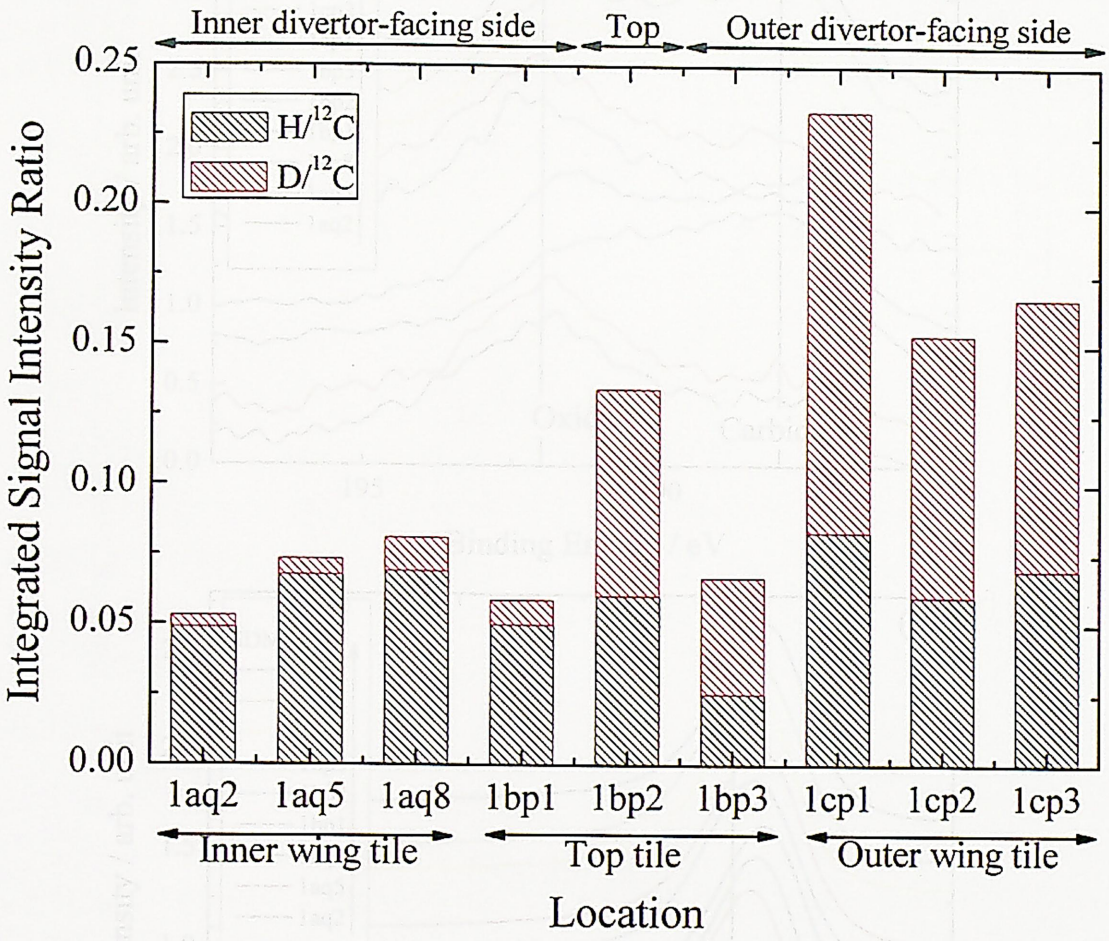

Fig. 6.4 Comparison of H and D retentions within 1.7 μm depth, given as the integrations of $H/^{12}C$ and $D/^{12}C$ signal ratios in the depth for all samples.

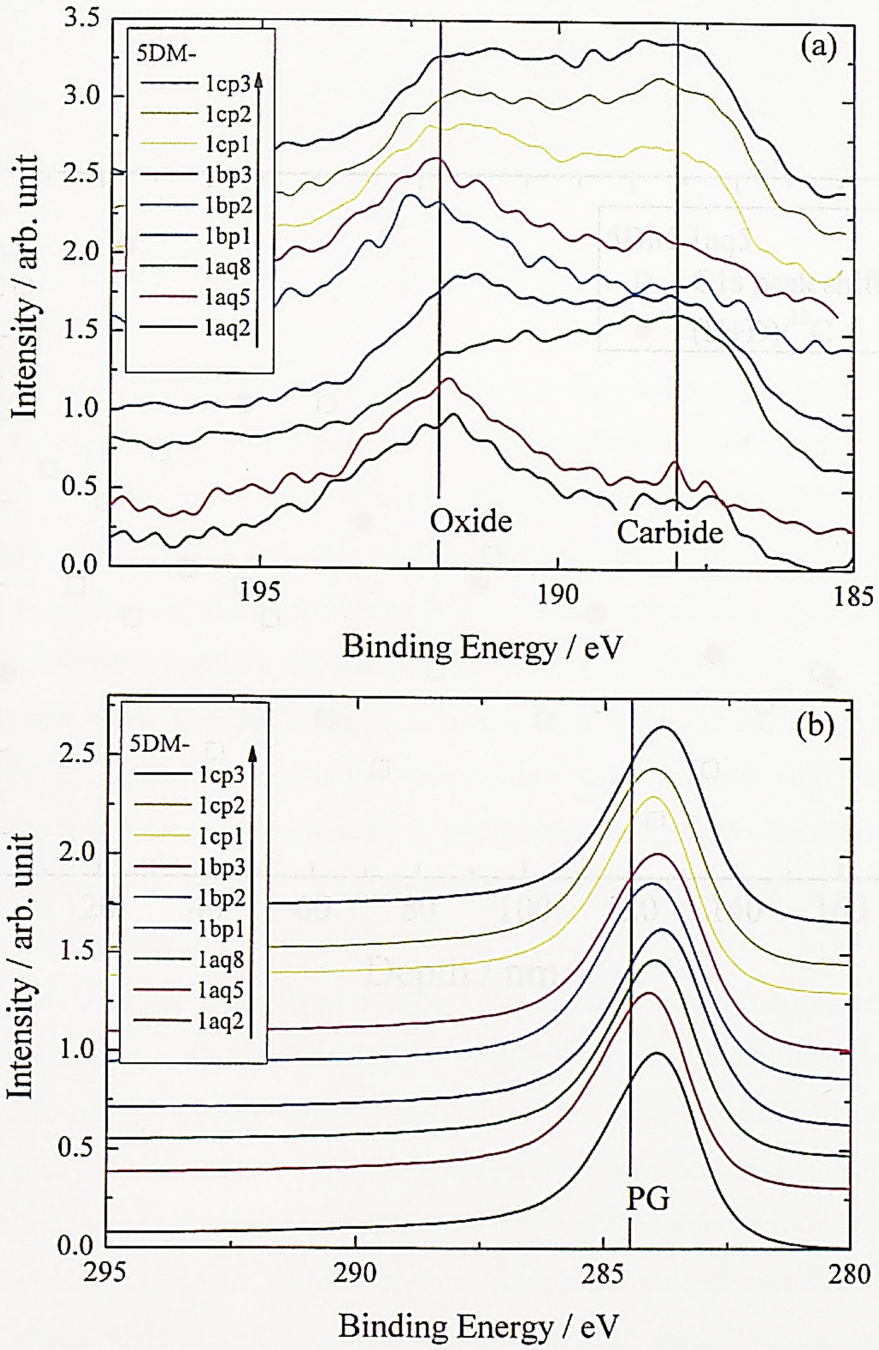

Fig. 6.5 Comparisons of XPS spectra of (a) B1s and (b) C1s observed on the inner divertor-facing (5DM-1aq2, 1aq5 and 1aq8), the dome top (5DM-1bp1, 1bp2 and 1bp3), the outer divertor-facing (5DM-1cp1, 1cp2 and 1cp3) tiles and Pyrolytic Graphite (PG) after Ar^+ sputtering for 6 min (removing 60-70 nm).

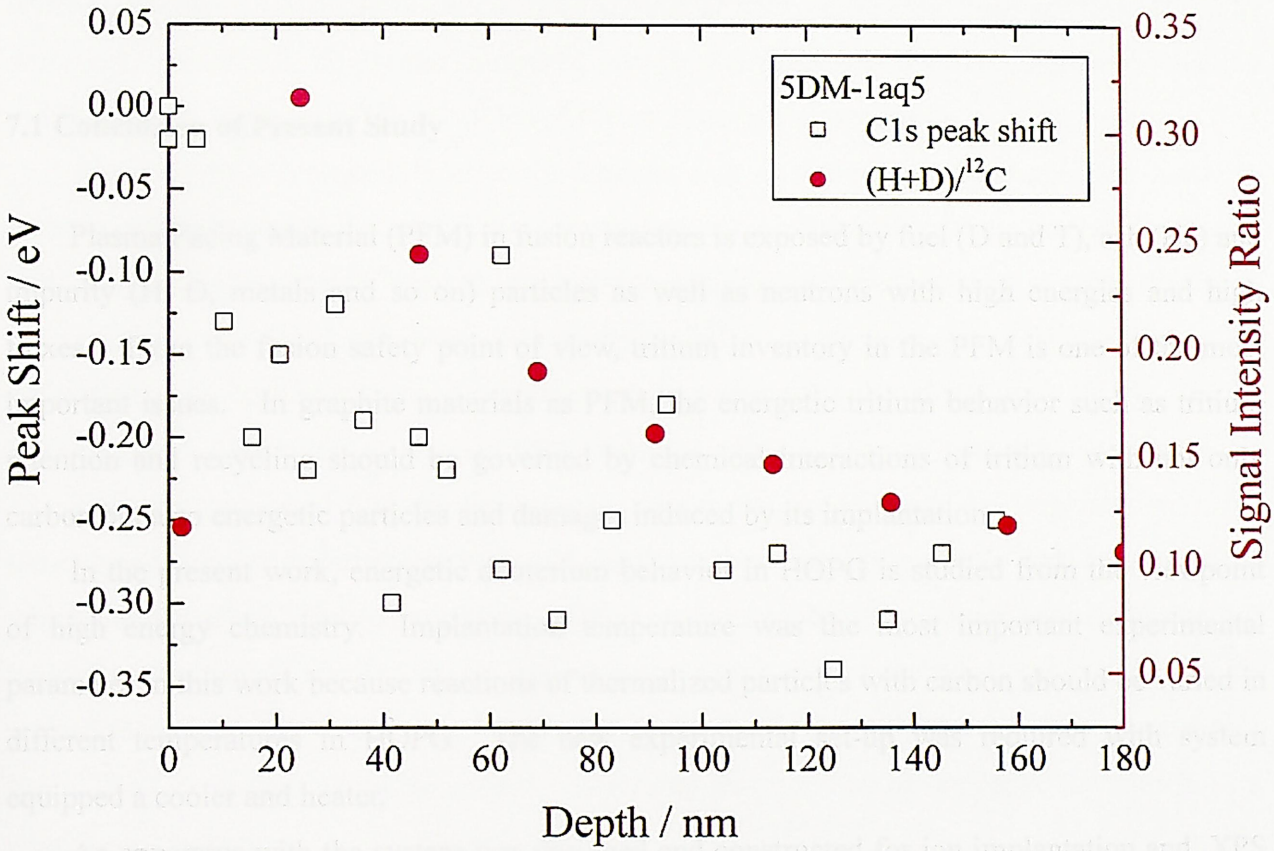

Fig. 6.6 Comparison between depth profiles resulted from XPS and SIMS for 5DM-1aq5.

CHAPTER VII

CONCLUSION

7.1 Conclusion of Present Study

Plasma Facing Material (PFM) in fusion reactors is exposed by fuel (D and T), ash (He) and impurity (H, O, metals and so on) particles as well as neutrons with high energies and high fluxes. From the fusion safety point of view, tritium inventory in the PFM is one of the most important issues. In graphite materials as PFM, the energetic tritium behavior such as tritium retention and recycling should be governed by chemical interactions of tritium with not only carbon but also energetic particles and damages induced by its implantation.

In the present work, energetic deuterium behavior in HOPG is studied from the viewpoint of high energy chemistry. Implantation temperature was the most important experimental parameter in this work because reactions of thermalized particles with carbon should be varied in different temperatures in HOPG. The new experimental set-up was required with system equipped a cooler and heater.

An apparatus with the system was designed and constructed for ion implantation and, XPS and TDS measurements. The system made a sample to be cooled and heated in ranging from 123 K to 1473 K using a cooling module and a PBN heater. This temperature region is very unique and introduced expectation of new knowledge for studies on the chemical interactions.

In the present work, chemical interaction of implanted deuterium into HOPG with carbon was investigated using XPS with various implantation conditions concentrated to ion fluence and energy. The chemical shift and FWHM change during D_2^+ implantation resulted in that new electron states. Investigation on the chemical shift with Ar^+ implantation found out forming sp^3 carbon and electron localized state. Successional implantation with D_2^+ induced relaxation of the disordered structure by forming C-D bond.

The deuterium implanted into HOPG was desorbed by heating and TDS spectra were measured with QMS. The TDS experiments were carried out with different heating rates for HOPG after the implantation with various fluences at a temperature ranging from 173 to 773 K. The TDS spectra demonstrated the deuterium desorption in the forms of D_2 and hydrocarbons. However, almost retained deuterium was desorbed with forming D_2 (CD_4/D_2=0.02 at 173 K).

The D_2 desorption spectra consisted of two processes which attributed to detrapping from the sp^3 and sp^3 neighbored with sp^x state C. The both process was limited by recombination reactions after detrapping. On the other hand, the desorption behavior of CD_x consisted of single process which attributed to the recombination of CD_{x-1} and D after detrapping from sp^3 state C. The desorption behavior of deuterium implanted into HOPG suggested that the disordered structure in HOPG was also annealed from sp^3 to sp^2 via sp^x state by detrapping D.

The amount of retained D after the implantation at various temperatures was found to decrease with increasing the implantation temperature. An increasing of the saturated retention with decreasing temperature even at lower temperature is clearly established in contradiction to the assumption of fixed maximum concentration below room temperature [1, 2] and to the estimation of the tritium inventory in a plasma-facing area using 0.4 of H/C ratio [3, 4]. As the thermal release of deuterium trapped with carbon forming C-D bond was not observed below 773 K it was suggested that the ion-induced release occurred during the implantation. The ion-induced release occurred by any collisional processes in the graphite and progressed by which the deuterium trapped by carbon could recombine to deuterium successional coming and migrate to the surface as molecules. This process is high energy chemical reaction because the activation energy is not concerned. After desorption due to the ion-induced release the trapping site without deuterium could be annealed easier and that was one of the cause for reducing the retention of deuterium.

Graphite tiles used in tokamak, JT-60U, was also investigated. It was found that the inner divertor-facing side of the dome unit was erosion dominated, while the outer divertor-facing side was covered by the re-deposited layers. This is opposite to the observations in most tokamaks. Nevertheless, deuterium retention in the re-deposited layer on the outer divertor-facing side was the highest, and was least at the eroded inner divertor-facing side as often observed for high hydrogen retention in re-deposited layers. The chemical shift of C1s XPS peak clearly correlated with hydrogen retention, but its FWHM did not, indicating the nature of tile surfaces. The characteristics of the deposited layers for hydrogen seems to depend quite on its temperature history, which controls the hydrogen retention.

7.2 Application of Present Study for Fusion Reactor

Over the last two decades, carbon materials, in the form of graphite or carbon composites,

has been the material of choice for lining the walls and divertors of most tokamaks. However, in ITER, the carbon materials will only used in a part of the divertor. This is because the carbon materials would retain extremely large amounts of tritium [3, 4].

When a hydrogen atom is implanted into carbon materials at temperature below about 800 K, it is effectively immobile [3-7] because the hydrogen in the materials is trapped by carbon forming chemical bonding. The trapped hydrogen is saturated in the carbon materials with atomic ratio (H/C) of 0.4 at RT. The hydrogen to carbon ratio in the saturated layer is quite dependence on the temperature [4] as nicely shown by Doyle *et al.* [8] and referred here. Fig. 5.4 shows the H/C in the saturated layer decreased with increasing the implantation temperature, regardless of the thermal annealing at temperature. The tritium inventory in the carbon materials for tokamaks is 0.4 in H/C ratio when the materials are kept near RT. A total tritium inventory is estimated to be 1 g using 0.4 (0.2 T/C for D-T) for large fusion reactor with a plasma-facing area of 100 m^2 [4]. However, temperatures on PFCs (Plasma Facing Components) such as first-wall and divertor for ITER are estimated to be in the region from ~560 K to ~1500 K [9]. In this temperature region, the H/C in the saturated layer should decrease to less than 0.2 (0.1 T/C for D-T) and a total tritium inventory of <0.5 g will result for the large fusion reactor, using the results in this study. Moreover, if the wall temperature kept being 773 K the tritium inventory could be critically decreased to be ~0. In fact, the hydrogen to carbon ratio was determined to be <0.05 in the divertor kept being > 573 K in graphite wall machine, JT-60U.

It will implicate perspective for tritium retention and recycling in fusion reactors that the tritium retention in the carbon materials was decreased during the implantation at lower temperature than 800 K where the tritium desorbs thermally from the materials. The decreasing of the hydrogen retention is high energy chemical reaction during the implantation. In JT-60U the deuterium retained vicinity of tile surface was exchanged by hydrogen as observed in this work. This could be induced by ion irradiation that is ion-induced release which would be progressed by that deuterium trapped by carbon is extracted by hydrogen and hydrogen coming continuously is trapped by carbon. Therefore the process governing the tritium retention and recycling during the plasma operation in fusion reactors can be applied with the high energy chemistry.

References

[1] D. K. Brice, *et al.*, *J. Nucl. Mater.*, **111-112**, 598 (1982).

[2] W. Möller and B. M. U. Scherzer, *J. Appl. Phys.*, **64**, 4860 (1988).

[3] R. A. Causey, *et al.*, *Fusion Eng. Des.*, **61-62**, 525 (2002).

[4] R. A. Causey, *J. Nucl. Mater.*, **300**, 91 (2002).

[5] R. A. Causey, *et al.*, *Carbon*, **17**, 323 (1979).

[6] M. Saeki, *J. Nucl. Mater.*, **131**, 32 (1985).

[7] H. D. Rohrig, *et al.*, *J. Am. Ceram. Soc.*, **59**, 323 (1979).

[8] B. L. Doyle *et al.*, *J. Nucl. Mater.*, **111-112**, 513 (1982).

[9] G. Federici *et al.*, *J. Nucl. Mater.*, **266-269**, 14 (1999).

ATTACHMENT

LIST OF PUBLICATIONS

Associated Paper

Paper

1. **Y. Morimoto**, T. Sugiyama, S. Akahori, H. Kodama, E. Tega, M. Sasaki, M. Oyaidu, H. Kimura, and K. Okuno, Study on energetic ion behavior in plasma facing materials at lower temperature, *Phys. Scr.*, **T103**, 117-120 (2003).

2. **Y, Morimoto** and K. Okuno, Correlation between annealing effect of damages and implanted deuterium release from graphite, *J. Nucl. Mater.*, **313-316**, 595-598 (2003).

3. **Y. Morimoto**, H. Kimura, M. Sasaki, K. Sakamoto, T. Imai and K. Okuno, X-ray Photoelectron Spectroscopy Study on Change of Chemical State of Diamond Window Implanted Ions, *Fusion Eng. Des.*, **66-68**, 651-656 (2003).

4. **Y. Morimoto**, Y. Oya, Y. Hirohata, H. Kodama, H. Yoshida, K. Kizu, J. Yagyu, K. Masaki, Y. Gotoh, N. Miya, T. Hino, S. Tanaka, K. Okuno, and T. Tanabe, Correlation Between Hydrogen Isotope Profiles and Surface Structure of Divertor Tiles in JT-60U, *J Nucl.Mater.*, to be published.

5. K. Iguchi, **Y. Morimoto**, T. Sugiyama, S. Akahori, K. Okuno, H. Nakamura, and M. Nishi, Chemical behavior of energetic deuterium implanted into SiC, Si, and Graphite, *Fus. Sci. Technol.*, **39**, 905-909 (2001).

6. Y. Hirohata, Y. Oya, H. Yoshida, **Y. Morimoto**, H. Kodama, K. Kizu, J. Yagyu, Y. Gotoh, K. Masaki, K. Okuno, N. Miya, T. Hino, S. Tanaka and T. Tanabe, The depth profiles of deuterium and hydrogen in graphite tiles exposed to DD plasma discharges of JT-60U, *Phys. Scr.*, **T103**, 15-19 (2003).

7. Y. Oya, Y. Hirohata, **Y. Morimoto**, H. Yoshida, H. Kodama, K. Kizu, J. Yagyu, Y. Gotoh, K. Masaki, K. Okuno, T. Tanabe, N. Miya, T. Hino and S. Tanaka, Hydrogen isotope behavior in in-vessel components used for DD plasma operation of JT-60U by SIMS and XPS technique, *J. Nucl. Mater.*, **313-316**, 209-213 (2003).

8. Y. Oya, **Y. Morimoto**, Y. Hirohata, H. Kodama, H. Yoshida, K Kizu, J. Yagyu, Y. Gotoh, K. Masaki, K. Okuno, N. Miya, T. Hino, S. Tanaka and T. Tanabe, Chemical States of Graphite Tiles exposed to DD Plasma by XPS, *JAERI Review*, **2003-029**, 140-143 (2003).

9. Y. Hirohata, Y. Oya, H. Yoshida, **Y. Morimoto**, H. Kodama, K. Kizu, J. Yagyu, Y. Gotoh, K. Masaki, T. Arai, K. Okuno, N. Miya, T. Hino, S. Tanaka and T. Tanabe, The Depth Profiles of Deuterium and Hydrogen in Graphite Tiles Exposed to DD Plasma Discharges of JT-60U, *JAERI Review*, **2003-029**, 136-139 (2003).

10. Y. Ishimoto, M. Miyamoto, **Y. Morimoto**, H. Yoshida, K. Matsuhiro, H. Iwakiri, Y. Hirooka, Y. Yamamura, K. Morita and the PWI-Taskgroup, Plasma-Wall Interaction Fata Compendium-3 "Hyrogen Retention Property, Diffusion and Recombination Coefficients Database for Selected Plasma-Facing Materials", *NIFS-MEMO*, **42** (2004).

11. Y. Oya, **Y. Morimoto**, M. Oyaidzu, Y. Hirohata, J. Yagyu, Y.Miyo, Y. Gotoh, K. Sugiyama, K. Okuno, N. Miya, T. Hino, S. Tanaka and T. Tanabe, Analyses of Hydrogen Isotope Distributions in the Outer Target Tile used in the W-shaped Divertor of JT-60U, *Phys. Scr.*, (2004) in press.

12. H. Kimura, **Y. Morimoto** and K. Okuno, Kinetic Study on Chemical Interaction of Deuterium during Implantation into Pyrolytic Graphite, *J Nucl.Mater.*, to be published.

13. M. Sasaki, **Y. Morimoto**, H. Kimura, K. Takahashi, K. Sakamoto, T. Imai, and K. Okuno, Energetic Deuterium and Helium Irradiation Effects on Chemical Structure of CVD Diamond, *J Nucl.Mater.*, to be published.

14. Y. Hirohata, Y. Oya, H.Yoshida, **Y. Morimoto**, T.Arai, K. Kizu, J. Yagyu, K. Masaki, Y.Gotoh, K. Okuno, N. Miya, T. Hino, S. Tanaka and T. Tanabe, Depth Profile and Retention of Hydrogen Isotopes in Graphite Tiles Used in the W-Shaped Divertor of JT-60U, *J Nucl.Mater.*, to be published.

Oral Presentation

1. 異方性グラファイトにおける高エネルギー重水素の化学的挙動
   静岡大・理・放射研　○森本泰臣 奥野健二
   平成 11 年度 第 3 回 PSI 研究会, 2000 年 2 月 17, 18 日, 九州大学応用力学研究所

2. 異方性グラファイトにおける高エネルギー重水素の化学的挙動
   静岡大・理・放射研　○森本泰臣 杉山友章 井口一成 奥野健二
   日本原子力学会 2000 年春の年会, 2000 年 3 月 28～30 日, 愛媛大学

3. 静岡大におけるプラズマ対向材料中水素同位体の高エネルギー化学的挙動の研究
   静岡大・理・放射研　○森本泰臣 奥野健二
   日本原子力学会 第5回「核融合炉材料中における水素同位体挙動」研究専門委員会, 2000 年 7 月 1 日, 静岡大学

4. Chemical Behavior of Energetic Deuterium in Anisotropic Graphite
Y. Morimoto*, T. Sugiyama, K. Iguchi and K. Okuno
Radiochemistry Research Laboratory, Faculty of Science, Shizuoka University
Japan-US Workshop on High Heat Flux Components and Plasma Surface Interactions for Next Fusion Devices, Nov. 6-9, 2000, at Senri-Hankyu Hotel, Osaka, Japan

5. プラズマ対向材料中の水素同位体挙動の高エネルギー化学的研究(Ⅲ)
静岡大・理・放射研　○森本泰臣　杉山友章　奥野健二
九大総理工・応力研　　宮本光貴　岩切宏友　吉田直亮
RIAMフォーラム 2001, 2001 年 6 月 7, 8 日, 九州大学筑紫地区共通管理棟 3階大会議室

6. 静岡大学における TDS 実験
静岡大・理・放射研 ・○森本泰臣　奥野健二
山村作業会, 2001 年 7 月 27 日, 核融合科学研究所

7. グラファイトにおける高エネルギー重水素の化学的挙動 (III) – グラファイトの電子状態 –
静岡大・理・放射研　○森本泰臣　杉山友章　児玉博　奥野健二
日本原子力学会 2001 年秋の大会, 2001 年 9 月 19-21 日, 北海道大学

8. グラファイト中の高エネルギー重水素の化学的挙動
静岡大・理・放射研　○森本泰臣　奥野健二
PSI 合同研究会, 2002 年 8 月 20, 21 日, 九州大学応用力学研究所

9. TDS データ解析 #3
静岡大・理・放射研　○森本泰臣
森田作業会, 2002 年 9 月 3 日, 核融合科学研究所

10. TDS データ解析 #3 ver.2
静岡大・理・放射研　○森本泰臣
森田作業会, 2002 年 12 月 17 日, 核融合科学研究所

11. TDS データ解析 #3 ver.3
静岡大・理・放射研　○森本泰臣
森田作業会, 2003 年 7 月 25 日, 核融合科学研究所

12. グラファイトにおける高エネルギー重水素の化学的挙動 (IV) –イオン照射温度依存性–
静岡大・理・放射研　○森本泰臣　木村宏美　布目智之　竹田剛　奥野健二
日本原子力学会 2003 年秋の大会, 2003 年 9 月 24-26 日, 静岡大学

Poster Presentation

1. 低Z材料中の高エネルギー重水素の化学的挙動
   静岡大・理・放射研　○森本泰臣 杉山友章 井口一成 奥野健二
   原研　　中村博文 西正孝
   第3回核融合エネルギー連合講演会 -21世紀が求めるエネルギー-, 2000年6月12, 13日, 中部大学

2. ANNEALING EFFECTS OF DAMAGES ON CHEMICAL BEHAVIOR OF DEUTERIUM IMPLANTED INTO GRAPHITE
   Y. Morimoto, S. Sugiyama, and K. Okuno
   Radiochemistry Research Laboratory, Faculty of Science, Shizuoka University
   10th International Conference on Fusion Reactor Material, Oct. 14-19, 2001, Kongresshaus, Barden-Barden, Germany

3. Correlation Between the Annealing Effects of Damage and Implanted Deuterium Release from Graphite.
   Y. Morimoto and K. Okuno (1)
   Graduate School of Science and Engineering, Shizuoka University
   (1) Radiochemistry Research Laboratory, Faculty of Science, Shizuoka University
   15th International Conference on Plasma Surface Interactions in Controlled Fusion Devices, May 27-31, 2002, Nagaragawa Convention Center, Gifu, Japan

4. Study on Energetic Ions Behavior in Plasma Facing Materials at Lower Temperature
   Y. Morimoto, T. Sugiyama, S. Akahori, H. Kodama, E. Tega, M. Sasaki, M. Oyaidu, H. Kimura(1), and K. Okuno(1)
   Shizuoka University, Graduate School of Science and Engineering
   (1) Shizuoka University, Faculty of Science, Radiochemistry Research Laboratory
   International workshop on "Hydrogen Isotopes in Fusion Reactor Materials", May 22-24, 2002, University of Tokyo, Tokyo, Japan

5. グラファイト中の重水素照射欠陥に対する熱アニール効果と重水素放出の相関関係
   静岡大・理・放射研 ○森本泰臣 児玉博 小柳津誠 佐々木政義 奥野健二
   第4回核融合エネルギー連合講演会 -新しい展開にむけて-, 2002年6月13, 14日, 大阪大学コンベンションセンター

6. X-ray Photoelectron Spectroscopy Study on Change of Chemical State of Diamond Window Implanted Ions
   Y. Morimoto, H. Kimura (1), M. Sasaki, K. Sakamoto (2), T. Imai (2), and K. Okuno (1)
   Graduate School of Science and Engineering, Shizuoka University
   (1) Radiochemistry Research Laboratory, Faculty of Science, Shizuoka University
   (2) Naka Fusion Research Establishment, Japan Atomic Energy Institute
   22nd Symposium on Fusion Technology, Sep. 9-13, 2002, Marina Congress Center, Helsinki, Finland

7. Hydrogen Isotopes Behavior in Divertor Tiles of JT-60U
Y. Morimoto, H. Kodama and K.Okuno
Graduate School of Science and Engineering, Shizuoka University,
Y. Oya and S. Tanaka
The University of Tokyo
Y. Hirohata, H. Yoshida and T. Hino
Hokkaido University
K. Kizu, J. Yagyu, K. Masaki, Y. Gotoh and N. Miya
Japan Atomic Energy Research Institute,
T. Tanabe
Nagoya University
15th Topical Meeting on the Technology of Fusion Energy, Nov. 17-21, 2002,
Washington, D.C.

8. Correlation Between Hydrogen Isotope Profiles and Surface Structure of Divertor Tiles in JT-60U
Y. Morimoto, H. Kodama, K. Okuno,
Shizuoka University, Ohya, Shizuoka 422-8529, Japan
Y. Oya, S. Tanaka
The University of Tokyo
Y. Hirohata, H. Yoshida, T. Hino
Hokkaido University
K. Kizu, J. Yagyu, K. Masaki, Y. Gotoh, N. Miya
Japan Atomic Energy Research Institute
T. Tanabe
Nagoya University
11th International Conference on Fusion Reactor Materials, Dec. 7-12, 2003 Kyoto, Japan

Other Paper

Paper

1. **Y. Morimoto**, S. Akahori, A. Shimada, K. Iguchi, K. Okuno, M. Nishikawa, K. Munakata, A. Baba, T. Kawagoe, H. Moriyama, K. Kawamoto and M. Okada, Correlation between tritium release and thermal annealing of damages in neutron-irradiated Li_4SiO_4, *Fus. Sci. Technol.*, **39**, 634-638 (2001).

2. K. Iguchi, **Y. Morimoto,** A. Shimada, N. Inuzuka, K. Okuno, H. Nakamura, and M. Nishi, Chemical behavior of energetic deuterium implanted into Silicon Carbide, *J. Plasma and Fusion Res. SERIES*, **3**, 337-341(2000).

3. K. Munakata, Y. Yokoyama, A.Baba, T. Kawagoe, T. Takeishi, M. Nishikawa, R.-D. Penzhorn, K. Kawamoto, H. Moriyma, **Y. Morimoto** and K. Okuno, Tritium Release from Catalytic Breeder Materials, *Proceedings of 9th International Workshop on Ceramic Breeder Blanket Interactions*, 49-56 (2000).

4. K. Munakata, Y. Yokoyama, A. Baba, T. Kawagoe, T. Takeishi, M. Nishikawa, R.-D. Penzhorn, H. Moriyma, K. Kawamoto, **Y. Morimoto** and K. Okuno, Tritium Release from Catalytic Breeder Materials, *Fusion Eng. Des.*, **58-59**, 683-687 (2001)

5. S. Akahori, **Y. Morimoto**, E. Tega, K. Okuno, M. Nishikawa, K. Munakata, Y. Yokoyama, H. Moriyama, K. Kawamoto and M. Okada, Correlation Between Tritium Release Processes and Thermal Annealing of Damage Induced by Neutron Irradiation in Li_4SiO_4, *Proceedings of 6th Japan-China Symposium on Materials for Advanced Energy System and Fission & Fusion Engineering*, (2001).

6. T. Sugiyama, **Y. Morimoto**, K. Iguchi, K. Okuno M. Miyamoto, H. Iwakiri and N. Yoshida, Effects of Helium Irradiation on Chemical Behavior of Energetic Deuterium in SiC, *J. Nucl. Mater.*, **307-311**, 1080-1083 (2002).

7. H. Kodama, **Y. Morimoto**, Y. Oya, A. Sagara, N. Noda and K. Okuno, Study on Retention and Chemical States of Implanted Deuterium into Boron Thin Film, *Proceedings of 7th China-Japan Symposium on Materials for Advanced Energy System and Fission & Fusion Engineering*, 352-358 (2002).

8. Y. Oya, Y. Makide, K. Chiba, S. Tanaka, **Y. Morimoto**, H. Kodama, K. Okuno T. Kawano, Y. Asakura and T. Uda, Hydrogen behavior on the surface of SS-304 and Fe for cooling pipe, *Proceedings of 7th China-Japan Symposium on Materials for Advanced Energy System and Fission & Fusion Engineering*, 359-336 (2002).

9. M. Nishikawa, K. Munakata, T. Takeishi, A. Baba, N. Nakashima, K. Hashimoto, Yokoyama, K. Okuno, **Y. Morimoto**, H. Moriyama, and K. Kawamoto, Out-pile tritium release experiment from various ceramic breeder materials in KUR, *Fus. Sci. Technol.*, **41**, 1025-1029 (2002).

10. K. Munakata, Y. Yokoyama, A. Koga, N. Nakashima, S. Beloglazov, T. Takeishi, M. Nishikawa, R-D. Penzhorn, K. Kawamoto, H. Moriyama, **Y. Morimoto** and K. Okuno, Effect of Catalytic Materials on Tritium release from Ceramic Breeder Materials, *J. Nucl. Mater.*, **307-311**, 1451-1455 (2002).

11. H. Kodama, T. Sugiyama, **Y. Morimoto**, Y. Oya, K. Okuno, N. Inoue, A. Sagara, and N. Noda, Thermal Annealing Effects on Chemical States of Deuterium Implanted into Boron Coating, *J. Nucl. Mater.*, **313-316**, 153-157 (2003).

12. M. Miyamoto, K. Tokunaga, T. Fujiwara, N. Yoshida, TRIAM group, **Y. Morimoto**, T. Sugiyama and K. Okuno, Material properties of co-deposition formed on plasma facing materials in all-metal machine TRIAM-1M, *J. Nucl. Mater.*, **313-316**, 82-86 (2003).

13. Y. Oya Y. Makide, **Y. Morimoto**, H. Kodama, K.Okuno, K.Chiba, S. Tanaka, T. Kawano, Y. Asakura and T. Uda, Hydrogen Isotope Behavior in Stainless Steel for Cooling Pipe in Fusion Reactor, *Fus. Sci. Technol.*, **44**, 359-363 (2003).

14. H. Kodama, Y. Morimoto, M.Sasaki, M. Oyaidu, Y. Oya, A. Sagara, N. Noda and K. Okuno, Chemical Behavior of Energetic Deuterium Implanted into Boron Coatings, *Fus. Sci. Technol.*, **44**, 420-424 (2003).

15. K. Munakata, A. Koga, Y. Yokoyama, S. Kanjo, N. Nakashima, S. Beloglazov, D. Inovski, T. Takeishi, M. Nishikawa, R-D. Penzhorn, K. Kawamoto, H. Moriyama, **Y. Morimoto,** S. Akahori and K. Okuno, Efect of Water Vapor on Tritium release from Ceramic Breeder Material, *Fusion Eng. Des.*, **69**, 27-31 (2003).

16. S. Akahori, E. Tega, **Y. Morimoto**, K. Okuno, M. Nishikawa, K. Munakata, H. Moriyama, K. Kawamoto, and M. Okada, Hot atom chemical behavior of tritium produced by ^{6}Li (n, α) ^{3}H in Li_4SiO_4, *J. Radioanal. Nucl. Chem.*, **255**, 257-260 (2003).

17. M. Oyaidzu, **Y. Morimoto**, M. Sasaki, H. Kimura, K. Munakata, M. Nishikawa, K. Kawamoto, M. Okada and K. Okuno, ESR Study on Annihilation Process of Radiation Defects Induced by Neutron Irradiation, *Phys. Scr.*, (2003) in press.

18. Y. Oya, H. Kodama, M. Oyaidzu, **Y. Morimoto**, M. Matsuyama, A. Sagara, N. Noda and K. Okuno, Study on Implanted Hydrogen Isotope Retention and Its Chemical Behavior in Boron Thin Film for Wall Conditioning, *J Nucl.Mater.*, to be published.

19. H. Kodama, M. Oyaidzu, M. Sasaki, H. Kimura, **Y. Morimoto**, Y. Oya, M. Matsuyama, A. Sagara, N. Noda, and K. Okuno, Studies on Structural and Chemical Characterization for Boron Coating Films Deposited by PCVD, *J Nucl.Mater.*, to be published.

20. G. Smolik, R. Pawelko, **Y. Morimoto**, K. Okuno, R. Anderl, D. Petti, and T. Terai, Mobilization Measurements from Flibe under Argon and Air Flow, *J Nucl.Mater.*, to be published.

21. M. Oyaidzu, **Y. Morimoto**, H. Kodama, M. Sasaki, H. Kimura, K. Munakata, M. Nishikawa, M. Okada, K. Kawamoto, H. Moriyama and K. Okuno, The Correlation between the Annihilation Process of Radiation Defects and Tritium Release Process in Li_2TiO_3, *J Nucl.Mater.*, to be published.

Oral Presentation

1. 中性子照射した Li_4SiO_4 におけるトリチウムと照射欠陥の相互作用
   静岡大・理・放射研　○森本泰臣 島田亜佐子 井口一成 奥野健二
   九大・総理工　西川正史 宗像健三 馬場淳史 川越孝宏
   京大炉　森山裕丈 川本圭造 岡田守民
   日本原子力学会 1999 年秋の大会, 1999 年 9 月 10～12 日, 新潟工科大学

2. 固体における高エネルギーイオンのホットアトム化学的過程に関する研究(Ⅱ)
   -Si 中の高エネルギー重水素の化学的挙動-
   静岡大・理・放射研　○森本泰臣 井口一成 島田亜佐子 奥野健二
   原研　中村博文 西正孝
   日本放射化学会 第 43 回放射化学討論会, 1999 年 10 月 13～15 日, つくば国際会議場

3. SiC における高エネルギー重水素の化学的挙動に与える He 照射の影響
   静岡大・理・放射研　○森本泰臣 杉山友章 井口一成 奥野健二
   九大・総理工　宮本光貴
   九大・応力研　岩切宏友 吉田直亮
   日本原子力学会 2000 年秋の大会, 2000 年 9 月 15～17 日, 青森大学

Poster Presentation

1. CORRELATION BETWEEN TRITIUM RELEASE AND THERMAL ANNEALING OF DAMAGES IN NEUTRON IRRADIATED Li_4SiO_4
   Y. Morimoto*, S. Akahori, A. Shimada, K. Iguchi and K. Okuno
   Radiochemistry Research laboratory, Faculty of Science, Shizuoka University
   M. Nishikawa, K. Munakata, A. Baba and T. Kawagoe
   Department of Advanced Energy Engineering Science, Kyusyu University
   H. Moriyama, K. Kawamoto and M. Okada
   Research Reactor Institute, Kyoto University,
   14th Topical Meeting on the Technology of Fusion Energy,
   Oct. 15-19, 2000, Park City, Utah, USA.